Materials for Nonlinear Optics: Semicontinuous Gold Films and Fast Saturable Absorbers

by

Giovanni Piredda

Submitted in Partial Fulfillment

of the

Requirements for the Degree

Doctor of Philosophy

Supervised by

Professor Robert W. Boyd

The Institute of Optics
The College
School of Engineering and Applied Sciences

University of Rochester
Rochester, New York

2008

Al di là dei monti e del mare, mi spiegò l'Assistente, esisteva un sapiente di nome Onsager, del quale lui non sapeva nulla salvo che aveva elaborato una equazione che pretendeva di descrivere il comportamento delle molecole polari in tutte le condizioni, purché si trovassero allo stato liquido. L'equazione funzionava bene per le soluzioni diluite; non risultava che nessuno si fosse curato di verificarla per soluzioni concentrate, per liquidi polari puri, e per miscele di questi ultimi.

Primo Levi, Il sistema periodico, Potassio.

Curriculum Vitae

Giovanni Piredda was born in Cagliari, Italy, on Dec. 3rd 1970. He graduated with a Laurea in Physics from the University of Trieste in 1997 with 110/110 e lode; his Laurea thesis dealt with theoretical Seismology. After the Laurea he served for ten months in the Italian National Civil Service as an administrative assistant at the "Ospedale Maggiore" in Trieste; in 1998 and 1999 he worked at the Science Museum "Immaginario Scientifico" in Trieste preparing hands-on physics demonstrations for middle- and high-school students. He began the PhD program at the Institute of Optics, University of Rochester, in 1999; in 2000 he joined the group of Prof. Robert W. Boyd, under whose direction he has worked on photorefractive optics, techniques for the measurement of the ultrafast component of the nonlinear refractive index, the optics of metal-dielectric composite materials and slow light. From the Fall of 1999 to the of Spring 2002 he received an Optical Science Purpose Trust fellowship.

Publications

"Nonlinear optical properties of a gold-silica composite with high gold fill fraction and the sign change of its nonlinear absorption coefficient", G. Piredda, D. D. Smith, B. Wendling and R. W. Boyd, *Journal of the Optical Society of America B* **25**, 945 (2008)

"Anisotropic nonlinear response of silicon in the near-infrared region", Q. Lin, J. Zhang, G. Piredda, R. W. Boyd, P. M. Fauchet, and G. P. Agrawal, *Applied Physics Letters* **91**, 071113 (2007)

"Wavelength dependence of silicon nonlinearity in the near infrared region", Q. Lin, J. Zhang, G. Piredda, R. W. Boyd, P. M. Fauchet, and G. P. Agrawal, *Applied Physics Letters* **91**, 021111 (2007)

"Optical solitons in a silicon waveguide", J. Zhang, Q. Lin, G. Piredda, R. W. Boyd, G. P. Agrawal and P. M. Fauchet. . *Optics Express* **15**, 7682-7688 (2007)

"Slow light by means of coherent population oscillations: laser linewidth effects", G. Piredda and R. W. Boyd, *Journal of the European Optical Society: Rapid publications* **2**, 07004 (2007)

"Measurement of the intensity-dependent refractive index using complete spatio-temporal pulse characterization", G. Piredda, C. Dorrer, E. M. Kosik, I. A. Walmsley and R. W. Boyd. *Journal of Nonlinear Optical Physics and Materials* **14**, 9- 20 (2005)

"Enhanced nonlinear optical response of one-dimensional metal-dielectric photonic crystals", N. N. Lepeshkin, A. Schweinsberg, G. Piredda, R. S. Bennink and R. W. Boyd. *Physical Review Letters* **93**, 123902 (2004).

Conference Papers

"Saturable Absorption in Nanocomposite Gold-Silica Materials with High Gold Fill Fraction", G. Piredda, D. D. Smith, Y. Yoon, R. W. Boyd, R. Xiao and B. Wendling; CLEO, Baltimore, MD, May 2007 (poster)

"Why Do Coherent Population Oscillations (CPOs) Lead to Slow Light When the Laser Linewidth Exceeds the Width of the CPO Transparency Window?" G. Piredda and R. W. Boyd; FiO, Rochester, NY, October 2006 (oral presentation)

"Room temperature slow light with 27 GHz bandwidth in semiconductor quantum dots", G. Piredda, A. Schweinsberg and R. W. Boyd; OSA topical meeting "Slow and Fast light", Washington DC, July 2006 (oral presentation)

"Metal-dielectric composites as nonlinear optical materials", N. N. Lepeshkin, G. Piredda, A. Schweinsberg and R. W. Boyd; OSA topical meeting "Photonic Metamaterials: From Random to Periodic", Grand Bahama Island, The Bahamas, June 2006 (oral presentation)

"Real-time imaging through fog by a self-referencing interferometric technique", G. Piredda, Y. Gu, J. E. Heebner and R. W. Boyd; FiO, Rochester, NY,October 2004(oral presentation).

"Nonlinear optical properties of noble metals at the interband transition threshold"; N. N. Lepeshkin, G. Piredda, A. Schweinsberg and R. W. Boyd; CLEO, Baltimore, MD, June 2003 (oral presentation).

"Applications of nonlinear optics in ultrashort pulse metrology and vice versa", I. A. Walmsley, E. Kosik, C. Dorrer, R. W. Boyd and G. Piredda; The 15th Annual Meeting of the IEEE Lasers and Electro-Optics Society, Glasgow, Scotland, November 2002 (oral presentation)

"A semiclassical approach to Van der Waals - Casimir forces", G. Piredda, The Institute of Optics, Rochester, NY, October 2002;

"Measurement of the intensity dependent refractive index using complete spatiotemporal ultrashort pulse characterization", C. Dorrer, G. Piredda, E. M. Kosik, I .A. Walmsley and R.W. Boyd; CLEO, Long Beach, CA , May 2002(oral presentation).

"Measurement of the intensity dependent refractive index using complete spatiotemporal ultrashort pulse characterization", C. Dorrer, G. Piredda, E. M. Kosik, I. A. Walmsley and R.W. Boyd; Winter College on Ultrafast Non-linear Optics, Abdus Salam ICTP, Trieste, Italy, February 2002 (oral presentation).

"Nondestructive, contrast enhanced imaging of biological tissues using photorefractive recycling", G. Piredda, A. Schweinsberg, J. E. Heebner, R. W. Boyd, D. D. Smith, R. Richmond and K. L. Bors; CLEO, Baltimore, MD, May 2001 (oral presentation).

Acknowledgements

I wish to acknowledge the support and guidance of my thesis advisor Professor Robert W. Boyd. Working with him as a PhD student I have had the possibility to see the whole path of a scientific work, from the conception of the idea to the publishing of the paper, and I consider this an extremely valuable experience.

I would like to thank Dr. David D. Smith and Dr. Mark A. Nelson for the collaboration from which my experiments on semicontinuous gold film resulted. In particular I owe to Dr. Smith the perspective on the nonlinear optics of percolation systems in which I have developed my own ideas.

Dr. Nick Lepeshkin contributed to form my interest in the optics of metals, first showed to me how to perform a "z-scan" experiment, and gave me valuable technical suggestions on the measurements; Per Adamson assisted me with a critical part of the experiments; Andreas Liapis and Brian McIntyre took for me the SEM images of some of the samples on which I have performed measurements; Dr. Nelson brought to Rochester his own samples on which I performed the first successful experiment; Dr. Bettina Wendling, whom I have never had the pleasure to meet, fabricated the samples on which I obtained most of the data for my thesis.

I would like to thank Aaron Schweinsberg for the collaboration on the experimental part of the "slow-light" work; when I started my work on the subject he had already considerable experience in the topic of slow light and the work with him has been purposeful and enjoyable.

The qualifying exam committee and the thesis committee have been the source of many important insights; for this I thank Profs. Chunlei Guo, Lukas Novotny, Lewis Rothberg and the president of the thesis committee Prof. Paul Fulkenbusch.

I thank all the staff of the Institute of Optics for the constant excellent support: Joan Christian, Noelene Votens, Lissa Cotter, Maria Schnitzler, Betsy Benedict, Gina Kern, Lori Russell, Barbara Schirmer, Marie Banach, Michael Koch and once more Per Adamson and Brian McIntyre.

The atmosphere in the laboratory and offices has been productive and stimulating thanks to the members of my group. I wish to acknowledge collaboration and many discussions with all of them, past and present, and they will not be offended if I single out Petros Zerom that has been my room-mate for two years and Matt Bigelow (together with his family) that introduced me to the Rockies and to "real" American life for once.

It seems that I never have enough of discussing, so I particularly would like to thank people outside of my research group who stopped to discuss Physics and other topics with me. These include, among the physicist, opticians or engineers, Dr. Alberto Marino, Dr. Mike Beversluis, Dr. Jorge Zurita-Sanchez, Dr. Manuel de la Cruz-Gutierrez, Dr. Nick Usechak, Dr. Matthias Danckwerts, Dr. Jin Wang, Dr. Stefano Palomba, Prof. Chunlei Guo, Yu Gu, Aleksandr Radunsky, Renee Pedrazzani and for an additional reason Prof. Miguel Alonso, Dr. Lin Qiang, Jidong Zhang, Dr. Svetlana Lukishova, Dr. Ansgar Schmid and Prof. Lukas Novotny that in different

occasions offered to me the opportunity to take part in their own research projects. The people that I have not listed explicitly can be sure that they are remembered and this includes all of those who have helped me, often very generously, at the Institute of Optics and at the University of Rochester at large.

On a different front there are people that I have met as friends while in Rochester, and I would like to mention in particular Drs. Claudio Campanale, Alessandro Riboni and Luca Guazzotto, the family of Ernesto Meli and Valeria Zanferli and the family of Dr. Arkadiusz and Iwona Bibillo.

Looking at the other shore of the ocean I need to acknowledge the friendship and concrete support of the late Prof. Gallieno Denardo of the Abdus Salam International Center for Theoretical Physics and Dr. Miltcho Danailov of the Elettra Synchrotron in Trieste that introduced me to the field of optics.

I gratefully acknowledge the constant friendship of many people abroad among which I want to mention Davide Zedda and his family, Alberto Dalle Coste, Gaspare Andreella and his family, Giuseppe Latino, Roberto Sedda and Maria Bonaria Loi, Laura Todde, Giorgio Erby, Dr. Piero Cau, Dr. Giuseppe Colizzi, Gianluca Perniciano, Cristiano Gnesutta, Gianluca Rotaris, Sara Peric and all the people from the CVS group, Dr. Giuliana Verbanac and Marijana Fajgl. There have been also people that I have met only through the Internet; the newsgroup it.arti.cinema has been in particular a constant reference point for stimulating discussion on movies and many other topics.

I wish also to thank all of the members of my family for being always present in my life; they won't be offended if the only name that I mention explicitly is that of aunt Vittoria.

Finally, I dedicate this thesis to my parents Efisio and Edelvais together with my sister Claudia and her family, my aunt Rina and my grandmother Elisabetta.

The citation in the dedication page is from a book by Primo Levi whom I very much like as a writer; he is describing succinctly his Laurea thesis work: it was nice to find out that he worked on the verification of an effective medium formula in high fill fraction conditions.

Abstract

In this thesis I have investigated two types of materials that have the potentiality, in different ways, to contribute to practical applications of nonlinear optics: semicontinuous gold films and fast saturable absorbers.

Metals have extremely high values of the third-order nonlinear optical susceptibility (they are approximately 10^6 times more nonlinear than silica) and a very fast response time (on the order of 2 ps); this high nonlinearity makes them attractive candidates for applications such as all-optical switching. On the other hand, as everyday experience teaches, they do not let light pass through.

One way to make light penetrate more deeply into metals is mixing them with dielectrics. In particular in my thesis I have studied the nonlinear properties of collection of gold nanoparticles embedded into silica or deposited onto it. These nanoparticle systems possess special resonances, the "plasmon resonances", that are absent from either bulk metal or bulk dielectric but only arise when the two are combined at the nanoscale.

In the linear optical response these resonances produce extinction bands that for gold in silica are situated in the visible. At the resonance wavelength the electric field is concentrated inside the nanoparticles, and this field concentration produces an enhanced nonlinear optical response.

In my work I have experimentally characterized the nonlinear absorption in these kind of samples over a wide range of composition and wavelength, and have proposed

an explanation for the fact that under certain conditions these materials are saturable absorbers while gold itself is an optical limiter.

A separate part of my work has examined the use of fast saturable absorbers to slow down light using the mechanism of coherent population oscillations.

Using quantum dots as saturable absorbers I have demonstrated the slow propagation of pulses of ≈ 30 ps duration.

Contents

List of Tables

List of Figures

Chapter 1

Introduction

Nonlinear optical effects are useful for many different applications. Some examples of areas of science and technology in which nonlinear optics is applied are nonlinear microscopy [1], ultrafast laser systems [2], wavelength conversion [3], material processing [4–6], the characterization of surfaces [7], optical routing and switching both on networks [8–10] and on chips [11].

Research is active in expanding the scope of these applications and refining those which are already mature. One striking example of a mature technology is the mode locking of lasers; lasers that produce pulses of fs duration by means of fast saturable absorbers are so reliable that they can be used in ophthalmologic surgery [12]. On the other hand, for example, the application of nonlinear optics to high bandwidth optical switching is at an earlier stage of evolution [13].

There are in fact, broadly speaking, two classes of optical switches [10]; the devices

belonging to one class, "space-domain switching", switch an entire channel between two or more outputs, and their response time can be relatively slow (even ms); the devices belonging to the other class, "time-domain switching", switch individual data packets or even bits, and they must respond in a time scale of a few ps or even shorter. One of the difficulties in developing optical switches is finding materials whose nonlinearity is at the same time strong and ultrafast while their linear and nonlinear absorption is small; a synthetic description of the potentiality of a material for optical switching can be given with figures of merit [8]. Among the materials that are taken into consideration are conjugated polymers [14], semiconductors [15] (both their free carrier nonlinearities and their Kerr nonlinearities can be used) and chalcogenide glasses [16].

Studies on materials must then be looked at in the perspective created by microstructures (such as photonic crystals) [17–19] which can be used to enhance nonlinear effects.

Another application for which the development of new materials with particular nonlinear optical properties is important is optical limiting [6].

Metals have a fast and strong nonlinear response [20], and may be good candidates for nonlinear optical applications if they are combined in an opportune way with dielectrics [21, 22]. Combining metals and dielectrics has two main purposes. One is allowing light to enter more deeply into metals, and this can be achieved for example by cancelling reflections by interference; the other is achieving light localization which

in turn leads to an enhanced nonlinear response [21].

A part of the work of my thesis has been spurred by these considerations; in particular I have examined experimentally nonlinear absorption in gold nanoparticle systems embedded in silica at high gold concentrations.

The interest in metal nanoparticles is not limited to the field of optics; important reasons for this interest [23] are that metal nanoparticles can be synthesized and modified chemically with ease and their properties are suited to many applications. Restricting ourselves to optics, an outstanding property of metal nanoparticles is the presence of extinction bands in the visible or infrared that result from the so-called "plasmon resonances"; these resonances do not exist in bulk metals, can be interpreted as a result of the confinement of free electrons in a space smaller than one wavelength of the light and controlled by changing the shape of the nanoparticle and its orientation with respect to the electric field.

Plasmon resonances in metal nanoparticles can be put to many practical uses; for example they enhance the sensitivity of optical sensors [24] and show great potential to be applied in the therapy of cancer [25]. Plasmon resonances are also the reason why the nonlinear optical properties of nanoparticle systems are enhanced with respect to those of bulk metals [26]; I examine this effect in detail in the work of my thesis.

A design for an optical switch based on the nonlinear optical response of metal has been recently presented in the literature by Min and coworkers [27]

Another area of research where the development of materials with particular non-

linear optical properties is important is slow light [28].

The first demonstration of dramatic slowing down of light was presented in a famous Nature paper by Hau and coworkers [29] where a speed of light of 17 m/s was observed in an ultracold gas. The work of the research group of which I am a member has shown that the same concepts that led to slow propagation of light in an ultracold gas could be applied successfully to solid state systems at room temperature [30].

This observation marked the start of a wide effort in finding new materials and effects that could lead to slow light. The establishment of this new field of research was made "official" when the first OSA Topical Meeting on Slow and Fast light was held in Baltimore in 2006.

The physical means of obtaining slow light are divided into two main classes. One can slow light down by propagation effects in several kind of structures or by material effects, creating a large swing of the index in a certain material and consequently a very big or very small group index.

The work of my thesis has dealt with the second approach and in particular I have worked to find materials that would permit extension of the effect of Coherent Population Oscillations used in [30] to ps time scales.

1.1 Overview of the thesis

The thesis is organized as follows. In Chapter 2 I introduce the optics of metal-dielectric composite materials. The effects that I have studied in my thesis can be

interpreted in terms of the "effective medium" concepts which are discussed in Section 2.2; to be able to apply these concepts to metal-dielectric composite one must know the linear and nonlinear optics of metals which are reviewed in Section 2.1.

Chapter 3 presents the results that I obtained on the nonlinear optics of gold nanoparticle systems and the methodology that I used; the observation that the composite material is a saturable absorber is explained with a model of plasmon damping that complements another explanation published earlier by my co-worker Dr. David D. Smith [31].

Chapter 4 presents my studies on slow light, in particular my discussion of some details of the theory of Coherent Population Oscillations and a demonstrative experiment of slowing down pulses of ps duration.

Conclusions are drawn in Chapter 5.

Chapter 2

Metal-dielectric composite materials

Metals possess high optical nonlinearities; for example, the Kerr coefficient of gold is $\approx 10^{-8}$esu, that is 10^6 times more than silica (the datum for gold can be found in [32] and for silica in [33]). It is difficult to take advantage of this high nonlinearity because light penetrates into metals for only tens of nanometers (the "skin depth"). However, most of the light is not absorbed, but reflected; if most of the light were absorbed it would be a hard task to use metals in optics (they would not indeed be even good as mirrors): since light is reflected, one can search for situations in which reflection is reduced.

Light can penetrate more deeply into metals when they are mixed together with dielectric materials; this opens the possibility to use metals in applications in which

light is transmitted through them rather than just as reflectors.

There are two broad classes of composite materials: nanocomposites, in which all the dimensions of the components are much smaller than the wavelength of light, and photonic crystals, in which the components are arranged in a periodic structure and at least some of the dimensions of the components are comparable with the wavelength of light. The optical properties of nanocomposites can often be described by effective dielectric constants; that is, the composite material behaves as a homogeneous medium whose dielectric constant is determined both by the dielectric constants of the components and the microscopic geometry. The behaviour of light inside photonic crystals is influenced by interference and the concept of effective dielectric constant is less useful.

If the optical properties of a nanocomposite material are described by an effective dielectric constant, then some information about its value is immediately available if one knows just some macroscopic quantities. In particular, if one knows only the dielectric constants of the components and the volume fill fraction of each, and if the dielectric constants are both real and positive, one can obtain the Wiener limits (since the original work of O. Wiener is hard to find, I refer to the review on optical properties of nanocomposites by Gehr and Boyd [34])

$$\sum_i f_i \varepsilon_i \geq \varepsilon_{\text{eff}} \geq \left[\sum_i f_i / \varepsilon_i \right]^{-1} . \tag{2.1}$$

where ε_i is the dielectric constant of the i-th constituent and f_i its volume fill fraction.

If in addition one knows that the effective medium is isotropic, the more restrictive

Hashin and Shtrikman limits [35] apply:

$$\varepsilon_1 + f_2 / \left(\frac{1}{\varepsilon_2 - \varepsilon_1} + \frac{f_1}{3\varepsilon_1} \right) \leq \varepsilon_{\text{eff}} \leq \varepsilon_2 + f_1 / \left(\frac{1}{\varepsilon_1 - \varepsilon_2} + \frac{f_2}{3\varepsilon_2} \right) \qquad (2.2)$$

where it is assumed that $\varepsilon_1 < \varepsilon_2$.

Even tighter limits can be found if one knows some other effective bulk parameter

of the composite [36].

Both the Wiener and the Hashin and Shtrikman limits have been extended to the

case in which the dielectric constants of the components can be complex by Milton [37]

and Bergman [38]. It is worth noting here that if the dielectric constants of the

components of a two-component mixture are of opposite sign the Wiener limits of

Equation 2.1 are already written in a wrong form because the expression $\left[\sum_i f_i/\varepsilon_i \right]^{-1}$

is not necessarily smaller than $\sum_i f_i\varepsilon_i$. It is exactly from this fact that many of the

interesting properties of the metal-dielectric composites treated in this thesis come.

If one wants to predict with more precision the effective dielectric constant of a

composite medium it is necessary to take the microstructure into account. Nanocom-

posite materials can be classified into several categories [34] (let us limit ourselves,

for simplicity, to materials that are made of two constituents); different theories are

suited to describe the different categories.

The first category is the "Maxwell Garnett" nanoparticle systems, in which one

constituent forms inclusions which are dispersed in the other constituent. They were

first described theoretically by J. C. Maxwell Garnett [39] who found the expression for their effective dielectric constant which brings his name. The main feature in the optical properties of these materials is the appearance of a resonance in their absorption spectrum, the "plasmon resonance" when one of the constituents is a dielectric and the other is metal [1].

Materials in the second category are composed of constituents that are interspersed in each other in such a way that none of them forms a homogeneous "background". There are two different points of view for this category, because not always an effective medium description is adequate, especially for the description of the nonlinear optical properties of these materials.

According to the first point of view one tries to devise a different effective medium theory. The first effective medium treatment which has been proposed for these kinds of media was proposed by Bruggeman [40] (in German - the same analysis can be found in the English language in the work by Landauer [41]). The most important features of Bruggeman's formula for the effective dielectric constant are that the plasmon resonance is missing and that a new phenomenon is predicted: the effective dielectric constant of the composite as a function of fill fraction of one of the two constituents has a sudden change of slope at a certain value of the fill fraction. This sudden change of slope can be connected to the physical concept of percolation: as the volume fraction of one component increases from very small

---

[1]The "classic" localized plasmon resonance case happens when the inclusions are metallic and the host is a dielectric, but a similar resonance appears also when it is the dielectric that forms inclusions in a metallic matrix

values, the grains of that component begin to aggregate and form structures in the background formed by the other component, till these structures join in a network that spans macroscopic distances. This percolation is linked to many important physical phenomena; the name comes from the Latin verb "percolare" (to seep through) and it refers to the fact that when holes form an interconnected network in a solid, liquids can seep through it (of great importance in Earth science [42] [2]). In material science the percolation threshold marks, for example, the transition between insulator and conductor in metal-dielectric composite materials.

Composite materials that are at or very close to the percolation threshold have the characteristic that they possess variations in physical properties at a large range of length scales. In this case an effective medium theory like the one by Bruggeman does not capture the effects that the field fluctuations have on the optical properties of these materials and a second point of view comes into play; it is necessary to take fluctuations explicitly into account.

An early attempt to include in the treatment some features of the microstructure is the work of Ping Sheng [43, 44].

Of all the important work that has been done on the physical phenomena related with field fluctuations in complex random nanostructures in optics in recent years I cite some papers by Shalaev and collaborators [45–47] that, using sophisticated numerical methods able to describe efficiently the local behaviour of the fields in complicated structures, predicted a very large enhancement of the optical nonlin-

---

[2]The liquid for example could be oil.

earities. The presence in these kind of structures of complicated field configuration including hot spots has been verified in several experimental studies (a partial review of this line of research can be found in [48] and a recent article is [49]).

Finally there are layered composites. If each layer is much thinner than a wavelength these media too behave as an effective medium that is anisotropic; see for example [50] for the theory and [51] for an experimental demonstration of nonlinear optical behaviour.

As the layers' thicknesses become large interference phenomena become important and the composite medium becomes a photonic crystal; in the immense scientific literature dedicated to photonic crystals there are just a few publications that treat the case were both a metal and a dielectric are part of the material. The fundamental reason for studying these composites is that they allow light to penetrate into metals [22] opening in this way one more avenue for the possible use of metals in practical optical devices.

My work as a doctoral student has just briefly touched the subject of photonic crystal; I have participated in a work that has shown enhanced nonlinear optical properties in a copper-silica metallo-dielectric band-gap structure [52]. It has mainly concentrated on the nonlinear optical properties of nanoparticle Maxwell Garnett systems from small to high metal fill fraction below the percolation threshold.

2.1   Optics of metals

The dielectric constant of the dielectric materials, glass and air, used in the composites that I studied, has a quite simple behaviour in the wavelength range of interest. Even that of glass can be considered purely real and constant without introducing any significant error in the analysis of the data. It is also possible to neglect any nonlinearity of glass and air because they are dwarfed by the nonlinearities of the metal.

Both the linear and nonlinear optical behaviour of metals are more complex and we analyze them in the following subsections.

2.1.1   Linear optics

The first step in understanding the optical properties of metals is considering the optical response as arising only from the response of free electrons. More precisely, one treats in a classical way the response of the electrons in the conduction band to the incident radiation; if one assumes that the otherwise free electrons of charge e and mass m are subject to random collisions with a mean frequency $\gamma = 1/\tau$ one obtains the following dielectric function [53]

$$\varepsilon\left(\omega\right) = 1 + \frac{4\pi i \sigma}{\omega\left(1 - i\omega\tau\right)} \tag{2.3}$$

with $\sigma = Ne^2\tau/m$ where N is the number of free electrons per unit volume. Expres-

sion 2.3 is called the Drude expression for the dielectric constant of a metal.

The value of the relaxation time τ when the metal forms very small structures can be considerably smaller than the value for bulk metal because electrons can scatter at the surfaces of the nanostructures besides than just with phonons. I include this effect in the analysis of my data in Section 3.4.

Equation 2.3 predicts that metal are good reflectors for all frequencies up to the "plasma frequency"

$$\omega_p = \sqrt{\frac{4\pi N e^2}{m}} \tag{2.4}$$

and that light can penetrate into them for frequencies larger than ω_p. The predicted transition is very sharp if the mean time between collisions τ is large, and softer for small values of τ in which case the collisions dissipate energy which is therefore neither transmitted nor reflected.

A typical value for N is $5.9 \times 10^{22}/\text{cm}^3$; the transition from the reflecting to the transmitting state should therefore happen in the ultraviolet. It can be observed for example in alkali metals, and the book by Born and Wolf [54] lists the calculated and observed value of the transition: for lithium the calculated value is 150 nm and the observed value is 205 nm, and for the other alkali the correspondence is equal or better.

The optical behaviour of noble metals is more complicated; silver looks white, which does not distinguishes it "at sight" from a Drude metal, but copper is reddish

and gold is yellow, which indicates that they do not reflect equally well all visible light even if the plasma wavelength for both is in the ultraviolet. Some of the visible light is in fact absorbed by transitions from the so-called d-band electrons into conduction band levels. The threshold for these "interband" transitions is about 2 eV for both gold and copper, while it is at around 4 eV for silver, that explains its uniform reflectivity in the visible range.

The interband transitions from the d-band to the conduction band play as well an important role in the nonlinear optics of metals, as we will see in Section 2.1.2.

The dielectric constant for various metals has been accurately measured for various metals by Johnson and Christy [55]. A comparison between the data obtained for gold by these authors and the prediction of Drude model for $\omega_p = 1.36 \times 10^{16}\,\mathrm{s}^{-1}$ and $\tau = 9 \times 10^{-15}\,\mathrm{s}$ is shown in Figure 2.1; the Drude model is corrected allowing for the presence of a background dielectric constant $\varepsilon_\infty = 9.9$; the onset of interband transitions can be seen in the Johnson and Christy data at around 600 nm.

A consequence of this combination of interband absorption and long-wavelength reflection given by the free electrons is that a very thin gold film looks green in transmission. The green color also distinguishes a percolated film from a film made by isolated nanoparticles.

Another consequence of the presence of free electrons in metals is the possibility of charge density oscillations called "plasma oscillations" [53]. These oscillations can be understood in terms of a simple model (Figure 2.2). Displacement of the free
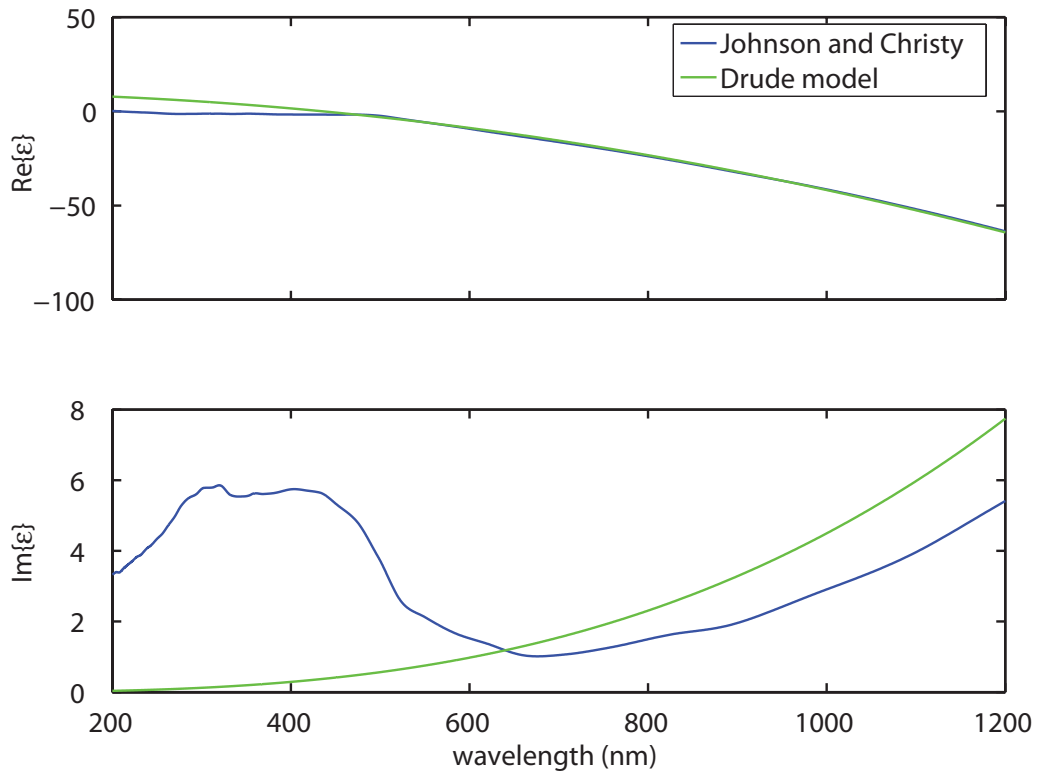
Figure 2.1: Dielectric constant of gold plotted against the wavelength. The data of Johnson and Christy [55] are compared to the Drude model with $\omega_p = 1.36 \times 10^{16}\,\mathrm{s}^{-1}$ and $\tau = 9 \times 10^{-15}\,\mathrm{s}$; the Drude model is corrected allowing for the presence of a background dielectric constant $\varepsilon_\infty = 9.9$. The onset of interband transitions can be seen at around 600 nm.

electrons in a block of metal as a whole gives rise to surface charges and consequently a restoring uniform electric field; this system acts as a harmonic oscillator with natural frequency given by Equation 2.4.

The plasma oscillations exist for any wavevector k and from Maxwell equations we find that their oscillation frequency is given by the relation $\varepsilon\left(\omega_p\right) = 0$; that is, they are not dispersive. A more careful analysis finds that a certain amount of dispersion is introduced by the fact that the dielectric constant of metal also has a wavevector

σ = Nde   Electrons

$$E = 4\pi Nde$$

Ions   σ = -Nde
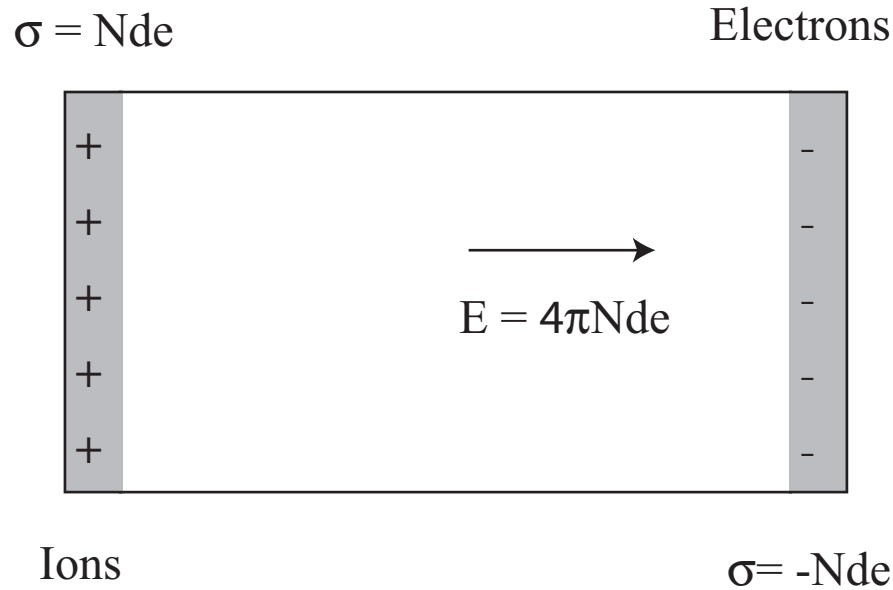
Figure 2.2: Plasma oscillations. The free electrons are uniformly displaced by a distance d, creating two zones of surface charge at each end of the medium.

dependence [56].

Another important feature of the bulk plasma oscillations is that they are not coupled to travelling electromagnetic waves. In fact the fourth Maxwell equation $\nabla \times \mathbf{B} = (4\pi/c)\,\mathbf{J} + (1/c)\,\partial\mathbf{E}/\partial t$ is satisfied by the plasma oscillations with $\mathbf{B} = 0$: the electric field couples only with the current; the second Maxwell equation $\nabla \times \mathbf{E} = -(1/c)\,\partial\mathbf{B}/\partial t$ is identically satisfied because the electric field coupled to plasma oscillations is irrotational.

Plasma oscillations can couple to travelling electromagnetic waves and become important in optics in two context. One is when they couple to the electromagnetic field at the surface of a metal forming the surface plasmon-polariton [57] (these are travelling electromagnetic waves that are confined to an extended surface); another

is when charge oscillations are excited in structures that are much smaller than the wavelength of light forming the localized surface plasmons which play a key role in the optical response of metal-dielectric composite materials including the ones analyzed in this thesis; a discussion of this point is postponed till Section 2.3. A paper that includes a review of bulk and surface plasmons from a physical point of view with many references is [58].

In a spherical metallic nanoparticle which is so small that its interaction with light can be described by its static polarizability the presence of a resonance can be seen in the expression for its polarizability α:

$$\alpha_i = R^3 \varepsilon_h \frac{\varepsilon_i - \varepsilon_h}{\varepsilon_i + 2\varepsilon_h}, \tag{2.5}$$

where R is the nanoparticle radius, ε_i its dielectric constant and ε_h the dielectric constant of the surrounding medium. This expression has a pole for $\varepsilon_i + 2\varepsilon_h = 0$ and the resonance can be interpreted in term of plasm oscillations just as in Figure 2.2 with the opportune adjustment for the different geometry. This kind of plasmons play a crucial role in the enhanced nonlinear optical effects described in Chapter 2.

2.1.2 Nonlinear optics - the case of gold

In reporting about the nonlinear optical properties of metals I limit myself to the case of gold. The other noble metals are described in a similar way but with differences due to the different band gaps from the d-band to the conduction band.

The nonlinear optical response of gold derives from four main contributions; I base my discussion on the works of Hache and collaborators [59, 60]. The first is due to the nonlinear behaviour of the conduction electrons when they are confined in the small volume of the nanoparticles, and does not exist in bulk gold; the second is the saturation of of interband transitions; the third is the so-called "hot-electron" contribution, the fourth, linked to the third, is an increase in electron-electron scattering rate when their equilibrium distribution is modified by an intense laser pulse (not described in the Hache's papers and proposed as an important mechanism in a work by a German group [61]).

The first contribution to the nonlinearity comes from the confinement of otherwise free electrons; the mechanism is the same as the one active in conjugated polymers (and described for the case of polymers in the book by Boyd [33] for example) and is described theoretically in the same way. In conjugated polymers one considers electrons that can move only along one spatial direction in a rectangular box; in gold nanoparticles Hache [60] considers a system of independent electrons in a spherical box. The nonlinearity appears for nanoparticles of diameter smaller than 100 nm and is size dependent. The imaginary part of the nonlinear susceptibility coefficient resulting from this mechanism is positive and the time response is quasi instantaneous.

The interband transitions from the d-band to the conduction band can be saturated by high optical intensities. This interband contribution to the nonlinearity is size-independent (down to very small sizes) and ultrafast.

The nature of the hot-electron contribution is more complex. Part of the optical radiation that is incident on gold is absorbed by the conduction electrons; the specific heat of these electrons is small and they can be raised to elevated temperatures. The electrons come to thermal equilibrium between themselves much earlier than with the crystalline lattice; thus their Fermi-Dirac distribution is modified and part of the energy levels below the Fermi level are emptied while part of the energy levels above the Fermi level become occupied (see Figure 2.3); this mechanism is called also the "Fermi smearing". The interband absorption becomes therefore modified; for gold in the vicinity of 530 nm this mechanism more precisely leads to an increase in absorption; it is a positive contribution to the imaginary part of $\chi^{(3)}$.

The Fermi smearing has been studied with thermomodulation techniques by Rosei and coauthors for silver [62,63] and for aluminum, gold and copper [64], and by Eesley with pulses of ps duration for copper [65] that made possible to time-resolve the heating of the electrons and the heating of the lattice; the electron-phonon relaxation was studied as well with pulses of $\approx 200\,\text{fs}$ duration by Elsayed-Ali and coauthors [66]. The conclusion from the time-resolved studies is that the electrons relax to the lattice temperature in a few ps.

Studies with finer temporal resolution have resolved the thermalization of the electron gas on its own which happens on the time scale of a few hundred fs [67, 68] and is influenced both by electron-electron scattering and by heat transport at the Fermi velocity over distances of the order of tens of nm. This last conclusion is reached

by comparing experiments on thin and thick gold films; in the thick films only a gold layer up to the skin depth is heated and heat is exchanged across the sample's depth; monitoring with a probe beam the time-dependent reflectivity on both sides of the sample when a pump hits one side allows to resolve some details of this heat transport mechanism.

A paper that describes in detail the combined dynamics of electron thermalization and electron-lattice thermalization is the work by Sun et al. [69]. In this work reflection and transmission changes in a 20 nm thick gold film were measured using an infrared pump and a probe tunable between 440 and 532 nm (corresponding to the transitions from the d-band to the Fermi level in the conduction band) and were interpreted with a model that using Boltzmann transport equation takes into account the whole kinetic of electron thermalization (20 nm gold film is a "thin" film by and therefore no heat transport needs to be taken into account).

The fine point that this paper explains both in quantitative detail and with a clear discussion is how the peak change of reflectivity and transmissivity is delayed with respect to the peak of the pump pulse. This can be seen in a descriptive way noting that the pump pulse imparts energy to electrons all over the conduction band; then change in occupancy are therefore at the beginning distributed over a broad range of energies and result in an instantaneous but small change in reflectivity and transmissivity distributed over a broad frequency range. As the electron gas thermalizes the changes in occupancy become concentrated in the vicinity of the Fermi level and

consequently a larger but more localized in frequency optical response arises.

Another consequence of the rapid thermalization of the conduction electrons and their consequent large temperature increase is the increase in the rate of electron-electron scattering, mechanism suggested in [61] to explain the transient broadening of the plasmon resonance observed under laser irradiation with pulses of fs duration. Electron-electron scattering is restricted by Pauli principle to the electrons that are not farther than kT from the Fermi level; and an increase in temperature leads to increased damping. The relative importance of the increased e-e scattering and the change in transition rates from the d-band to the conduction band has been evaluated in a work of a Japanese group [70] that with a sophisticated fitting procedure on their experimental data on time-resolved absorption spectra of a gold nanoparticle system concluded that among the two the change in transition rates is the most effective mechanism of dielectric constant change.

After a hundred of ps or so the lattice heating is transferred over longer distances and a more properly "thermal" nonlinearity ensues.

A short synthesis of the time scales involved is the following. The quasi-instantaneous response is composed by the interband and intraband contributions; the response of the "hot electrons" develops in hundreds of fs and decays in a couple of ps; the localized lattice heating is transferred to the surrounding medium in hundreds of ps.

On the time scale of the pulses I used in the experiments I performed (around 25 ps) the hot-electron contribution dominates and gold at 532 nm is expected to be an

optical limiter (positive sign of the imaginary part of $\chi^{(3)}$).

A measurement of nonlinear absorption of ps pulses in a thin gold film has been published by David D. Smith et al. who found that gold is an optical limiter at 532 nm and assigned to $\chi^{(3)}$ a value of $-1 \times 10^{-8} + 5 \times 10^{-8}i$ esu.
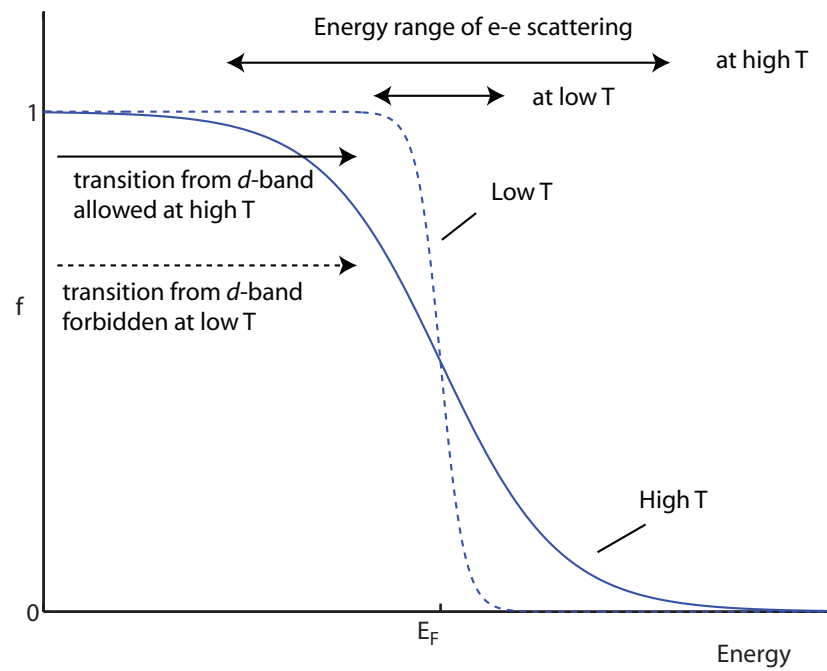
Figure 2.3: Fermi smearing mechanism. The lines represent the Fermi-Dirac distribution of conduction electrons at low (dashed) and high (solid line) temperature. The same transition from the d-band to the conduction band is forbidden at low temperature (dashed arrow) and allowed at high temperature (solid arrow); moreover the energy range in which electron-electron scattering is allowed increases with temperature.

2.2 Nanoparticle systems

In this thesis we look for the macroscopic nonlinear response of a composite medium. That is we admit implicitly that it makes sense to think of our composite media as having an effective homogeneous response.

We briefly touched on several theories that lead to effective parameters for the optical response of composite materials at the beginning of this Chapter and in this Section we discuss more in depth the one developed by J. C. Maxwell Garnett in 1904.

A procedure that describes an object endowed with a microstructure in terms of macroscopic parameters is called a homogenization procedure; I found a synthetic and precise definition of the meaning of homogenization in a book by Ari Sihvola, Electromagnetic mixing formulas and applications [71], and I report it here verbatim: *"What is homogenisation? Certainly it is something more than averaging. We may think that homogenisation of a heterogeneous material is a process leading to its macroscopic characterization with fewer parameters than those needed for a full description of the original object. For example, the whole microstructure with the dielectric variation of a sample is reduced to an effective permittivity."*

2.2.1 Maxwell Garnett nanocomposites

The theory proposed by J. C. Maxwell Garnett (MG theory) for the effective dielectric constants of nanoparticles dispersed in a host medium [39] is developed in the same

way as the Clausius-Mossotti theory for the dielectric constant of a gas. To obtain the polarization density of the composite medium one has to add the polarization of the host and the polarization of the nanoparticles; the polarization of the nanoparticles is calculated from their static polarizability taking into account that each of them is subject to the Lorentz local field rather than the macroscopic field. The details of the calculation are given in Appendix B.

The result is the Maxwell Garnett (MG) formula

$$\frac{\varepsilon - \varepsilon_h}{\varepsilon + 2\varepsilon_h} = f\,\frac{\varepsilon_i - \varepsilon_h}{\varepsilon_i + 2\varepsilon_h}, \tag{2.6}$$

which expresses the effective dielectric constant of the composite medium ε as function of the dielectric constant of the host ε_h, the dielectric constant of the inclusions ε_i and the volume fraction of the inclusions in the composite f (often called "volume fill fraction" or simply "fill fraction").

Studies on the range of applicability of the Maxwell Garnett formula

It is interesting to report here the results of some modern theoretical analyses that clarify the range of applicability of the theory.

Let us first analyze two features of the derivation given in Appendix B. The first feature is that each nanoparticle reacts to the mean field and does not "see" the individual fields of the other nanoparticles. This leaves open the question on how dense the nanoparticles can be for the theory to be applicable. The second

feature is the quasistatic approximation. The quasistatic approximation consists in the observation that when applying the Helmholtz equation for the electric field

$$\nabla^2\mathbf{E} + k^2\mathbf{E} = 0 \tag{2.7}$$

to a nanoparticle embedded in a host the term $k^2\mathbf{E}$, that expresses the retardation effects, is negligible with respect to the term $\nabla^2\mathbf{E}$ that is the electrostatic term. The Laplace equation

$$\nabla^2\mathbf{E} = 0 \tag{2.8}$$

is therefore used to describe the mesoscopic field[3] inside and around the nanoparticles. The derivation that retraces the steps of the Clausius-Mossotti theory uses the quasistatic approximation in the calculation of the polarizability of the nanoparticles. A more explicit use of the quasistatic approximation is made by Aspnes in the "averaging" treatment (see for example [72]) in which the macroscopic electric field $\mathbf{E}$ and electric displacement field $\mathbf{D}$ are obtained with a spatial average of the fields calculated with the quasistatic approximation in and around the nanoparticle.

The quasistatic approach indicates that the MG theory is valid only for small nanoparticles; the separation between particles, and thus the filling fraction, also should count because it gives another characteristic size to the system. Using the

---

[3]The mesoscopic field is the field considered at the spatial resolution at which a nanoparticle is large but an atom is small.

Clausius-Mossotti or the Aspnes procedures it is not possible to find out what precisely the limits of validity are.

Treatments based on scattering [73–75] are useful to clarify these aspects. These treatments consider a unit cell, representative of the composite material, immersed in an yet unknown effective medium. The unit cell that represents spherical nanoparticles embedded in a host is a sphere made of the inclusion material coated by a spherical layer made of the host material. The radius of the internal sphere and the outer radius of the spherical layer are chosen so that the amount of the two materials respects the proportions present in the composite. Next the scattering from the coated sphere is calculated; the dielectric constant of the surrounding medium such that scattering from the unit cell is zero is taken to represent the effective dielectric constant of the composite.

In the scattering calculation one can take into account only the first order, obtaining in this way the Maxwell Garnett expression, or subsequent orders, obtaining corrections to the MG theory. If the spheres of the embedded material are too large the inner sphere of the unit cell becomes too large for the first order expansion to be valid, and if the fill fraction is too small it is the outer layer that becomes too large (it represents a large separation between particles).

The limiting values that are found by [75] are that the size and separation of the particles can be as large as $0.2\,\lambda$.

The derivations based on scattering from a unit cell do not say anything on the

role played by how the nanoparticles are distributed inside the host; moreover they take into account only single scattering. A recent paper by Mallet et al. [76] examines in detail these issues. The paper follows this logic: one can consider a sphere in which dipolar scatterers (with a polarizability given by the Clausius-Mossotti formula B.4 with a radiative correction) are dispersed and a sphere of the same volume made of an "effective medium" and calculate scattering of a plane wave from both; scattering from the collection of dipolar scatterers is calculated by a series solution of the so-called Foldy-Lax equations (see the Mallet paper for references), while scattering from the homogeneous sphere is calculated using the Born series (as detailed in the paper). The two series are compared and it is found that they can be made equal at all orders if there are no correlations between the positions of the particles.

The main results of the analysis in [76] is that the fill fraction of the inclusions can be arbitrarily high as long as there are no correlations between particle positions; but there can be interactions between particles in the near-field as well because the full Green functions are used in the constructions of the two series. Moreover there is no limit to how low the fill fraction can be (how much the particles can be separated), in contrast with the conclusions of [73–75]; the requirement is that there are enough particles so that sums over the scattering of many of them yields plane waves, but not that the separation is small enough so that quasistatic approximations hold.

Of course when the nanoparticles start touching and forming aggregates then their polarizability is not described anymore by Equation B.4 and moreover their radiation

is not anymore the one of a dipole, so the analysis by Mallet et al. breaks down.

Main features of the Maxwell Garnett effective medium

An example of the predictions of the Maxwell Garnett theory is shown in Figure 2.4
for a gold-silica system with gold fill fraction equal to 0.2. The predictions of the
Maxwell Garnett model are quite different from a weighted average of the dielectric
constants of gold and silica, and as we anticipated a large resonance, the plasmon
resonance, can be observed at a wavelength of around 530 nm.
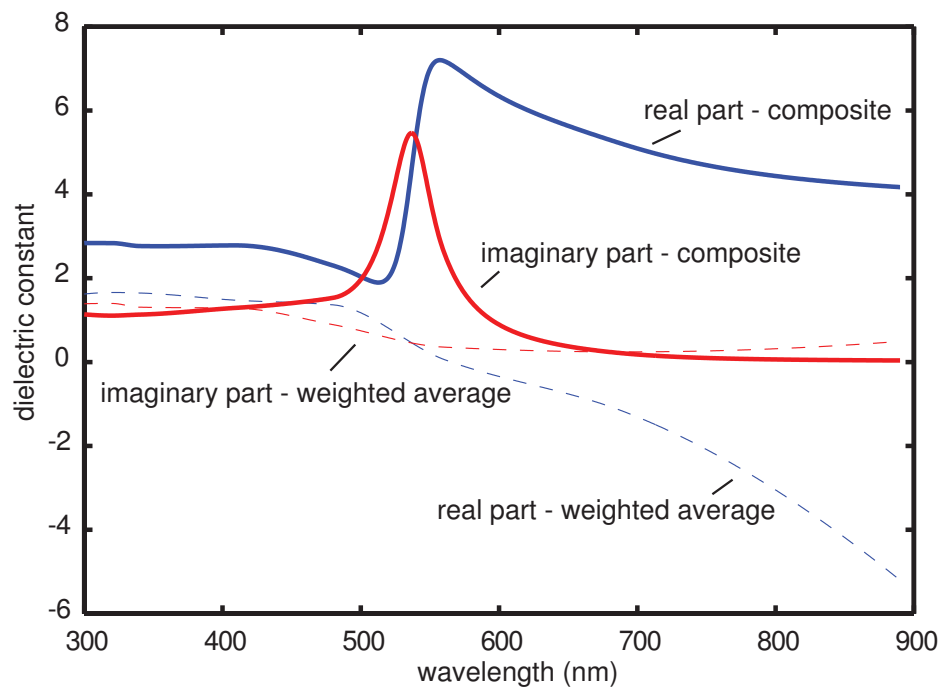
Figure 2.4: Effective dielectric constants according to the model of Maxwell Gar-
nett for gold nanoparticles dispersed in SiO_2. The gold fill fraction is 0.2. The
plasmon resonance can be observed at a wavelength of around 530 nm. The predic-
tions of the Maxwell Garnett model are quite different from a weighted average of
the dielectric constants of gold and silica.

If we solve Equation 2.6 for the effective dielectric constant ε we can see the plasmon resonance appear:

$$\varepsilon = \varepsilon_h \frac{\varepsilon_i (1 + 2f) + 2\varepsilon_h (1 - f)}{\varepsilon_i (1 - f) + \varepsilon_h (2 + f)}. \tag{2.9}$$

The denominator in Equation 2.9 is equal to zero for $\varepsilon_i = -\varepsilon_h (2 + f) / (1 - f)$ and in view of the complex character of the dielectric constants of metal the effective dielectric constant resonates at a wavelength at which

$$\mathrm{Re}\{\varepsilon_i\} = -\varepsilon_h \frac{2 + f}{1 - f}, \tag{2.10}$$

which moves to the red as the metal fill fraction is increased (one needs to recall that the dielectric constant of metals increases in magnitude for increasing wavelength).

For f very small one recovers the plasmon resonance of a single nanoparticle (as derived from Equation 2.5).

At the plasmon resonance there is a strong concentration of electric field inside the metallic component of the composite; this field concentration is responsible for the increased dissipation and I will discuss it more in detail in Section 2.3.

Experimental studies on the Maxwell Garnett formula

Let's briefly review some experimental work on the verification of the Maxwell Garnett mixing formula.

The first observation is that if the two materials that are mixed together in a

composite medium possess real and positive dielectric constants, then the Hashin-Shtrikman limits alone give an excellent prediction. For example for an isotropic mixture of two dielectrics of dielectric constants equal to 5 and 1 respectively, if one takes as effective dielectric constant one half of the sum of the Hashin-Shtrikman limits then the limits guarantee that the prediction is within 10% of the actual value in the worst case (which is reached for a fill fraction of approximately 0.5) and of course much better if one or the other material predominates in the mixture.

When metal nanoparticles (with negative real part of the dielectric constant) are dispersed inside a dielectric the situation is different because as I remarked at the beginning of Chapter 2 in this case the Hashin-Shtrikman limits must be reinterpreted and are not anymore so stringent. This is why the Maxwell Garnett theory's prediction of a resonance in the absorption spectrum is non trivial and also why the title of Maxwell Garnett original paper is "Colours in Metal Glasses and in Metallic Films".

The first test of the Maxwell Garnett theory is that when one looks at a glass containing metal nanoparticles he sees its typical color; gold doped glass is red when looked in transmission, which means that it absorbs green as the theory predicts. The first comparisons were performed by Maxwell Garnett himself in his 1904 paper for glasses with a very small metallic content (silver, copper, gold, and potassium/sodium together at fill fractions on the order of 10^{-6}) and were satisfactory.

An early quantitative comparison appeared in two papers by Doremus in 1964 and

1965 [77, 78]. Doremus compared the data on absorption of silver- and gold-doped glasses to a formula obtained by summing the dipolar Mie scattering of independent spherical particles; this formula, whose derivation can be quickly reconstructed by combining two formulae in the book by Bohren and Huffman on scattering of light by small particles [79][4], is equivalent to Maxwell Garnett formula if the local field effects are neglected, that is justified at very low fill fractions. He found that he could obtain readily an agreement between the location of the absorption peaks predicted and measured, but that if he wanted to correctly calculate the width of the resonance he needed to admit that the linear dissipation in very small metal nanoparticles depended on particle size and was higher than in bulk metal. The mechanism that provides this increase in dissipation is the scattering of free electrons on the surface of the nanoparticle. Once that the dielectric function of metal was corrected (in a phenomenological way) to take surface scattering into account, then a very nice fit was obtained for silver and a more than decent one for gold. In my thesis too I need to take into account surface scattering of the free electrons to obtain a good theoretical fit of the data. It is also important, when evaluating these papers, to take into account that at the time the author did not have a precise knowledge of the dielectric constant of gold and silver (the work of Johnson and Christy [55] appeared in 1972).

---

[4]In the edition of the book published in 2004 by WILEY-VCH these formulae are formula (3.41), that gives the effective refractive index of a collection of scatterers as a function of their "vector scattering amplitude", and formula (5.17), that gives the vector scattering amplitude for a small spherical particle.

It is more difficult to test precisely the Maxwell Garnett theory at higher fill fraction because (depending on the method of preparation used) the small particles could aggregate already at a fill fraction smaller than 1%.

A nice work in which a very good fit is obtained between the measured and calculated absorption of nanoparticle systems at high fill fractions is again by Doremus [80]; good correspondence is observed up to $f = 0.40$. In this case the nanoparticles are spherical and well separated.

Effects that would make the effective dielectric constant of a nanoparticle system deviate from the Maxwell Garnett result include the non-sphericity of the particles and coalescence. Experimental studies that deal with these issues are the one by Granqvist and Hunderi [81], that studies the effects of coalescence at low fill factors, and the one by Cohen and coauthors [82], in which the effect of non-sphericity is studied, and the data span the whole range of fill fractions from 0.1 to 0.9 so that the effect of percolation can be seen; in this paper, for wahat regards more strictly the Maxwell Garnett model in particular is shown that as the metal fill fraction grows the plasmon resonance shifts to the red as predicted by Equation 2.9 and the amount of this shift is also decently predicted by the MG theory.

A recent study that compares spectro-ellipsometric data of $Au : SiO_2$ nanocomposites with a few percent of gold fill fraction to the MG formula and obtains an excellent accord is [83].

The Maxwell Garnett theory cannot capture the effect of percolation. One clear

example is in [84] where it is shown that in silver-silica films with 40% silver the Maxwell Garnett theory greatly overestimates the absorption at resonance.

2.3   Nonlinear properties of metal-dielectric composite materials

The surface-mediated enhancement of the electromagnetic field is the main cause of the spectacular increase of the effective cross sections of optical effects (such as Raman scattering) emanating from molecules in the dielectric at or close to a rough metallic surface [85]. Since these enhancements of nonlinear effects are due to the concentration of electric field next to the metal particles, it is reasonable to expect that the third-order nonlinear properties of the particle system, that depend on the electric field inside the particle, are also enhanced. I paraphrased this reasoning from the first study that, pointing this out, measured the third-order nonlinear properties of metal nanoparticles systems [26]. In this paper D. Ricard and coworkers used the technique of optical phase conjugation [86] to measure the modulus of the third-order nonlinear optical susceptibility $\chi^{(3)}$ of gold and silver colloids in water. At the low volume fill fractions at which they worked (between 10^{-6} and 10^{-5}) the Maxwell Garnett theory is applicable; according to this theory the mesoscopic local field inside each nanoparticle is given by

$$\mathbf{E}_{in} = \frac{\varepsilon + 2\varepsilon_h}{\varepsilon_i + 2\varepsilon_h}\mathbf{E} = q_i\mathbf{E} \tag{2.11}$$

where $\mathbf{E}$ is the macroscopic field, ε_h, ε_i and ε are the dielectric constants of the host, of the nanoparticles and of the effective medium respectively while q_i is the "local field factor". Starting from the knowledge of the local field one can derive (we do so in Appendix B) the following expression for $\chi^{(3)}$ of the collection of nanoparticles in the hypothesis that the metal is the only nonlinear material (hypothesis justified by the fact that metals are much more nonlinear than glasses):

$$\chi^{(3)} = f\chi_i^{(3)}q_i^2\left|q_i\right|^2. \tag{2.12}$$

A more complete expression for the effective nonlinear susceptibility of a Maxwell Garnett composite medium in which both inclusions and host are allowed to be nonlinear has been derived by Sipe and Boyd [87] and includes Equation 2.12 as a special case.

The prediction of Equation 2.12 is therefore that the nonlinear polarization depends on the fourth power of the enhancement factor q_i and the power in the phase conjugation signal on the eight power of q_i. The measurements in reference [26] compared phase conjugated reflectivities off and on resonance for both gold and silver colloids using pulses of duration $\approx 30\text{ps}$ and obtained values in general accord with the theoretical predictions. In the same paper the first time-resolved study of the

nonlinear response appears; the data showed that the response is composed of an extremely fast main component (not resolvable with pulses 30 ps long) and a weaker slower component.

Let's illustrate the predictions of the nonlinear Maxwell Garnett model by plotting the effective nonlinearity of a gold-silica Maxwell Garnett composite with gold fill fraction $f = 0.2$ against wavelength (Figure 2.5).
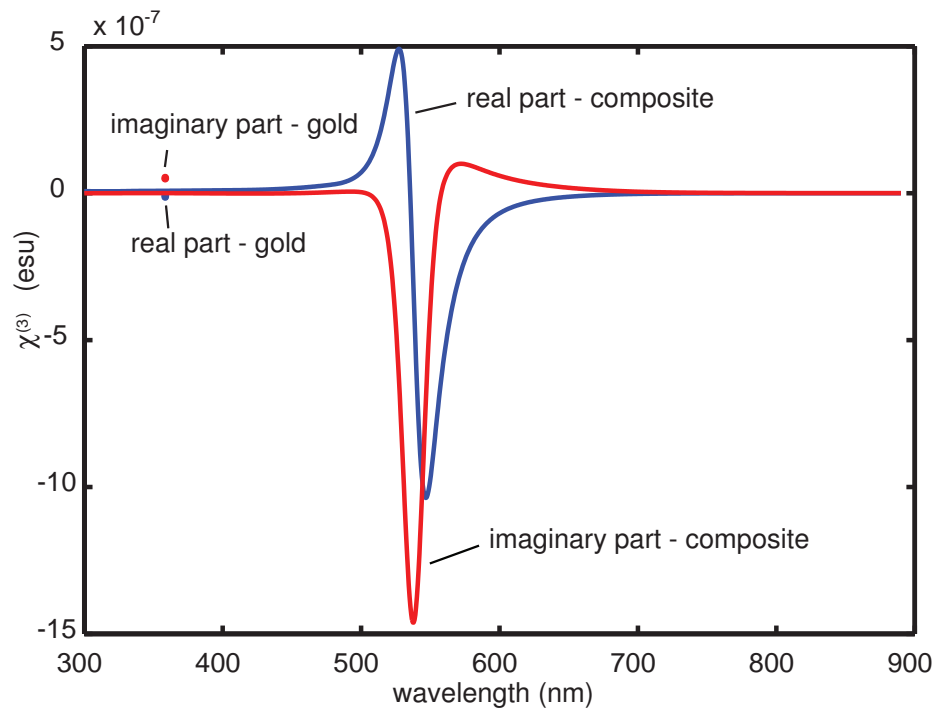
Figure 2.5:   Effective nonlinear susceptibility $\chi^{(3)}$ according to the model of Maxwell Garnett for gold nanoparticles dispersed in SiO_2 . The gold fill fraction is 0.2. The plasmon resonance can be observed at a wavelength of around 530 nm. The nonlinear susceptibility of gold is considered constant in the whole wavelength range and equal to $-1 \times 10^{-8} + 5 \times 10^{-8}i$ esu and it is plotted at just one wavelength for graphical convenience. Note that at the plasmon resonance the sign of $\mathrm{Im}\left\{\chi^{(3)}\right\}$ of the composite is opposite with respect to that of $\mathrm{Im}\left\{\chi^{(3)}\right\}$ of gold, as discussed in the text.

It is evident a large enhancement of the nonlinearity in correspondence of the

plasmon resonance. A gold-silica composite with 20% fill fraction is, according to the Maxwell Garnett theory, around 20 times more nonlinear than pure gold. Note that at the plasmon resonance the sign of $\mathrm{Im}\left\{\chi^{(3)}\right\}$ of the composite is opposite with respect to that of $\mathrm{Im}\left\{\chi^{(3)}\right\}$ of gold. I will return on this effect in Section 3.4.

In subsequent papers [59, 60] a more detailed study of the origin and frequency dependence of the third-order nonlinearity appeared. The results of these papers for what regards the origin of the nonlinearity are reported in Section 2.1.2; here I add just a few details about their experiment. First, the experiment of measuring the optical phase conjugation signal as a function of the diameter of the nanoparticles showed that there is no significant dependence in the range 6-20 nm. Second, the authors were able to measure the phase of $\chi^{(3)}$ as well: a phase conjugation experiment can be in fact made sensitive to the phase if one uses an interference technique as explained in [59].

The result was that the Kerr response of the gold spheres is mainly imaginary. Moreover the $\chi^{(3)}_{xyxy}$ was found to be opposite in sign with respect to the other components: it was imaginary negative while the other components were imaginary positive. This means that the hot-electron nonlinearity, which does not contribute to the $\chi^{(3)}_{xyxy}$ susceptibility, is positive and larger than the interband contribution, which in turn is negative.

It is also worthy of note that in this paper the fact that the third-order nonlinear susceptibility of a collection of metal nanoparticles has opposite sign with respect to

the susceptibility of bulk metal is mentioned for the first time. This change of sign is one of the subjects of the work of this thesis and is discussed in detail in Section 3.4.

Subsequent experimental work on the nonlinear optical properties of metal-dielectric composites has proceeded along several lines: the dependence of the nonlinear susceptibility on the size of the nanoparticles, the dynamics of the nonlinear response, the determination of the phase of $\chi^{(3)}$, the dispersion of the nonlinearity as a function of wavelength, the nonlinearity of composites with large metal fill fraction or with aggregation and the behaviour of layered systems.

Size dependence of the optical nonlinearity

Let us examine the literature on the size dependence of the nonlinearity.

The work on gold by Hache and coauthors had not evidenced any significant dependence of nonlinearity on size. An early work that in contrast found a size effect was published in 1994 by Yang and coworkers [88]. These authors measured the absolute value of $\chi^{(3)}$ in a copper nanoparticle system with pulses of 35 ps duration at the wavelength of 532 nm which is off the plasmon resonance. They observed that $\chi^{(3)}$ increases with decreasing diameter of the nanoparticles when the diameter is approximately below 10 nm. The difference between the observations of Hache et al. [59] and the observations of Yang et al. could be explained in the following way.

Hache et al. measured the nonlinear susceptibility in resonance conditions, while Yang et al. off resonance (the plasmon resonance for copper is located at around 565

nm while the measurement was performed at 532 nm). The dielectric enhancement factor q_i (defined in Equation 2.12) depends on the imaginary part of the dielectric constant of the metal nanoparticles; but this dependence is much more marked on resonance than off resonance. Since the dissipation in the nanoparticles increases with decreasing size, it is quite possible that effects of the increase in nonlinear susceptibility and the increase in dissipation cancelled each other in the measurements of Hache et al. while they did not in the measurements of Yang et al.

In the same year a paper by a different group [89] obtained results similar to the ones of Yang et al. The measurements in [89] were obtained under conditions of resonance with pulses 7 ns long on both copper and silver nanoparticles; the length of the pulses does not allow one to exclude purely thermal effects in the measurement, but the paper calls attention to the need of considering the size dependence of the dielectric constant of the nanoparticles when analyzing the data.

A paper that partly corrects some of the defects of the previous studies has been written more recently by a Spanish group [90]. In this case the nonlinear thermal effects were carefully separated from the electronic effects by means of a sophisticated fitting procedure of high-quality z-scan data, and the size dependence of the linear dissipation was taken into account. Moreover the nanoparticles were prepared with a procedure of pulsed laser deposition that produces very narrow size distributions. As a comment, it would still be nice to perform measurements that can exclude thermal contributions without requiring particular fitting procedures.

In conclusion the size dependence of the nonlinear susceptibility of small metal particles has observed in the literature but the results in at least one but probably two out of the three papers I cited (Uchida's [89] and Ballesteros' [90] works) are put into question by the possible presence of thermal effects. Moreover, more work is needed to test the observed behaviour against theoretical expressions (as found for example in [59]); in fact in all of the published work too few data points appear to discriminate conclusively between different possible dependences.

Dynamics of the nonlinear response

The time dynamics of the nonlinear response has been studied in several papers. It is quite reasonable that time-resolved studies on nanoparticle systems should share many features with time-resolved studies on bulk metals. Some of the papers [61, 70] that have been cited in the discussion on the origin and time response of the nonlinearities of gold are indeed works on nanoparticle systems. The subtle differences between the behaviour of bulk metal and metal nanoparticles that are observed on a fs time scale [91] are not relevant to the experiments in this thesis that were performed with pulses of ≈ 25 ps duration.

A paper by Liao and coworkers [92] compared the nonlinear optical response of gold nanoparticle systems as measured on different time scales. More precisely these authors measure the modulus of $\chi^{(3)}$ of a $Au : SiO_2$ composite using pulses of three different durations: 200 fs, 35 ps and 70 ps respectively. The value of $\left|\chi^{(3)}\right|$ measured

with ps pulses is around 20 times larger than the value measured with fs pulses.

The difference is attributed to the fact that the hot-electron nonlinearities does not rise enough in 200 fs as explained in Section 2.1.2. In this work there is as well the observation that the difference in value between the values of $\left|\chi^{(3)}\right|$ measured with pulses of different duration increases with increasing gold concentration. This behaviour is investigated with a fs pump-probe experiment which shows that the decay time of the hot-electron nonlinearity is a function of concentration: at the fill fraction of 12% the hot electrons relax with the lattice in a few ps, while at 33% fill fraction the decay time is increased to about 10 ps. This behaviour is not very clear to the author of this thesis.

Determination of the phase of $\chi^{(3)}$

The first measurement of the phase of $\chi^{(3)}$ in nanoparticle systems was performed in the work of Hache et al. [59] which also detailed the discussion of the origin of the nonlinearity. The technique of DFWM can be modified to give the phase of the nonlinearity of an unknown material when the generated waves can be interfered with the waves generated by an adjacent nonlinear medium (the walls of the glass cuvette that contained the colloids in this case). In this paper there is for the first time the observation that the effective nonlinear susceptibility of the composite has opposite sign with respect to the nonlinear susceptibility of the metal component, and this fact is attributed to local field effects. I postpone a more detailed discussion

of this sign change to Section 3.4 since an alternative explanation (but completely compatible with the one based on local field effects) of this phenomenon is one of the main results of my thesis.

A few things are important and must be mentioned. The change of sign of the nonlinear susceptibility has been observed by other authors since the paper of Hache and coauthors. D. D. Smith and coauthors, for example, showed in [31] that this change of sign mechanism can be used, combining the nonlinear response of gold nanoparticles with the response of a nonlinear host, to fabricate a composite material that has a value of intensity dependent absorption equal to zero (at the lowest perturbative order). This is important because one of the nonlinear figures of merit for optical switching compares nonlinear refraction to nonlinear absorption and is best when nonlinear absorption is lowest [93].

Another observation of the change of sign was done for the nonlinear refractive index by Cattaruzza et al. [94]. Interestingly Polloni et al. [95] observed optical limiting in a copper/SiO_2 nanoparticle system at the wavelength of 532 nm. While copper is an optical limiter at wavelengths between 570 and 610 nm (I myself did the measurement in [52]) I do not know of direct measurements of the nonlinear absorption coefficient in bulk copper at this wavelength but the lack of sign reversal in this case can be explained by the same theory that explains the sign reversal in the other cases because the measurements were performed off the plasmon resonance (the detailed discussion is in Section 3.4).

Wavelength-resolved studies

The study of Ricard [26] already, by comparing measurements off and on the plasmon resonance wavelength, has some wavelength resolution. Many of the studies that have presented wavelength-resolved measurements (often in the context of an investigation focusing on other details of the nonlinear behaviour) were performed with phase conjugation or DFWM and show "only" that the nonlinearity is enhanced around the plasmon resonance [60, 92, 96] ([96] reports the phase of $\chi^{(3)}$ but for one data point only). Other studies that present wavelength-resolved data are the already cited [61, 70] that are pump-probe transmission measurements. A study in which the dispersion of nonlinear self-effects were analyzed for silver nanoparticles is [97]; the conclusions of this paper is that the observed dependence of the real and imaginary part of the nonlinearity on wavelength can be explained using the low-fill-fraction limit of the Maxwell Garnett theory.

Another work [98] finds the nonlinearity dispersion for gold nanoparticles in a quasi-zero-delay pump-probe experiment that is sensitive only to the intraband and interband contributions.

Studies of composite with high metal fill fraction

Experimental studies of the nonlinear optical response of metal-dielectric composites with high metal fill fraction are not many. It is possible to follow two distinct threads. One approach aims at following the evolution of the nonlinear response as more

metal is added to the composite; with the important detail that the preparation of the composite is such that nanoparticles do not tend to aggregate till the metal fill fraction is substantially high ($f > 0.4$ for example). In the other approach the formation of aggregates is promoted even at low fill fractions using particular methods of sample preparation; in this case the properties of the nanoparticle system differ from the properties of collections of single nanoparticles even at low fill fractions.

An experimental work that presents significant data and discusses nicely the different physical situations that are encountered as the metal fill fraction in the composite is increased is [99] by R. del Coso and coworkers. In this paper the modulus of $\chi^{(3)}$ of a $Cu : Al_2O_3$ composite is measured at the plasmon resonance wavelength ($\lambda \approx 585\,\text{nm}$) as a function of copper fill fraction starting from $f \approx 0.1$, fill fraction at which the nanoparticles are well separated, to $f \approx 0.45$ which is close to the percolation threshold.

These authors identify three different regimes of behaviour. In the first regime, ranging from $f = 0$ up to $f \approx 0.20$, the composite is well described by a Maxwell Garnett model and the value of the nonlinear susceptibility increases linearly with the fill fraction. In the second regime, between $f \approx 0.20$ up to $f \approx 0.35$, the data show a much faster increase of $\chi^{(3)}$ that according to the authors cannot be explained with the Maxwell Garnett theory because it does not follow the same linear slope as the data at lower fill fraction. The authors tried to fit the data using Bruggeman's effective medium model without success. The explanation for the failure of both models,

according to the paper, is that at these fill fractions multipolar interactions between particles become important because the particles get close together and sometimes coalesce further emphasizing multipolar effects. These effects are responsible for the additional enhancement of the nonlinearity.

In the third regime, for fill fractions above 0.35, the nonlinear susceptibility slowly decreases. The observation of the authors about this behaviour is that, since for $f \to 1$ the nonlinear susceptibility of the composite has to approach the susceptibility of pure copper and for $f = 0.35$ it is much larger than that, then it will have to decrease at some point. At the highest fill fraction at which data are reported, $f \approx 0.46$, the composite has approached but not yet reached the percolation threshold.

A small critical observation that can be addressed toward this paper is the following: it is not true that the Maxwell Garnett model predicts a linear dependence of the effective nonlinearity on the fill fraction. In fact in Equation 2.12 there are two distinct dependences on the fill fraction: the first is the factor f, the second is the local field factor q_i that depends on the fill fraction through the effective dielectric constant.

To conclude the examination of [99] it is worth noting some of the data of this paper disagree with the data in the work on size dependence of $\chi^{(3)}$ that I have analyzed earlier [90]; in more detail, according to the discussion in [99] there is no dependence on particle size for diameters between 2 and 4.5 nm, while according to the data in [90] there is a dependence ([99] itself points this out). For completeness of

information, these two papers are authored by workers belonging to the same group.

It is difficult to say what exactly is right or wrong, but let me make the following consideration: paper [90] seems to implicitly take into account the dependence of linear dissipation on particles size (their values for the imaginary part of the dielectric constant of metal are taken from a reference that does that in an explicit way) while paper [99] does not, which should not be correct. My opinion, as I discussed above, is that since the two contributions (linear dissipation and metal nonlinearity) to the effective nonlinearity tend to cancel each other then ignoring one of them can be rather confusing if one wants to draw some conclusion about the other. Besides this, these results suggest that separating thermal from electronic effects by means of a z-scan fit as was done in [90] is a quite difficult art. On the whole, I am inclined to give some credit to the size dependence of the nonlinearity that [90] found.

It is interesting to compare the data in the del Coso et al. paper with the theoretical predictions of Shalaev and coworkers [45]; at first sight it would seem that the highest enhancement of the nonlinear optical properties happens quite before the percolation threshold. One important study that would need to be done before more definite conclusions can be drawn on the subject is a series of frequency-resolved measurements; the theoretical prediction is in fact that around the percolation threshold the enhancement of the nonlinearity is not limited around the low-fill-fraction plasmon resonance wavelength but extends in a wide range up to the infrared. My own experimental studies on the subject were limited by the fact that often optical damage

occurs on the samples that I had available before any nonlinearity can be detected, as I discuss in detail in Chapter 3.

Other important data on the nonlinear optical properties of metal-dielectric composites can be found in a series of works by H. B. Liao and coworkers [92, 100–102]. All of the data in these works are obtained using DFWM in gold nanoparticles systems embedded in different dielectrics (SiO_2, TiO_2 and Al_2O_3). The data in these papers span a range of fill fractions that include the percolation threshold (a larger range than [99]), and they present approximately the same behaviour: the nonlinearity first increases, then decreases. The decrease starts at fill fractions lower than the percolation threshold.

As an example, on the other hand, of experimental results that are made suspicious by the likely presence of thermal effects I cite a work that was published recently in Optics Express [103] in which the nonlinearity of a semicontinuous silver film was measured with pulses of fs duration but at a repetition frequency of 76 MHz. In this case there is no guarantee that the large (up to 80%) variations in transmittance that were observed in the silver film are indeed ultrafast.

The effects of aggregation and coalescence can be studied in a fashion independent of the effects of high fill fraction if one performs measurements, for example, on fractal colloid aggregates. Besides the confirmations on the presence of hot spots given by near-field studies on semicontinuous films [48, 49] and by the enhancement of the cross section for Raman scattering [85], there are a few interesting studies on the nonlinear

optical properties of these aggregates that often are arranged in fractal geometries.

An important work [104] deals with photomodification of fractal aggregates of silver colloidal nanoparticles. In this work electron micrographs of the same silver particle aggregate were taken before and after irradiation with laser pulses of ns duration and of wavelength tunable between 440 and 1900 nm. The micrographs show that photomodification occurs in a small (subwavelength) region of the aggregate that decreases in size as the irradiation wavelength increases. This is a very strong experimental confirmation of field localization. Moreover photomodification leads to a formation of spectral holes in the absorption profile of the aggregates. This indicates that the positions of the hot spots depends on the wavelength of the incident light, so that the modification of particles that for example are in a spot that resonates at a wavelength of 1300 nm does not affect light at 530 nm.

Closer to the theme of this thesis is the work of Lepeshkin et al. [105]. These authors compared the modulus of $\chi^{(3)}$ for isolated silver nanoparticles and fractal aggregates; the measurements indicated a large enhancement (> 500) of the latter with respect to the former. These results can be interpreted as well in term of field fluctuations and hot spots.

Finally, for giving a flavor of how large is the range of nonlinear phenomena that one encounters in the study of percolation films, I want to briefly cite the work of Breit et al. on nonlinear light scattering [106]. Exciting semicontinuous gold films near the percolation threshold with near-IR pulses of fs duration these authors observed that

the second harmonic was generated with a broad angular distribution in addition to coherent reflected and transmitted beams. This broad distribution contrasts with the collimated linear reflection and transmission that is observed both at the excitation wavelength and at the second-harmonic wavelength, and it is once more a consequence of light localization in the fractal structure of the semicontinuous films.

An extensive theoretical treatment of the nonlinear optics of random metal composites can be found in the book by Shalaev [21] and, for example, in his and Sarychev's article in Physical Review B [45].

Layered composites

The study of layered metal dielectric composites includes the observation made by Bennink et al. [22] that the nonlinearity of a metal can be accessed much more easily when the metal is mixed with a dielectric in such a way to cancel reflections as much as possible. In fact as we remarked at the beginning of Chapter 2 and as is explained in detail in the work of Bennink et al. the strong attenuation that light experiences in a metal is given just in part by absorption (against which only optical gain would be a recourse) and therefore the concept of anti-reflection coating can be applied successfully to let light penetrate more deeply in the metal.

This theoretical concept was proven experimentally by Lepeshkin et al. [52] who demonstrated an enhancement of the nonlinear response of the metal-dielectric layered structure with respect to the response of bulk copper. At the spectral peak of the

bulk response of copper the enhancement factor is of about 4 times, and the layered structure responds in a much wider wavelength range then bulk copper. In fact nonlinear transmission changes of a 40 nm bulk copper film can be measured with ease using pulses of ps duration only in the 570-610 nm wavelength range, while the response of the metal-dielectric system (which contained 80 nm of copper) was present in the range 550-680 nm (using an 80 nm thick bulk copper sample would not have made any difference since the optical field intensity would have been too low in the additional 40 nm of copper to produce any nonlinear optical response).

Additionally, if a factor of 4 enhancement seems small, one must take into account that this enhancement is not accompanied by a concomitant increase of linear absorption as in the plasmon-enhanced nonlinearities and therefore represents a net gain in the figures of merit. As a last benefit of the layered structure I add that the depth of optical limiting that can be observed in the structure before the occurrence of optical damage is much larger than what can be observed in pure copper (60% reduction in transmission against 10%) and also much larger than the amount of saturable absorption that can be observed in high-fill-fraction gold films as I will show in detail in Chapter 3. I participated in this work by performing all of the published transmission and reflection z-scan measurements.

In closing this review of the layered composites I cite a theoretical work by Husakou and Herrmann [107] in which a different kind of metal-dielectric layered composite is studied, one in which the layers are much smaller than the wavelength of light; the

optical response of this composite is not determined by interference effects but can be studied in the quasi-static approximation and an effective dielectric constant can be attributed to the material. Husakou and Herrmann chose the composition (silver and SiO_2) and the layers's thicknesses so that the real part of the effective dielectric constant of the layered composite medium is close to zero. Nonlinearity in the metal can be used to push the value of the dielectric constant below zero or above zero, and in doing this the reflectance from the composite undergoes a quite large change. The composite material therefore has the characteristics of an optical switch.

Chapter 3

Measurements of nonlinear absorption in gold nanoparticle systems

Most of the work of my thesis has dealt with the measurement of nonlinear absorption in gold nanoparticle films in a wide range of fill fractions (always below the percolation threshold) and with pulses of around 25 ps duration.

The source of the pulses is either the second harmonic of a regeneratively amplified mode-locked Nd:Yag laser (EKSPLA PL2140) or the output of an optical parametric amplifier (OPA EKSPLA PG401VIR).

On the time-scale of these pulses the main contribution to the nonlinear absorption in gold at the wavelengths around the plasmon resonance (520 nm) is given by the

hot-electron mechanism discussed in section 2.1.2

3.1   Description of the samples and their linear optical properties

I have had at my disposal two kinds of samples prepared with different techniques and possessing different morphology.

The first kind of samples ("Wendling samples") have been prepared by Dr. Bettina Wendling at the University of Alabama in Huntsville by cosputtering gold and SiO_2 onto a quartz substrate using a multitarget magnetron sputtering system. The second kind of samples ("Nelson samples") have been prepared by Dr. Mark Nelson at the New Mexico State University by laser ablation in an argon atmosphere.

The different morphological characteristics of the two kind of samples allow to test different aspects of the nonlinear optical response of metal-dielectric nanocomposite materials. The investigation of the Nelson samples has been limited by the fact that under certain circumstances the samples suffer optical damage before it is possible to detect a reversible nonlinear optical response.

Let us describe in detail the samples starting with the Wendling samples.

Wendling samples

The Wendling samples are two 8-cm quartz wafers on which an approximately 200 nm thick gold-silica film was deposited by the cosputtering technique. During the sputtering the target and substrate were inclined with respect to each other, and as a result the concentration of gold varies across each of the samples; on one of them ("sample 5W") the gold fill fraction goes approximately from 0.05 to 0.40, on the other ("sample 7W") approximately from 0.05 to 0.56.

The appearance of the sample also varies across their surface. For both samples, the color that is observed in reflection goes from orange (at the low gold fill fraction side) to purple (in the middle) to gold-like (at the high fill fraction side). The color that is observed in transmission varies from orange (at the low fill fraction side) to purple (anywhere else); it is important to note that in no place the samples look green in transmission. This is a strong indication that, despite the high fill fraction, gold is not beyond its percolation threshold and forms isolated nanoparticles. This is confirmed by an examination of the samples under the Scanning Electron Microscope (SEM).

We present in Figure 3.1 two SEM micrographs of the samples, collected by Mr. Andreas Liapis using the Zeiss SUPRA 40 VP SEM microscope of the Institute of Optics. Figure 3.1(a) is the 5W sample at fill fraction $f = 0.05$; at this low fill fraction the diameter of most nanoparticles can be estimated as $<\approx 10$ nm. Figure (b) is the 7W sample at 0.55 (the highest fill fraction available in the Wendling samples); the

micrograph confirms the conclusion reached by judging the appearance of the sample that even at this high fill fraction gold forms isolated nanoparticles.
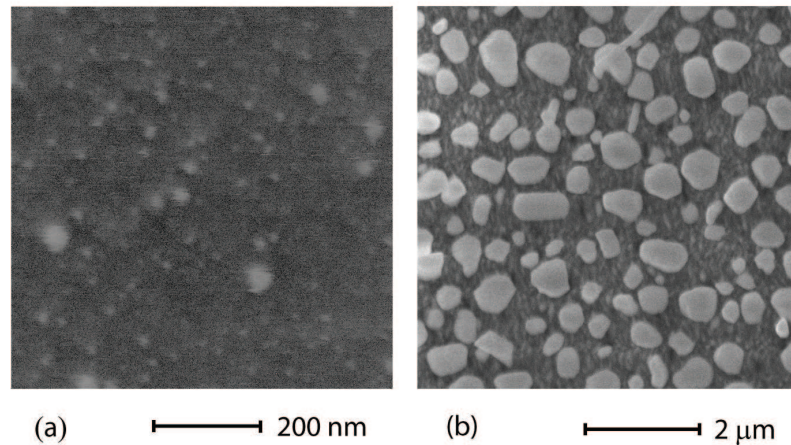

Figure 3.1: SEM micrographs of the Wendling samples. Lighter-colored areas in the micrographs represent gold. Part (a) is sample 5W at $f = 0.05$; the diameter of most nanoparticles can be estimated as $<\approx 10$ nm. Part (b) is sample 7W at $f = 0.55$; even at this high fill fraction the sample consists of isolated gold nanoparticles.

The composition of the samples and their linear optical attenuation have been characterized by B. Wendling on a grid of points. Tables 3.1 and 3.2 report the fill fraction, thickness and optical density at the wavelength of maximum attenuation for grid points in sample 5W and 7W respectively. Figure 3.2 shows the optical attenuation as a function of fill fraction. One can observe that optical attenuation first grows, up to approximately $f = 0.40$, then decreases.

The composition has been inferred by calibrating separately the deposition rates of gold and silica. The calibration was performed for each material by depositing it onto a grating and measuring the resulting thickness with a profilometer. The substrates
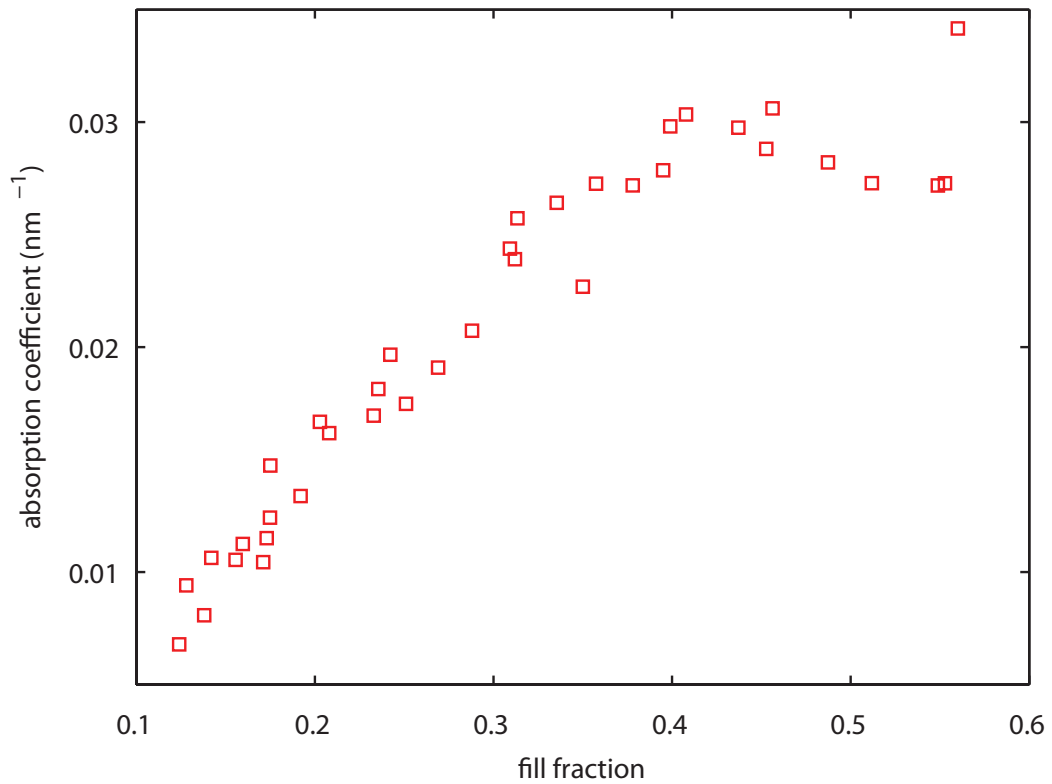
Figure 3.2: Linear attenuation of the Wendling samples as a function of fill fraction at the wavelength of maximum attenuation (2001 data).

for each of the samples were placed in the same position as the calibration gratings for cosputtering, and the fill fraction was calculated at each point from the known deposition rates. The thickness of the resulting film was determined by profilometry.

The linear optical attenuation was characterized as a function of wavelength by B. Wendling with a spectrophotometer. I repeated some of the measurements in order to verify features that appeared to me in contradiction with what I had observed in the nonlinear measurements. The results of my measurements differ from the data by B. Wendling and were more in accord with the nonlinear data as I will explain

Spot #	Au Volume Fraction	Optical Density	Thickness (nm)	Abs. Coeff. α (nm^{-1})
1	0.142	0.999	216	0.0106
2	0.208	1.337	190	0.0162
3	0.312	1.81	175	0.0239
4	0.399	2.04	158	0.0298
5	0.128	0.977	239	0.00941
6	0.175	1.33	207	0.0147
7	0.288	1.72	191	0.0207
8	0.395	2.14	177	0.0279
9	0.138	0.910	259	0.00808
10	0.192	1.29	222	0.0134
11	0.269	1.64	198	0.0191
12	0.378	2.17	184	0.0272
13	0.124	0.758	257	0.00678
14	0.173	1.12	223	0.0115
15	0.251	1.49	196	0.0175
16	0.35	1.78	181	0.0227

Table 3.1: Fill fraction, thickness and linear attenuation for Wendling sample 5W measured for a grid of points.

in detail in Section 3.4. The most natural explanation is that the properties of the sample changed with time. I present in Figures 3.3 and 3.4 both the attenuation spectra measured by B. Wendling and by me at 6 years of distance.

The plasmon resonance is evident in the attenuation spectra. It is situated at around 520 nm for low fill fractions, it increases in magnitude and shifts to the red as the fill fraction increases up to approximately $f = 0.40$ and then decreases and shifts back to the blue. For what regards the differences between the attenuation spectra measured in 2001 and the ones measured in 2007, in 2001 the wavelength shifts of the plasmon resonance were much larger and the peak reached up to 560 nm for $f = 0.41$;

Spot #	Au Volume Fraction	Optical Density	Thickness (nm)	Abs. Coeff. $\alpha \, (\mathrm{nm}^{-1})$
1	0.175	1.21	225	0.0124
2	0.242	1.70	199	0.0197
3	0.357	2.22	187	0.0273
4	0.456	2.32	175	0.0306
5	0.160	1.21	248	0.0113
6	0.236	1.76	224	0.0181
7	0.335	2.35	205	0.0264
8	0.453	2.45	196	0.0288
9	0.171	1.22	270	0.0104
10	0.233	1.72	234	0.0170
11	0.313	2.36	211	0.0257
12	0.437	2.62	203	0.0298
13	0.156	1.22	267	0.0105
14	0.203	1.68	231	0.0167
15	0.309	2.25	213	0.0244
16	0.408	2.62	199	0.0303
17	0.553	2.24	188	0.0273
18	0.549	2.35	199	0.0272
19	0.512	2.39	202	0.0273
20	0.487	2.40	196	0.0282
21	0.560	2.42	163	0.0342

Table 3.2: Fill fraction, thickness and linear attenuation for Wendling sample 7W measured for a grid of points.

in 2007 the shifts were limited to ten nanometers.

There is no particular reason to doubt the results of the spectrophotometer, but since the change of the attenuation spectra is a noteworthy fact I verified the plausibility of the results by measuring the attenuation at a few wavelengths using the laser system used for the nonlinear absorption measurements, obtaining a very good accord between the measurements made in the two ways. I do not have an explanation for the change of the attenuation spectra with time.
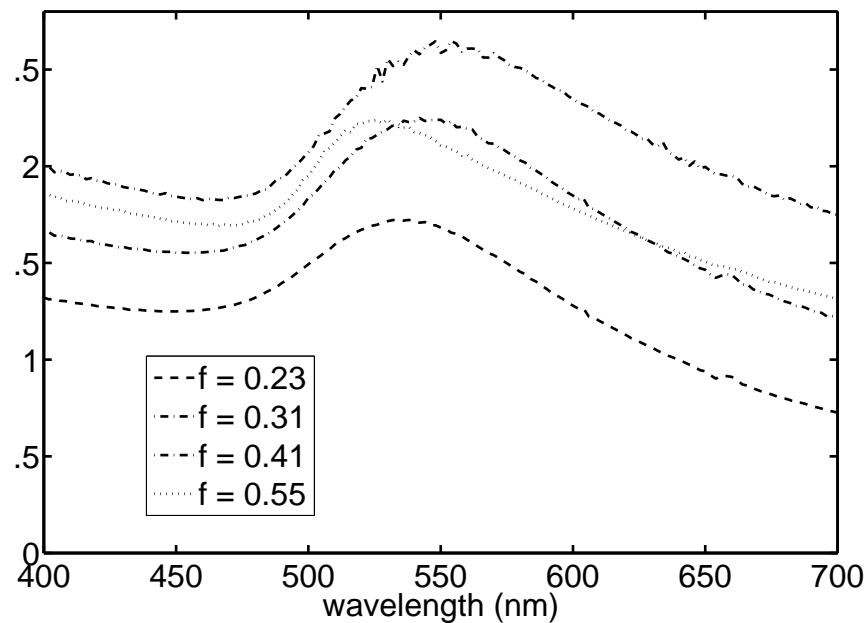
Figure 3.3: Linear attenuation of the Wendling samples for several fill fractions; measured in 2001.

Nelson samples

The Nelson samples are several 12 mm circular glass coverslips covered with approximately 30 nm (as measured by SNOM topography) of a discontinuous gold film.

Gold deposition was performed by the technique of laser ablation; pulses of 7 ns duration and energy ranging from 100 to 300 mJ were focused onto a gold target in an Argon atmosphere; the gold flakes ablated from the target fell onto the glass coverslips. The filling fraction of the samples was controlled by varying the distance of the coverslip substrate from the target between 3 and 12 cm and the deposition time between 10 and 50 minutes.

Laser ablation results in a film morphology quite different from the one obtained by
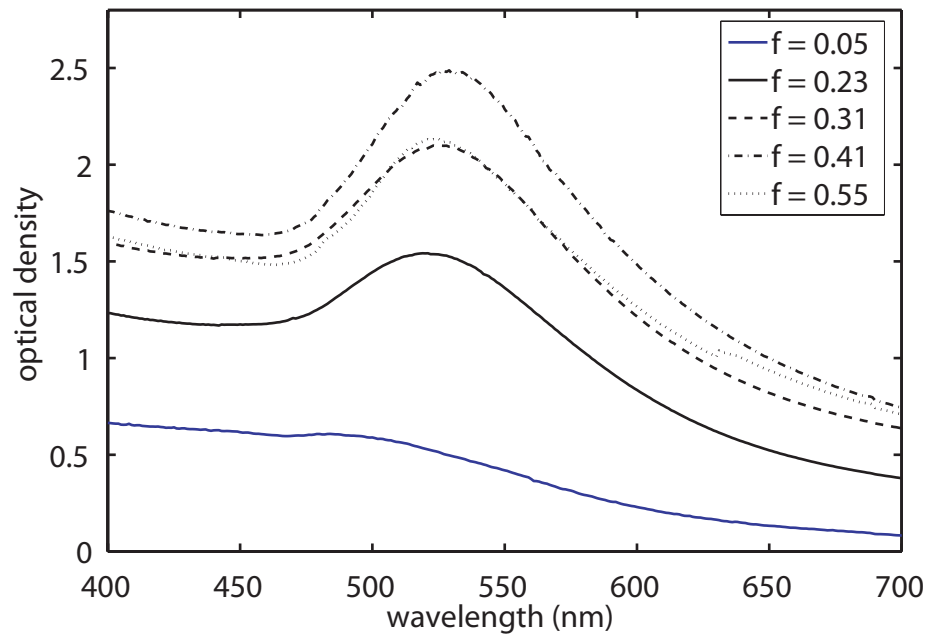
Figure 3.4: Linear attenuation of the Wendling samples for several fill fractions; measured in 2007.

co-sputtering gold and silica (as in the Wendling samples). In particular aggregation and the formation of clusters happen at lower fill fraction than for films prepared by silica-gold co-sputtering, as can be evinced from the data in Mark Nelson's PhD thesis [108]. This leads to optical properties that differ from the optical properties of the Wendling samples.

The Nelson samples cover a large range of filling fractions. I have obtained interesting results only with two of the samples, named "9-1-03 #4' and "9-1-03 #7", with fill fractions $f = 0.43$ and $f = 0.47$ respectively. The reason why I do not have extensive data on the nonlinear optical properties of this samples is that they are extremely susceptible to optical damage in such a way that the damage threshold is

often reached before any optical nonlinearity appears. Here is the characterization of these two samples.

Both samples have a purple color both in reflection and in transmission. The morphology of the samples is shown in Figure 3.5, which is a TEM micrograph of a semicontinuous gold film deposited on a silicon oxide coated TEM grid with deposition parameters similar to the ones for sample 9-1-03 #7. The image shows that the sample is below percolation (as is confirmed by electrical and optical measurements [108]) and that the arrangement of gold on the substrate is more complex than the one in the Wendling samples (compare Figure 3.1).
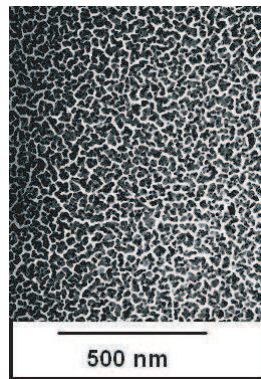
Figure 3.5: TEM micrograph of a semicontinuous gold film deposited on a silicon oxide coated TEM grid with deposition parameters similar to the ones for sample 9-1-03 #7.

The different morphology causes the optical attenuation spectra to be different from the attenuation spectra of the Wendling samples. Figure 3.6 shows the optical attenuation spectrum for sample 9-1-03 #4. The plasmon resonance is shifted to the red by almost 200 nm relative to the Wendling samples (compare with Figures 3.3 and 3.4).
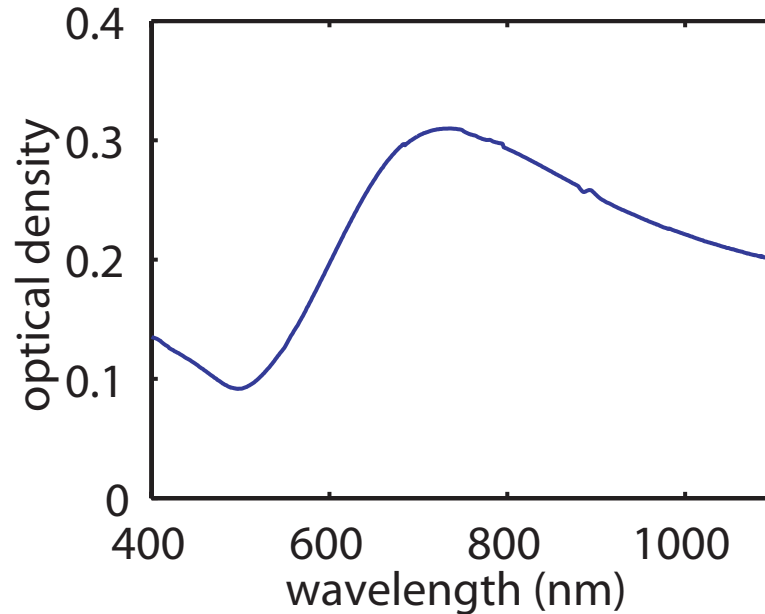
Figure 3.6: linear attenuation for sample 9-1-03 #4.

3.2 The z-scan technique applied to gold nanoparticle and semicontinuous film samples

In order to measure the nonlinear absorption in the metal-dielectric samples I used the open-aperture z-scan technique [109, 110]. The open-aperture z-scan technique, described in detail in Appendix C, is a refinement of the transmittance experiment with variable input energy.

In the open-aperture z-scan technique the transmittance through the sample is measured as a function of position as the sample is translated through the focus of a Gaussian beam. The transmission profile shows an increase or decrease in the proximity of the focus according to the sign of the nonlinear absorption coefficient β. For

pulses with a Gaussian temporal profile, a material with an instantaneous nonlinearity, small changes in transmission, and using integrating detectors to measure the transmitted energy for each pulse, the transmission normalized to its linear value can be fitted by the approximate expression

$$T\left(z\right) = 1 - \frac{q_0\left(z,0\right)}{2^{3/2}}, \tag{3.1}$$

where z is the sample position and $q_0\left(z,0\right) = \beta I_0\left(0\right) L_{\mathrm{eff}}$, with $I_0\left(0\right)$ the on-axis intensity at the peak of the pulse and L_{eff} an effective thickness of the sample that depends on the linear absorption coefficient.

The open-aperture z-scan improves the simpler experiment of measuring transmission varying the intensity using neutral density filters or crossed polarizers because it gives the possibility of varying the intensity incident on the sample over a large range and with high resolution without effort.

Figure 3.7 shows the setup I used in the z-scan measurements on the composite films.

There are some details that must be addressed with care when applying the technique to gold nanoparticle systems. The gold-silica samples are quite inhomogeneous (at a the scale of a few μm) and they easily suffer optical damage.

The inhomogeneity of the sample renders the z-scan traces difficult to interpret because the linear transmission varies as the sample is translated along the beam and this contaminates the nonlinear signal. The way to solve this problem has been
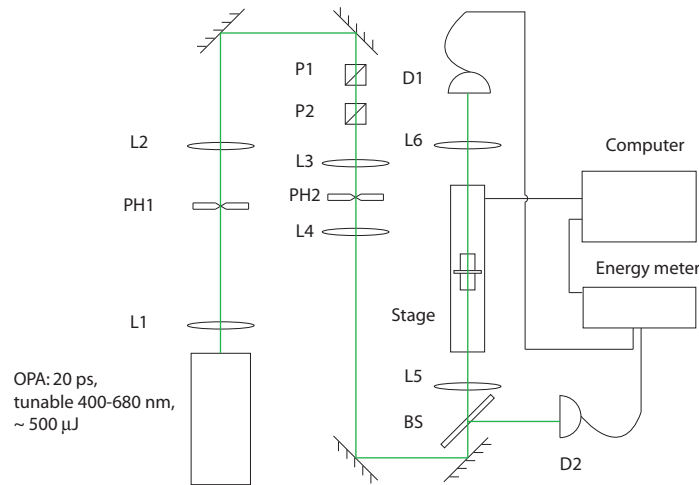
Figure 3.7: z-scan setup for measurements on composite materials. Lens L1 and pinhole PH1 compose the first spatial filter; lens L2 collimates the beam for proper incidence on the couple of polarizers P1 and P2 that are used to control the energy of the pulses incident on the sample which is placed on a motorized translation stage; lens L3 and pinhole PH2 form the second spatial filter; lens L5 forms the focused beam used for the z-scan measurement. The light is collected by large area detectors D1 (signal) and D2 (reference). The measurements are controlled by a computer.

indicated by Sheik-Bahae et al. [110]; one must compare a high energy scan to a low energy scan in which there is no nonlinear response even at the focus of the Gaussian beam.

There is an important requirement that may appear obvious but must be satisfied in a rigorous way in order that the measurement be successful: one must be able to change the energy of the pulses without changing their spatial profile; if the spatial profile of the pulses changes too much between scans at different energy, then again it will not be possible to distinguish between linear and nonlinear effects.

To appreciate this point better one needs to take into account that the maximum variation in transmission that can be induced in the samples by nonlinear effects

without inducing any damage is often on the order of 2%; it is therefore necessary that the linear part of the low and high energy scans (the part of the scans outside the Rayleigh range of the Gaussian beam) coincides with accuracy better than a few parts per a thousand.

Methods that change the spatial profile of the pulses too much and cannot be used are: changing the amplification of the laser amplifier, adding neutral density filters. The only method that guarantees that the change in the spatial profile of the pulses is small enough that linear effects do not contaminate nonlinear effects is the use of two crossed polarizers of good quality. The polarizer that rotates must have at least $\lambda/4$ surface quality; I have verified that a polarizer with nominal λ surface quality is not suited to the task. Moreover the polarizer that I selected had to rotate by less than $10°$ otherwise I would see an effect in the linear part of the scans. Since it is advisable to change the energy of the pulses by a factor of at least 3 or 4 times to differentiate well between low and high energy, it is then necessary to hit the polarizers with a very energetic pulse and orient them so that they are almost crossed, so that a very small motion of the first polarizer will induce a significant energy variation.

For my measurements I chose the input energy to the double polarizer setup to be on the order of $10 \, \mu\text{J}$ and the angle between polarizers so that the output energy was on the order of tens of nJ. In order to have a maximum sensitivity of the transmitted energy to the rotation of the first polarizer it is also necessary that there is no "leakage" out of the crossed polarizers, and the best way to realize this

condition is using crystal polarizers and collimating well the beam which is incident on them. I want to stress that all of the above conditions are essential and must be fulfilled otherwise the experiments will not work.

Another consideration of practical importance is the focal length of the lens used in the z-scan setup. All focal lengths are not equivalent because of the following considerations.

Some points of the Wendling samples have a transmittance smaller than 0.5% at the wavelength where their attenuation is maximum. The detectors that were available to me could measure a minimum energy of around 20 pJ with a precision sufficient to make the measurement possible. It is necessary therefore that the minimum energy incident on the sample (for the low energy scans) be of the order of 5 nJ. A lens must have focal length of at least approximately 200 mm in order that pulses with 5 nJ energy can be considered low intensity for the Wendling samples; a lens with a focal length longer than 300 mm is unadvisable because too long a scanning range could emphasize the linear effects of the inhomogeneities of the sample. For most of the scans I chose a 250 mm lens.

The possibility of optical damage to the samples poses two distinct problems. The first is that we must be able to detect small changes in transmittance (let us say of a few parts in a thousand) because the maximum change in transmittance that can be obtained before optical damage occurs can be as small as 2%. The second is that we must devise a method to verify that the sample has not been damaged after each

measurement.

The issue of measuring transmittance changes with a precision better than a few parts per a thousand can be addressed with the classic signal/reference detector setup. There is a crucial point; the laser system which I have used for the measurements has a 10 Hz repetition rate. A rough estimate of the time available for the experiment suggests that I cannot afford to average more than 200 shots per experimental point (one must take into account that some of the shots are rejected by the measurement system because they are not within prescribed energy limits). An average of 200 shots reduces the standard deviation of the mean by approximately 15 times with respect to the standard deviation of a single data point; since I need one part per a thousand precision in the mean, the standard deviation of the distribution of single data points must be on the order of 1.5%.

Measurements at the wavelength of 532 nm were performed with the SHG output of the laser which has an extremely good beam profile; the splitting ratio between reference and signal had a standard deviation of about 0.6%, adequate for the measurements.

Things are different when performing frequency-resolved measurements with the OPA. A not particularly painstaking spatial filtering of the OPA, that I had used for the measurement performed on the layered metal-dielectric composite material [52] yielded pulses whose splitting ratio between reference and signal had approximately 8% standard deviation.

The reason for this quite high standard deviation is that while at a superficial look the beam emerging from the low-numerical-aperture spatial filter I used for the work in [52] may appear to possess a good spatial profile, in fact it possesses inhomogeneities that vary from pulse to pulse and cause the measured splitting ratio to change. I have verified by placing a polarizer in front of the whole setup that the changing splitting ratio is not due to polarization variations that would have caused changes in the reflectance-transmittance of the beamsplitter; it was rather due to the fact that (in large part) the response of the detectors is not spatially homogeneous and (in smaller but unquantifiable part) that the splitting ratio of the beamsplitter may not be spatially homogeneous. The problem cannot be solved with the use of integrating spheres because the signal detector is already used at the lower limit of its detection range and because the sample transmittance itself is inhomogeneous; the only possibility is a careful spatial filtering of the pulses.

Spatial filtering of even moderate energy energy ps pulses is not the same task as spatial filtering of a cw beam because one must avoid damage to the pinhole; the nonlinear measurements require high energy which is very close to the damage threshold of the composite material under test when focused by a 250 mm lens; the materials of which the pinholes I used is made (I worked with both Cu and Mo) have a much higher damage threshold than the gold nanoparticle system, but it is important not to exaggerate with the f-number of the spatial filter lens because they too can be damaged and cannot be readily replaced; I reached a compromise with a

$25\,\mu$m pinhole which turned out to be small enough to be a good spatial filter but large enough to resist to pulses of few hundred nJ energy which is larger than the maximum that I needed for the experiments; for giving an idea that there is indeed a danger to be avoided, the first pinhole I used was damaged by a pulse with $< 1\,\mu$J energy. It is mandatory to put the double polarizer which controls the intensity before the spatial filter because the spatial filter cannot resist to a pulse of $10\,\mu$J. In this way I obtained on the average a standard deviation of about $1\,\%$ in the signal to reference ratio.

The OPA output spatial profile is extremely rough. If it were allowed to directly hit the polarizers (of course conveniently attenuated) this could cause additional unwanted problems of beam changing shape when the first polarizer is rotated; I did not verify the actual presence of this danger but I decided to prevent it anyway. It is then necessary to pre-spatially filter the OPA beam; the output energy of the OPA is about $500-800\,\mu$J. It has to be kept running at this high energy because the standard deviation of the energy of the output is lowest when the energy of the pulses with which it is pumped is high. I chose then as a spatial filter a $300\,\mu$m iron aperture and focused the OPA pulses on it with a 1 m focal length lens. The throughput is around $10\,\mu$J which is more or less what is needed as an input to the double polarizer setup to control the energy with the required stability in spatial profile; the reason the throughput is so low is that the spatial profile is extremely bad.

The second issue that derives from optical damage is that after each measure-

ment it is necessary to verify that no optical damage has occurred. The first sign of optical damage, in fact, is that the change in transmission which is provoked by the high energy pulses is irreversible; only at higher energies one sees a large spike in transmission which makes it immediately evident that there has been optical damage.

It is therefore necessary to perform a low energy scan before and after each high energy scan so that it can be verified that the low energy scan did not change. A devil's advocate could imagine that the position of the beam waist or the shape of the beam for the low energy scans does not exactly correspond with the one the beam takes at high energy and that therefore the low energy pulses do not sample the damage.

In order to investigate this issue I have taken some data (with the help of Per Adamson) and done a small simulation based on them. In synthesis, I have taken images of the waist of the beam for various positions of the polarizer P1 which is used to vary the energy of the pulses incident on the samples and then I have calculated what would the transmission of any of the beams be through some damage caused by one of them.

A more detailed explanation

I have taken images of the beam at the waist for different positions of the polarizer, using a camera with a pixel size of 4 microns. I have used a lens slightly longer than usual (500 mm rather than 300 mm) in order to have a larger beam waist. I have

also data with the usual 300 mm lens that show the same effect, but the beam shape is resolved less well, so it was nicer to use these data.

I have assumed that one of the pulses that are hitting the sample while the polarizer is at a position mark = 120 degrees (that corresponds to high energy pulses) has damaged the sample and the transmission of this pulse is 1.015 times the transmission through the undamaged sample.

I have modelled the damage in two ways.

In the first way the damage (damage = permanently increased transmission) happens in every position where the pulse intensity is larger than a given intensity, and it is uniform; that is, the transmission through the damaged area of the sample is uniform and is such that the overall transmission of the pulse which is inflicting the damage is 1.015.

In the second way the damage function is equal to the intensity of the pulse raised to a certain power, and I have taken this power ranging from 1 to 99. Again, the damage function represents the permanent change in transmission due to the damage and I normalize it so that the transmission of the pulse which is inflicting the damage is 1.015 times the transmission through the undamaged sample.

For both cases I have taken the new transmission function deriving from the damage and calculated the transmission of a pulse for different positions of the polarizer P1 (corresponding to low energy pulses) through it. Since in the transmission function there will be the "imprint" of the pulse, then the more a pulse will differ from

the pulse that has caused the damage (that is, the more I turn the polarizer away from the initial position), the less the pulse will feel the damage and the closer its transmission will be to the transmission through the undamaged sample (normalized to 1).

We can see from Figures 3.9 and 3.10 that even for the position of the polarizer which is farther away we should be able to "read" the damage if it occurs.

A separate calculation done using the same images shows that the center of the beam moves about 1% of the beam size for a 5 degrees rotation of the polarizer.

The data and calculations presented here also caution against an excessive rotation of the polarizer because the ability to detect damage becomes smaller.

3.2.1   Some representative examples of z-scan data

Figure 3.11 shows an example of a z-scan measurement for one of the points of the 7W sample. The measurement consists in three z-scans. The first one (green circles, 3.9 nJ energy) establishes a baseline for the linear transmission; one can see that the linear transmission is not a flat line, and the deviation from the flat line is an expression of the sample inhomogeneity. The second one (blue circles, 42.2 nJ) probes the nonlinearity; the final one (red circles, 4.2 nJ) verifies the absence of damage.

Figures 3.12 and 3.13 are examples of optical damage. Looking at Figure 3.12 we see that the first and the third scans (green and red circles respectively), performed at the same pulse energy and same position of the polarizer, present a suspicious
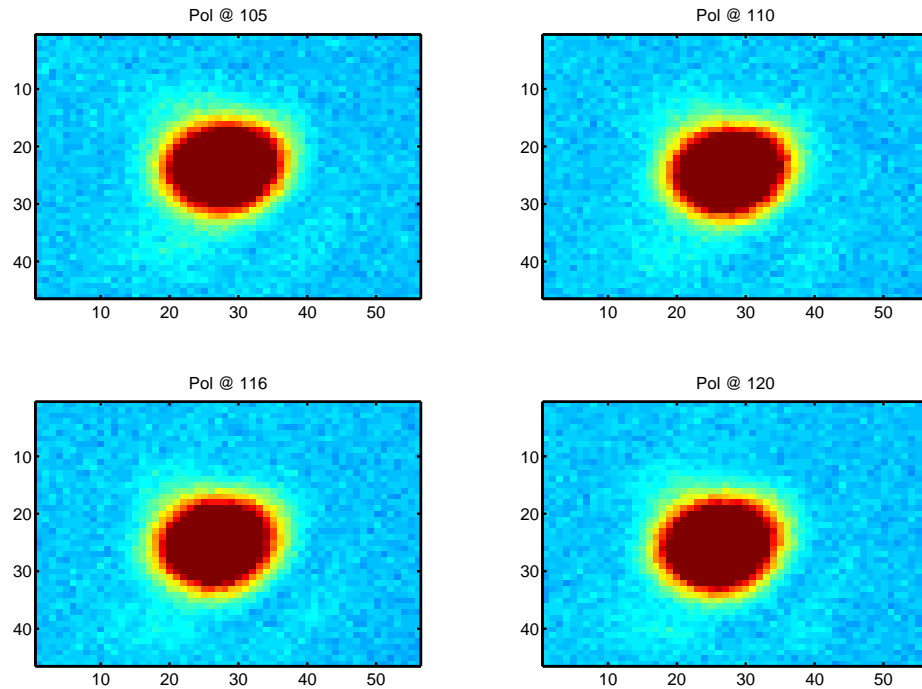
Figure 3.8: Beam profiles for different positions of the polarizer; the axes are labelled in pixel units; one pixel corresponds to 4 microns.

difference: even if the difference between each couple of corresponding points may be inside statistical error, the part of the third scan that corresponds to the waist of the beam is consistently higher in transmission than the first scan. This may point to optical damage.

I have taken this as an occasion to show the aspect of optical damage more clearly by repeating the set of three scans (low-high-low energy) at the same point with a particularly high energy "high" scan. The results are shown in Figure 3.13 and the occurrence of damage is evident: the excessive energy of the second scan has irreversibly changed the transmission of the gold films. It is important to note that
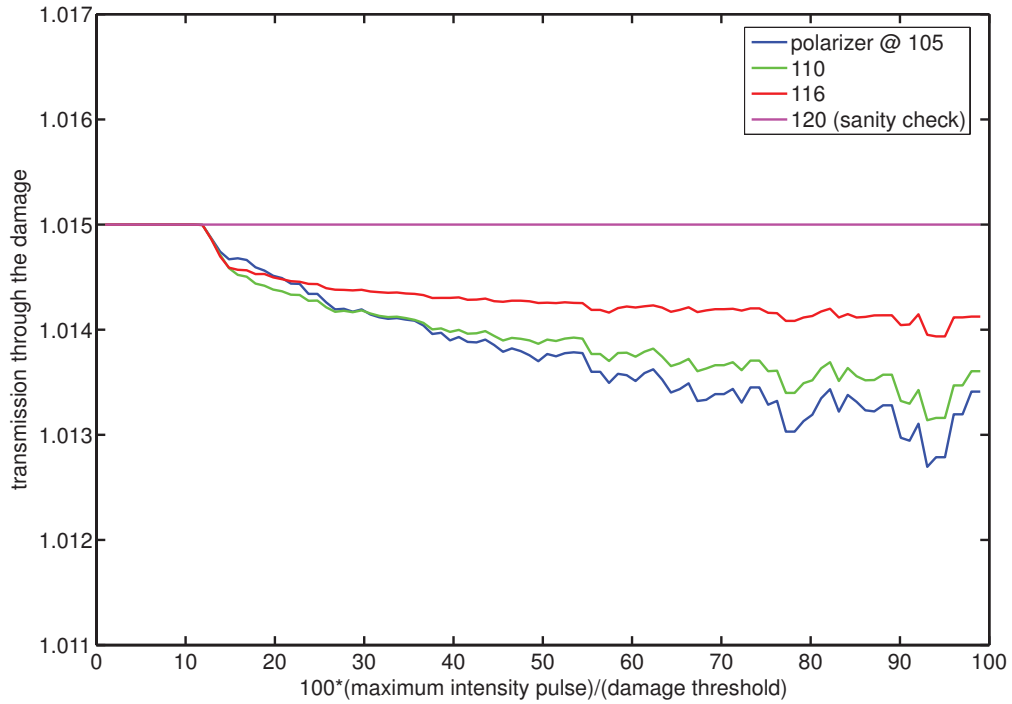
Figure 3.9: Transmission through damage produced by a pulse with polarizer @ 120, damage occurs only for $I > I_{th}$.

curve obtained in the high energy scan looks still quite like the typical open-aperture z-scan; damage can be established only with a linear control scan.

The solution for this particularly difficult case is to further reduce the energy of the "high energy" scan. I have obtained the data presented in Figure 3.14 which are compatible with the absence of optical damage. They are also the data with the lowest signal to noise ratio that I have used in the data set. The typical data quality is closer to the data of Figure 3.11.

Another aspect of the measurement that merits discussion is the step of the data reduction in which one goes from the measured energy to the intensity. In princi-
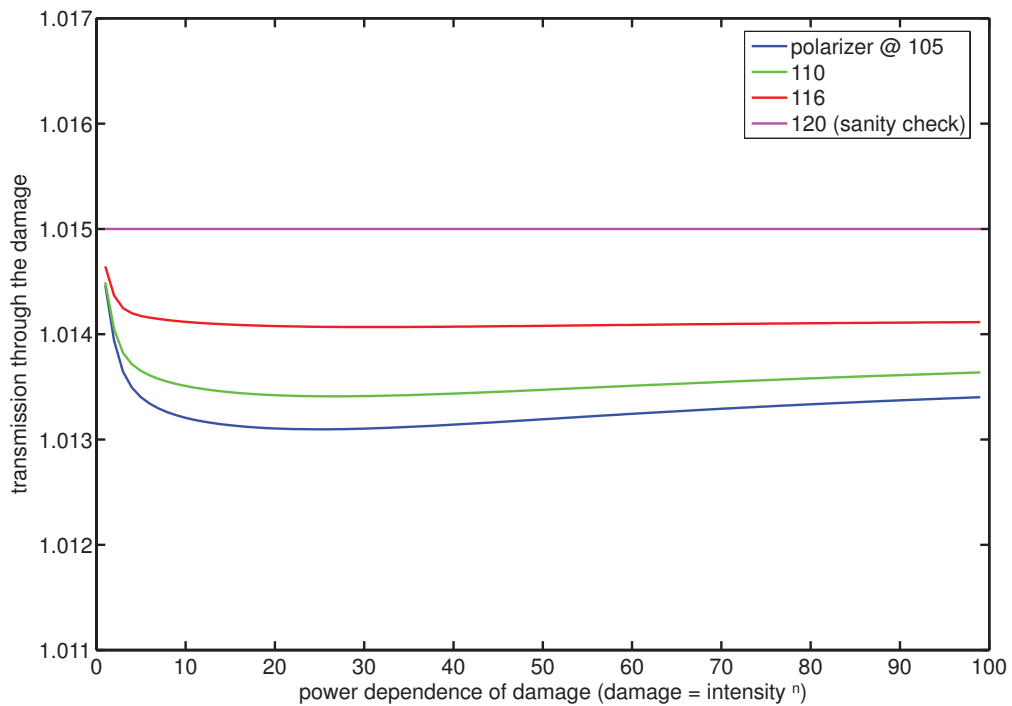
Figure 3.10: Transmission through damage produced by a pulse with polarizer @ 120, damage follows a power law I^n.

ple the most straightforward procedure is measuring the beam waist, perhaps with a knife edge method. Practical considerations have suggested me to limit myself to just a few of these measurements: one critical issue in the measurement is the performance of the EKSPLA OPA, which as I remarked earlier outputs pulses of energy distributed with relatively low standard deviation only if pumped at relatively high energy. This makes some of its components susceptible to repetitive pulse damage, requiring sometimes extensive realignment performed by an EKSPLA engineer. In view of this consideration I dedicated the maximum possible laser time to the measurement of nonlinearities and I used the values of the nonlinear absorption coefficient

Figure 3.11: z scans for point 15 of Wendling sample 7W. The first scan (green circles) establishes a baseline for the linear transmission of the samples; the second (blue circles) probes the nonlinearity; the third (red circles) verifies the absence of optical damage.

obtained for beam waist measurement performed at selected points as a reference to deduce the values at all other points.

3.2.2 z-scan data fitting and error analysis

I have analyzed the z-scan data using the first two terms (zeroth- and first-order) of the series C.17. For each scan I divided the normalized data (transmission at the first sample position being normalized to one) at high energy by the normalized data at

Figure 3.12: z scans for point 16. The first scan (green circles) establishes a baseline for the linear transmission of the samples; the second (blue circles) may exceed the damage threshold for the composite film; the third (red circles) raises suspicions that there may have been an irreversible transmittance change in the material.

low energy obtaining a curve for the normalized nonlinear transmission; an example of fitted data is given in Figure 3.17.

The effective length L_{eff} appearing in expression C.17 has been calculated on the basis of the data of tables 3.1 and 3.2. I have taken into account reflection from the sample (measured by me with the ps laser system at the wavelengths at which I performed the measurements) for calculating the actual energy inside the sample but I have attributed all the observed changes in transmission to nonlinear absorption; this is reasonable because the main contribution to the effective $\chi^{(3)}$ of the composite material is expected to be imaginary. Finally, I have considered the wavelength
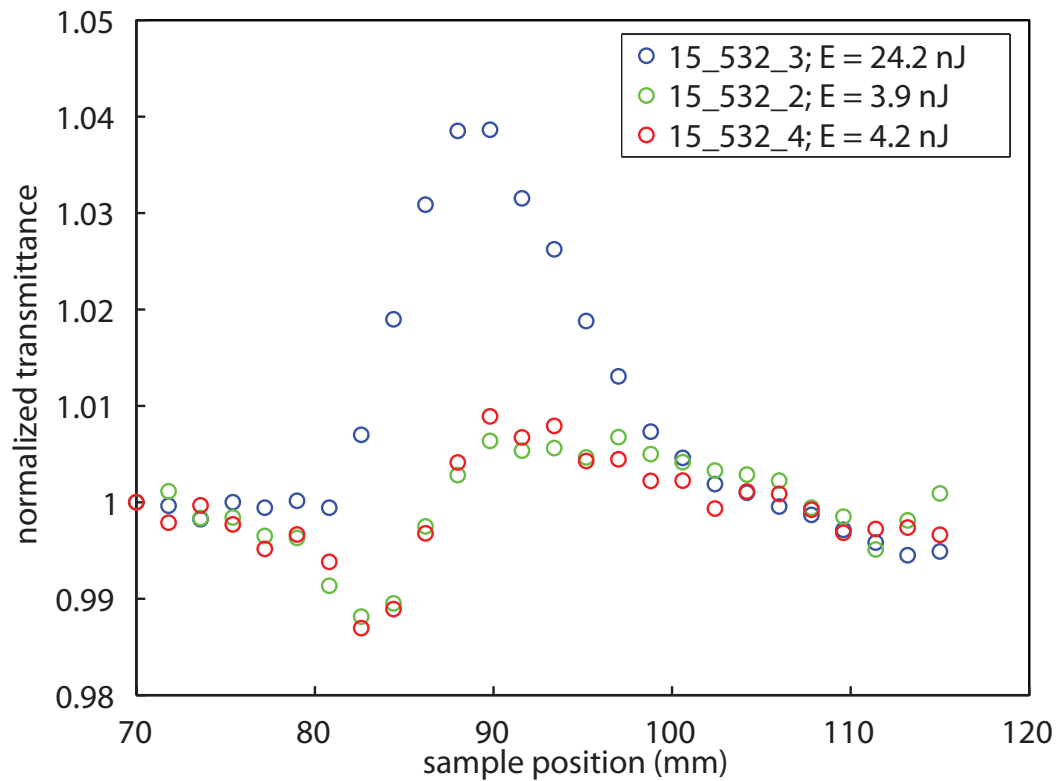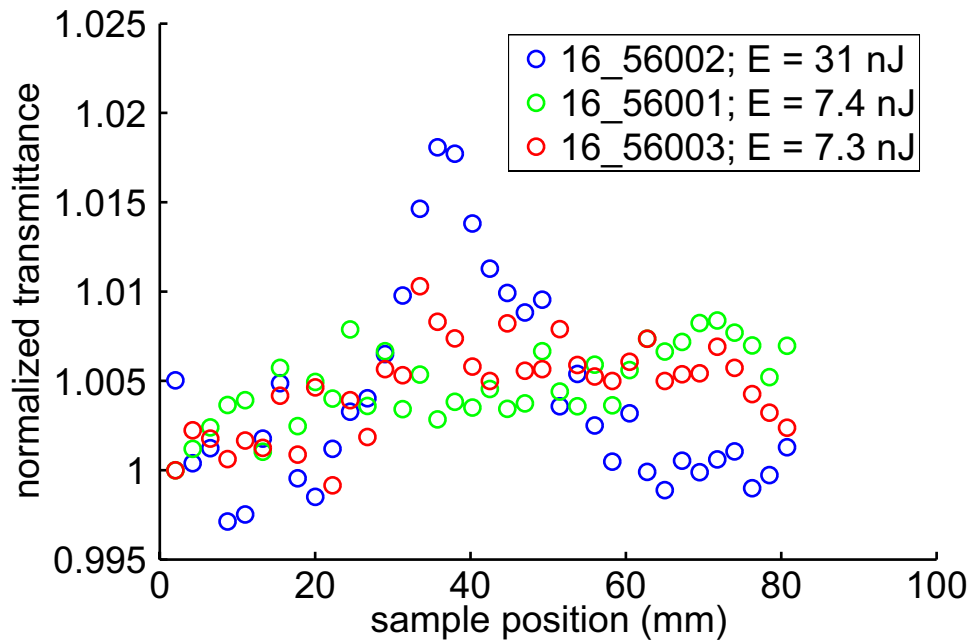
Figure 3.13: z scans for point 16. The first scan (green circles) establishes a baseline for the linear transmission of the samples; the second (blue circles) exceeds the damage threshold for the composite film; the third (red circles) shows that there has been an irreversible transmittance change in the material.

dependence of the detector's response (data furnished by the manufacturer Laser Probe).

There are many factors that contribute to experimental errors in a measurement of an optical nonlinearity. It is much easier to obtain an accurate value of the nonlinearity at a wavelength with respect to the nonlinearity at another wavelength or of another material at the same wavelength than an absolute measurement. In order to appreciate this point one can observe panels (a) through (d) of Figure 3.16 and compare them to panel (e) of the same Figure. It can be noted that the data point at 530 nm in the first four panels is lower than what one would expect by looking at
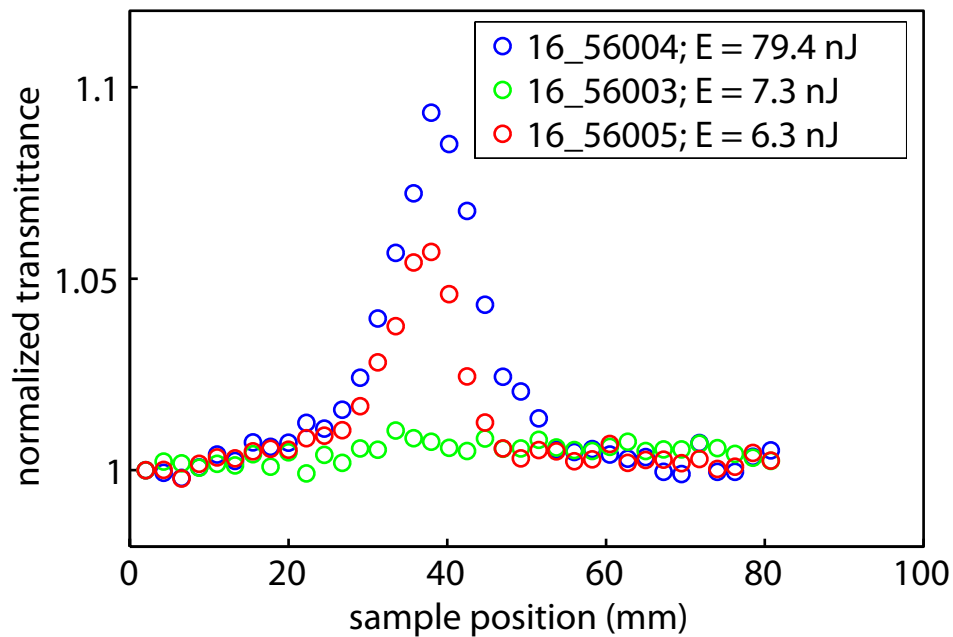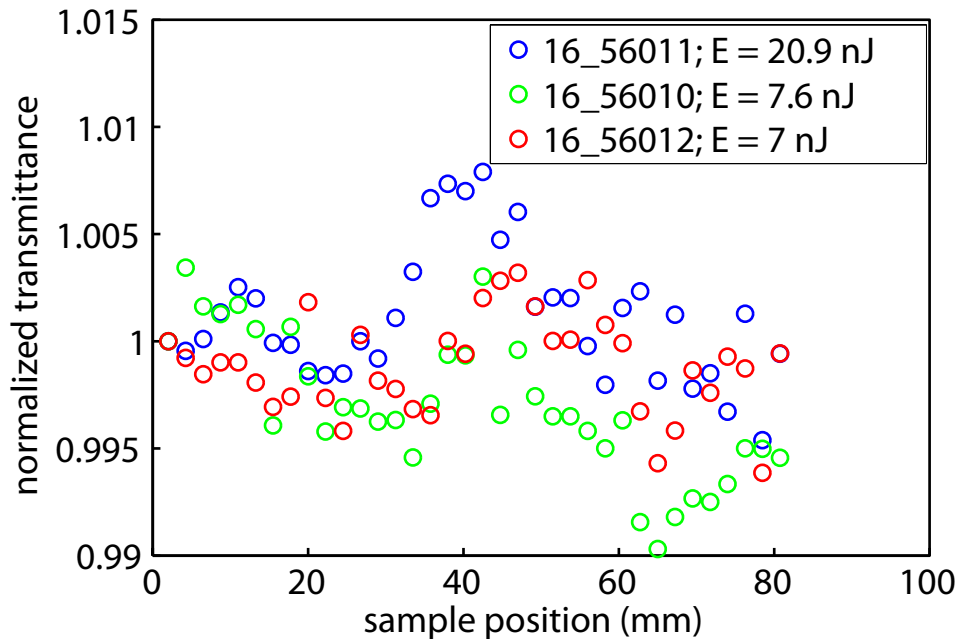
Figure 3.14: z scans for point 16. The first scan (green circles) establishes a baseline for the linear transmission of the samples; the second (blue circles) probes the nonlinearity; the third (red circles) is compatible with absence of optical damage.

the points at other wavelengths, but that this does not happen for the data in panel (e).

A very reasonable explanation is the following. First of all it is necessary to know that the "530 nm" data point in the first four panels was actually taken at a wavelength of 532 nm. I did it because the OPA output is more stable at that wavelength than at any other wavelength: a little bit of the second harmonic output of the ps laser seeps through the dichroic mirrors that are used to isolate the 355 nm third-harmonic pump and seeds optical parametric generation in the OPA, while at any other wavelength the signal and idler originate from noise. Measurements at 532 nm

therefore take much less time than measurements at 530 nm; the drawback is that most probably the temporal duration and possibly the spatial profile (even after spatial filtering) of the OPA output at 532 nm differs from that at all other wavelengths, and this causes the under-estimation of the nonlinear absorption coefficient.

I realized that the data point at 532 nm was anomalous after the measurements at the third fill fraction; it was impractical to re-take the data, but the measurements at the last two fill fraction show that measuring the nonlinearity at 530 nm made the "530 nm" data fall into better agreement with the rest of the data.

The errors in the measurement of the nonlinear absorption coefficient β are caused by: uncertainties in the knowledge of pulse duration (pulse duration can only be estimated as I didn't have any means of measuring the duration of a ps pulse in the visible part of the spectrum at the time of the experiments), beam waist, variations of beam waist between different experimental runs (it is necessary to readjust the position of pinhole PH2 for measurements at different wavelength and therefore the position of lens L4 which in turn affects the beam width and divergence at lens L5), uncertainties in the knowledge of pulse energy (not only the mean value affects the measurement but also the spread; the computer is instructed to accept only pulses with a nominal energy that does not differ by more than 10% from a selected value), uncertainties in the knowledge of the beam spatial and temporal shapes (which are approximated by Gaussians in the data analysis).

It is quite possible that the compounded error deriving from all of these effects

is larger than 30%. The relative error is however much smaller than 30% as the smoothness of the curves in Figures 3.15 and 3.16 attests.

Calculating the values of $\chi^{(3)}$ requires both knowledge of nonlinear absorption and of nonlinear refraction [32, 111]; I do not possess any data on nonlinear refraction therefore the comparison with theory is made by calculating the theoretical curves for the nonlinear absorption coefficient and comparing those to the data. The formula that relates β to $\chi^{(3)}$ is [33]

$$\beta = \frac{4\pi}{\lambda} \mathrm{Im} \left\{ \frac{12\pi^2}{n \mathrm{Re}\left\{n\right\}} \chi^{(3)} \right\}. \tag{3.2}$$

3.3 Data on the nonlinear absorption of gold-dielectric composites

I measured the nonlinear absorption coefficient β of the Wendling samples at the wavelength of 532 nm in the entire range of fill fraction; for five points I have obtained as well wavelength-resolved data.

I performed moreover a measurement of the nonlinear absorption coefficient at 532 nm for two of the Nelson samples.

Wendling samples

The data for the Wendling samples are shown in Figures 3.15 and 3.16. Figure 3.15 shows the data at the fixed wavelength of 532 nm over the whole fill fraction range and Figure3.16 shows the data at five different fill fractions as functions of wavelength.
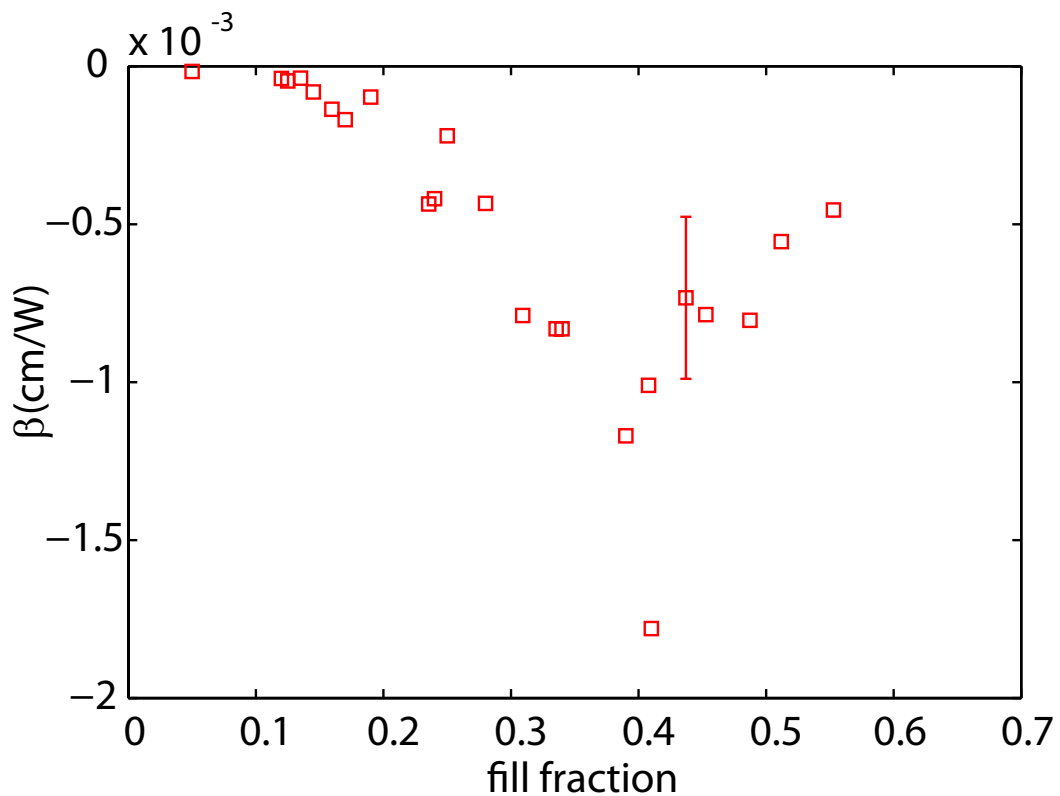
Figure 3.15: Nonlinear absorption coefficient of the Wendling gold-silica film plotted as a function of fill fraction at a wavelength of 532 nm. An error bar is shown for one data point; the estimated error is 35% for all data points.

The Wendling samples are found to act as saturable absorbers (that corresponds to having a negative value of β) for all fill fractions and at all wavelengths for which a measurement was performed. The nonlinearity first grows and then decreases as a function of fill fraction; this behaviour can be seen clearly in Figure 3.15 where we
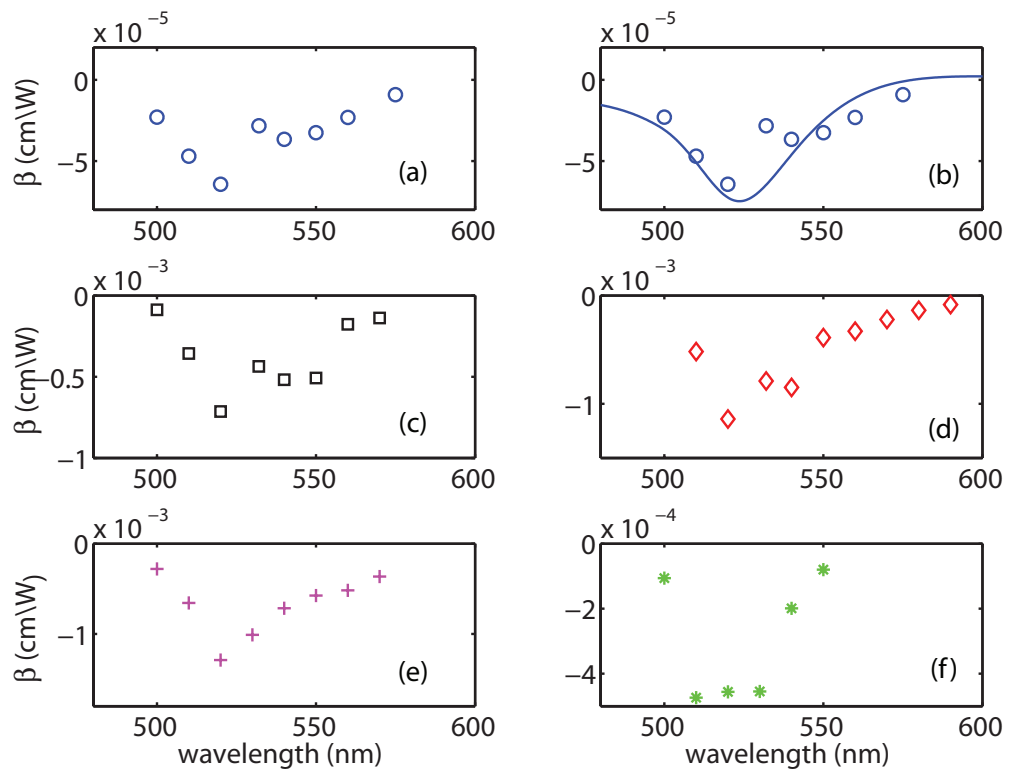
Figure 3.16: Nonlinear absorption coefficient of the Wendling gold-silica film plotted as a function of wavelength at fill fraction (a) $f = 0.05$, (b) again $f = 0.05$ fitted to the Maxwell Garnett theory,(c) $f = 0.23$, (d) $f = 0.31$, (e) $f = 0.40$, (f) $f = 0.55$. The Maxwell Garnett theory is not valid at higher fill fractions.

plot the nonlinear absorption coefficient against the fill fraction at fixed wavelength. Similar results (for the modulus of $\chi^{(3)}$) have been reported in other studies [99, 101, 102]. We also observe from Figure 3.16 that the peak of the nonlinear response as a function of wavelength does not shift much as the fill fraction is varied.

We obtain a useful insight into the nature of the optical response by noting that the nonlinear response (Figure 3.16) peaks at approximately the same wavelength as the linear response (Figure 3.4). The link between the linear and nonlinear properties is

of course the plasmon resonance; we shall examine this link in more detail in the next section and show how it determines the sign of the nonlinear absorption coefficient.

Nelson samples

The samples prepared by Mark Nelson offer the opportunity of widening our view on the optical nonlinearities of metal-dielectric composite sample; their morphology and linear optical properties are different from the morphology and optical properties of the Wendling samples and this creates some expectations for differences in the nonlinear optical properties as well.

Unfortunately the Nelson samples are even more susceptible to damage than the Wendling samples. In particular it has proven impossible to observe any nonlinearity at wavelengths corresponding to the plasmon resonance before the onset of optical damage. I have been able to perform several measurements outside the plasmon resonance. The success in this case is due presumably to the fact that outside the plasmon resonance the optical field is not strongly localized in the metal and cannot damage it as easily. I present here these results. The same results are presented in Mark Nelson's thesis; here they are discussed in the context of the mechanisms governing the nonlinearities of composite materials.

The successful measurements were performed on samples "9-1-03 #4" and "9-1-03 #7" at the wavelength of 532 nm. Both samples are optical limiters at this wavelength. The value of the intensity-dependent absorption coefficient is $1.8\,\mathrm{cm/GW}$

for both samples.

Figure 3.17 shows the processed data for sample 9-1-03 #4 together with the theoretical fit based on the open-aperture z-scan expression C.17.
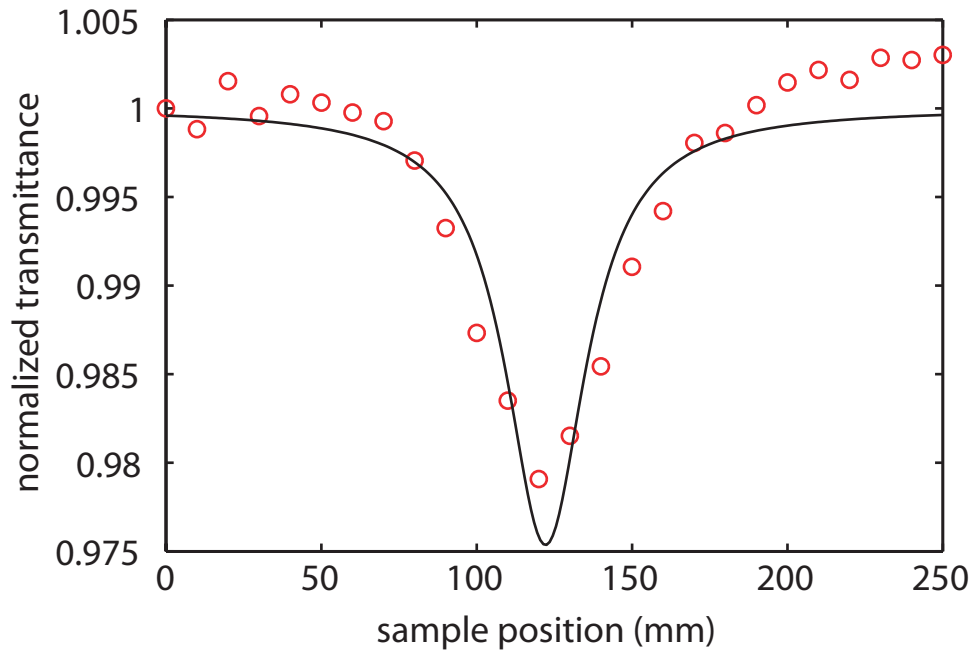
Figure 3.17: z-scan of one of the Nelson samples showing optical limiting.

The relationship between the optical limiting observed in the Nelson samples and the saturable absorption observed in the Wendling samples is discussed in Section 3.4

3.4 The change of sign of nonlinear absorption as an effect of plasmon damping

It is possible to understand the experimental results at low fill fractions through use of a modified version of the Maxwell Garnett theory which retains its spirit and all

of its fundamental approximations.

The need for modifications of the Maxwell Garnett theory comes from the fact that we want a formula that we can apply to very thin samples. The standard Maxwell Garnett theory calculates the local field in a composite sample at the location of a specified nanoparticle assuming that the nanoparticle is surrounded by an isotropic distribution of dipole density; this condition is not completely fulfilled for a sample that is only two hundred nanometers thick. A certain amount of work has been published in the scientific literature regarding the effective dielectric constants of thin films; a good example is [112] and the "GranFilm" software described in [113] and available online at http://www.insp.upmc.fr/axe2/Oxydes/GranFilm/GranularFilm.html. We have chosen to develop an extremely simple theory because it afforded us the possibility of interpolating in a simple way between the two-dimensional case and the usual three-dimensional case; moreover an extension to the nonlinear regime is promptly found.

We proceed in two steps. First we develop a theory valid for a planar (two-dimensional) sample. We then note that the formulae for the two-dimensional and the usual three-dimensional case can be written in the same form using a parameter D (for dimension) that takes the value 2 and 3 respectively. We then let the parameter D vary freely between 2 and 3 to represent the case of a sample that is neither truly two- nor three-dimensional. Details of the derivation of the two-dimensional Maxwell Garnett theory are given in Appendix B. The effective dielectric constant ε of a

D-dimensional Maxwell Garnett composite medium is thereby found to be given by the relation

$$\frac{\varepsilon - \varepsilon_h}{\varepsilon + (D-1)\,\varepsilon_h} = f\,\frac{\varepsilon_i - \varepsilon_h}{\varepsilon_i + (D-1)\,\varepsilon_h}, \tag{3.3}$$

where ε_h is the dielectric constant of the host and can be considered purely real while $\varepsilon_i = \varepsilon_i' + i\varepsilon_i''$ is the dielectric constant of the metallic inclusions. For small fill fractions, when the dielectric constant of the composite material is very close to the dielectric constant of the host, the dielectric constant of the composite material can be approximated by

$$\varepsilon \approx \varepsilon_h \left[1 + Df\frac{\varepsilon_i - \varepsilon_h}{\varepsilon_i + \varepsilon_h(D-1)} \right]. \tag{3.4}$$

In these small-fill-fraction conditions, the approximate expression for the linear absorption coefficient,

$$\alpha = \frac{\omega}{c}\mathrm{Im}\sqrt{\varepsilon} \approx 2\frac{\omega}{c}Df\sqrt{\varepsilon_h}\,\mathrm{Im}\left\{ \frac{\varepsilon_i - \varepsilon_h}{\varepsilon_i + \varepsilon_h(D-1)} \right\}, \tag{3.5}$$

simplifies greatly for a host with no loss to the following expression:

$$\alpha \approx \frac{\omega}{c}D^2 f\varepsilon_h^{3/2}\,\frac{\varepsilon_i''}{\left[\varepsilon_i' + (D-1)\,\varepsilon_h\right]^2 + \varepsilon_i''^2}. \tag{3.6}$$

Eq. (3.6), which is valid only in the limit of very small fill fractions, leads to the

reversal of the sign of the induced absorption with respect to that of pure gold for the following reason. Near resonance, that is for $[\varepsilon_i' + (D-1)\varepsilon_h]^2 \approx 0$, α is inversely proportional to ε_i''. Thus, as ε_i'' increases the overall absorption α decreases. The bulk properties of gold are such that $\mathrm{Im}\chi^{(3)}$ is positive, meaning that gold itself acts as a reverse saturable absorber, that is, as an optical limiter [32]. As the optical field strength E increases, the effective value of ε_i'' thus increases by an amount equal to $3\,\mathrm{Im}\chi^{(3)}\,|E|^2$, and the overall absorption decreases. Thus the composite material acts as a saturable absorber. We observe that this is similar to what happens in the case of a forced harmonic oscillator: at resonance, it is the most damped oscillator the one that dissipates the least power, because an oscillator at resonance oscillates with an amplitude inversely proportional to the damping constant.

The simple explanation just presented for the sign reversal, or that presented in ref. [31], cannot be applied to a situation in which the fill fraction of the metallic component becomes large. In this case, we can suggest the following more heuristic explanation. It has previously been established [61] that the surface plasmon resonance becomes broadened in the presence of intense optical radiation. The broadening of the resonance implies an increased damping for the surface plasmon. Thus the field enhancement within each nanoparticle is decreased and consequently the overall absorption is decreased. Thus, by this mechanism, the composite material is once again expected to act as a saturable absorber.

The explanation that we just presented complements, for the case the imaginary

part of the nonlinearity, the reasoning based on local-field effects that was presented in [31]. We briefly review that reasoning here. An expression for the nonlinear susceptibility of a Maxwell Garnett composite has been derived in [87] for the case of spherical inclusions. In Appendix B we give a brief derivation of the nonlinear susceptibility for the case of cylindrical inclusions that is valid when only the inclusions are nonlinear. The result for D dimensions is

$$\chi^{(3)} = f \, |q_i|^2 \, (q_i)^2 \, \chi_i^{(3)} \tag{3.7}$$

where q_i is the local field factor in the metal inclusions. The local field factor for D dimensions is

$$q_i = \frac{\varepsilon + (D-1)\,\varepsilon_h}{\varepsilon_i + (D-1)\,\varepsilon_h}. \tag{3.8}$$

Eq. (3.7) displays the sign-reversal effect that we have discussed starting from Eq. (3.6). At the plasmon resonance the condition $\varepsilon_i' + (D-1)\varepsilon_h = 0$ is approximately satisfied (exactly satisfied in the limit of very small fill fraction); the local field factor therefore becomes $q_i \approx D\varepsilon_h/i\varepsilon_i''$ which is imaginary. Thus q_i^2 is mainly real negative and the nonlinear susceptibility of the composite material is opposite in sign to that of the metal inclusions.

A comparison of the predictions of Eq. (3.7) and the experimental data is given in part (b) of Fig. 3.16. In order to obtain good agreement with the data we took the

parameter D to have a value of 2.38. Moreover we took into account that collisions of the free electrons with the boundaries of the nanoparticles modify the dielectric function of Au. We assume that this process influences the imaginary part of the dielectric function only. The relaxation time τ of the conduction electrons in the nanoparticles is taken to be described by the relation $1/\tau = 1/\tau_{bulk} + v_F/l$, where v_F is the Fermi velocity and l is the average mean path between two points on the surface of the nanoparticle, which for a sphere of radius R is $4R/3$ [114]. The imaginary part of the dielectric function of Au is therefore given by

$$\varepsilon_i'' \approx \varepsilon_{i(bulk)}'' + \frac{3\omega_p^2 v_F}{4\omega^3 R}.$$ (3.9)

We use the value 1.36×10^{16} Hz for the plasma frequency ω_p and 1.40×10^8 cm/s for the Fermi velocity v_F [53] of bulk gold; formula 3.9 is an excellent approximation at optical frequencies when $\omega >> 1/\tau$.

The fit of Fig. 3.16 is realized using a radius of 3 nm for the nanoparticles; it is reached assuming a third-order susceptibility for gold $\chi^{(3)} = (-2 + 10i) \times 10^{-8}$esu which is compatible with the value found in [115].

The Maxwell Garnett theory, and therefore Eq. (3.7), cannot describe quantitatively the sets of our data for the Wendling samples at points which have fill fractions f equal or larger than 0.23, but the concept described using Eq. (3.6) is still valid; the nonlinearity of the composite results from an intensity-dependent damping of the resonance, and it makes sense from a physical point of view that the nonlinear be-

haviour of the composite material at high fill fractions is similar to the behaviour at lower fill fraction if the character of the resonance is not modified drastically.

The data on the nonlinear absorption coefficient for the Nelson samples are compatible with the explanation based on plasmon damping. In fact, looking at Figure 3.6 one can see that the wavelength of 532 nm is at the wing of the plasmon resonance, where the field localization is not expected to be large. It is therefore plausible that an increase in the absorption of gold result in the increase in the absorption of the composite. If our physical situation were described by Equation 3.6 we would observe this behaviour as soon as $[\varepsilon_i' + (D-1)\,\varepsilon_h]^2 > \varepsilon_i''^2$. The behaviour of the composite under study is of course more complicated.

The heuristic considerations that we present should not be valid for composite materials with a more complicated morphology, as for example the films investigated by Seal and coworkers [49] where field fluctuations are present at all scales and can be best described by means of sophisticated numerical calculations such as the already cited ones by Shalaev and collaborators [45–47].

Chapter 4

Slow light in saturable absorbers

The velocity of propagation of light in a material system can be controlled and modified to a large extent; extreme values of pulse velocity ($\mathrm{v} \ll \mathrm{c}$, $\mathrm{v} > \mathrm{c}$, and v negative) have been reported [29, 116, 117].

The first demonstration of ultraslow light propagation has been in an ultracold atomic gas [29]; in this work the physical effect of electromagnetically induced transparency (see the paper for references) was used to create a hole in the absorption profile of a gas of sodium atoms. Causality requires that a hole in the absorption profile of a material be accompanied by a swing in the refractive index; a precise relationship between the two quantities is expressed by the Kramers-Kronig relations (reviewed in many places and for example in [33]).

The reason why a large refractive index swing leads to slow light propagation is the following. The usual refractive index n describes the velocity at which the

phase of a monochromatic wave propagates in a medium, which is called the "phase velocity" (v_p). A pulse can be thought of as the sum of many monochromatic waves over a certain frequency band (a "wavepacket" limited to a certain frequency band); it is constituted by a smooth envelope enclosing faster oscillations that vibrate at the central frequency of the wavepacket. The envelope does not travel at the phase velocity but at the so-called "group velocity" (v_g); the corresponding "group index" n_g is defined by

$$n_g\left(\omega_0\right) = \frac{c}{v_g} = n\left(\omega_0\right) + \omega_0\frac{dn\left(\omega_0\right)}{d\omega}. \tag{4.1}$$

where ω_0 is the central frequency of the wavepacket. One can see that if $dn/d\omega$ is large then n_g can be considerably different from n.

An often cited descriptive explanation of why a refractive index swing leads to a wavepacket propagation at the group velocity is the following. The envelope of a pulse is determined by an interference condition between the various frequency components of a wavepacket; we could imagine for example that the peak of the pulse (seen in the spatial domain) is the position at which all the frequency component are in phase and likewise there will be a specific phase relationship between different frequency components for each part of the pulse. The velocity of the pulse is determined, therefore, by the speed with which the condition of given phase relationship travels and not by the speed at which every single phase travels; for example the peak of the pulse will be situated where the monochromatic waves are again in phase, but not

where each of them has a certain specific phase.

Let us put this thought into equations. The phase of a monochromatic wave that propagates in the positive z direction can be written as

$$\phi(\omega) = kz - \omega t = [k_0 + k_1(\omega - \omega_0)]z - \omega t, \tag{4.2}$$

where we have admitted a linear dependence of the wavevector k on the frequency ω. This monochromatic wave travels at a speed $v_p(\omega) = \omega/k = \omega/[k_0 + k_1(\omega - \omega_0)]$ which in general is a function of frequency ω. The phase change $\Delta\phi$ for a time shift Δt and position shift Δz is

$$\Delta\phi = [k_0 + k_1(\omega - \omega_0)]\Delta z - [\omega_0 + (\omega - \omega_0)]\Delta t. \tag{4.3}$$

If we want to preserve the phase relationship between the waves at different frequencies then we need to request that $\Delta\phi$ does not depend on ω. We then find that Δz and Δt must be related by the condition

$$\Delta z = \frac{1}{k_1}\Delta t, \tag{4.4}$$

which defines a group velocity $v_g = 1/k_1$.

The phase change of each monochromatic component at a position at which condition 4.4 is satisfied is given by

$$\Delta\phi = k_0\Delta z - \omega_0\Delta t \qquad (4.5)$$

and is equal to zero if and only if $k_1 = k_0/\omega_0$, so if and only if all of the monochromatic waves propagate at the same speed; so in general the phases themselves will move with respect to the envelope.

To summarize, in the case of linear dispersion that we have used as an example, the envelope resulting from the interference of monochromatic waves propagates in general at a different speed from each of the component waves.

Higher order terms in the dependence of the wavevector on frequency give rise to various kinds of distortions in the pulse profile, the first of which is pulse spreading.

The concept of a refractive index swing associated to a feature in the absorption is represented graphically in panel (b) of Figure 4.1.

The work by Bigelow and colleagues [30] showed the successful application in a solid-state material at room temperature of the very same concept of the link between absorption and dispersion that was first demonstrated in the ultracold gas in [29]. This extension, that used the mechanism of Coherent Population Oscillations (CPO), has been a very important step towards practical applications; other material systems and physical effects that lead to slow light have been found, both based on the dispersive properties of a medium and on the properties of various kind of structures such as ring resonators, maybe coupled to waveguides, and photonic crystals; for a brief review one can refer to [118]; papers that present optical delay based on the

dispersive properties of a medium are for example [119] where slow light is obtained by means of Brillouin scattering and [120] where Raman scattering is used.

Current work aims at optimizing these effects in order to obtain large delays for undistorted output pulses [121, 122].

The potential of slow-light techniques for practical applications has been examined critically in the scientific literature; it is possible theoretically to delay a light pulse by an arbitrary amount [123] but the analyses presented in papers like [124–126] have shown that the conditions to obtain delays large enough to be useful in an applications such as optical buffering are such that electronic buffering is more convenient. More generally Miller showed that there is a limit to the maximum delay that can be obtained by propagation in a one-dimensional structure that depends only on the maximum contrast in dielectric constant in the structure itself irrespective of the method used [127]; more precisely the limit depends only (citing verbatim from the paper) on (a) the largest magnitude $\eta_{\max}$ of relative variation of the dielectric constant in the structure within the frequency range of interest and (b) the length L/λ_c of the structure in wavelengths, with the limiting number of bits of delay (and the delay-bandwidth product) being $\eta_{\max}L/\lambda_c$. At the same time the prospects for using slow-light techniques in other applications such as retiming a signal-carrying pulse in its bit slot remain excellent (for example see [128]), and, interestingly, other, completely different applications have emerged (slow-light interferometry [129, 130] and true-time-delays for beam forming systems [131]).

The work in my thesis has examined critically some aspects of the technique of CPO and investigated some materials that can be useful for its applications on pulses whose duration is in the ps regime.

4.1 Coherent Population Oscillations

Coherent Population Oscillations is an effect that is often studied in the context of the two-level atom [132, 133] but exists in any system in which there is saturation of the absorption.

We can describe this phenomenon referring to a pump-probe configuration. Let us imagine that a constant pump beam with a small superimposed modulation is incident on a saturable absorber; the small intensity modulation creates a modulation of the absorption, which in turn impresses on the pump beam a temporal modulation of the same frequency as that of the probe . The modulation acquired by the pump beam sums itself with the original modulation; the final effect is a decrease of the absorption of the modulated probe and a phase shift of the modulation, that is a delay.

The absorption profile of a probe beam when the CPO mechanism is active is shown in panel (a) of Figure 4.1; in panel (b) of the same figure a close up of the dip in the absorption profile is shown together with the refractive index swing and the corresponding group velocity. In Figure 4.1(b) I have indicated that the width of the absorption hole generated by CPO is equal to $1/T_1$, where T_1 is the recovery time of the saturable absorber; the maximum bandwidth of the modulations that is possible

to slow down with CPO is therefore limited to about $1/T_1$.
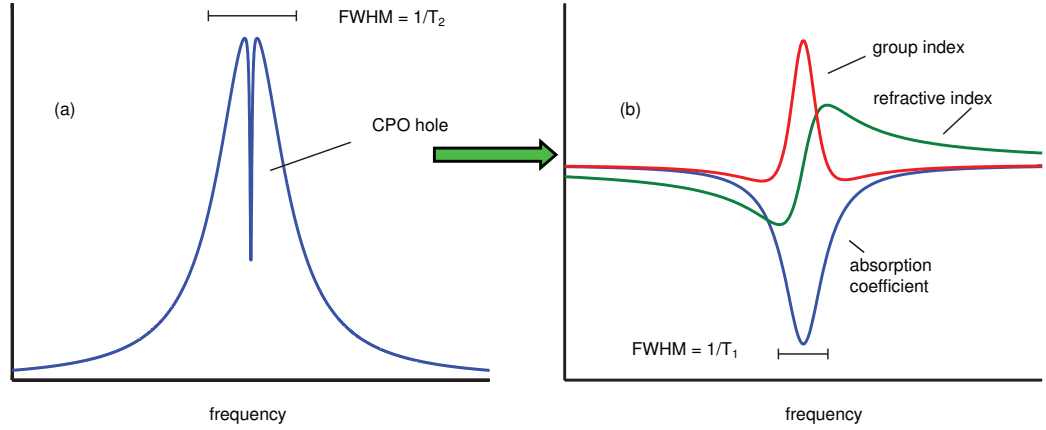
Figure 4.1: (a) schematic representation of an absorption profile with CPO hole (b) close-up of the CPO hole with the associated refractive index swing and the resulting group index.

We can write the modulated intensity as

$$I = I_0 + I_1 \exp\left(-i\delta t\right) + I_{-1} \exp\left(i\delta t\right) \tag{4.6}$$

with δ modulation frequency, and mathematically the effect can be described by an absorption coefficient α and a group refractive index n for the modulated part of the intensity (expanding from [134])

$$\alpha = \frac{\alpha_0}{\frac{I_0}{I_s} + 1} \left(1 - \frac{I_0}{I_s} \frac{\frac{I_0}{I_s} + 1}{(\delta T_1)^2 + \left(\frac{I_0}{I_s} + 1\right)^2} \right) \tag{4.7}$$

$$n_{\text{mod}} = \frac{\alpha_0 c T_1}{\frac{I_0}{I_s} + 1} \frac{I_0}{I_s} \frac{1}{(\delta T_1)^2 + \left(\frac{I_0}{I_s} + 1\right)^2} \tag{4.8}$$

where I_s and T_1 are respectively the saturation intensity and the recovery time of the saturable absorber.

Equations 4.7 and 4.8 can be obtained with two approaches [134]; in one approach one works only with intensities and a rate-equation model, in the other fields are considered; both approaches contribute to clarify some aspects of CPO.

4.1.1 Rate-equations approach to CPO

The rate equation approach uses a model similar to that of one of the early papers on CPO [135]. We assume that the dipole dephasing time T_2 of the material system is much smaller than the ground state recovery time T_1 and the inverse of the Rabi frequency associated with the applied laser fields. In this case, to good approximation we can describe the dynamics of the system through use of a rate equation. We describe the ground state population N by means of the equation

$$\frac{dN}{dt} = -\frac{N\sigma I_{\text{tot}}(t)}{\hbar\omega} + \frac{(\bar{N} - N)}{T_1} \tag{4.9}$$

where $\bar{N}$ is the total density of absorbers and $\hbar\omega$ is the energy of the photons of the laser field. The total intensity of the applied field is given by Equation 4.6. The solution of Equation 4.9 for an intensity of the form of 4.6 is given to lowest order for $I_1 << I_0$ by

$$N(t) = \frac{\bar{N}}{1 + I_0/I_{\text{sat}}} - \left[\frac{\bar{N}}{1 + I_0/I_{\text{sat}}} \left(\frac{I_1/I_{\text{sat}}}{1 + I_0/I_{\text{sat}} - i\delta T_1} \right) e^{-i\delta t} + \text{c.c.} \right] \quad (4.10)$$

where $I_{\text{sat}} = \hbar\omega/\sigma T_1$ is the saturation intensity.

We can now describe the propagation of the optical field according to

$$\frac{d}{dz} I = -\sigma N(t) I(t) \quad (4.11)$$

By extracting from this equation terms with identical time dependencies we see that the unmodulated and modulated portions of the field experience different levels of attenuation. In particular, we see that the unmodulated portion obeys the equation

$$\frac{d}{dz} I_0 = -\alpha_0 I_0 \quad (4.12)$$

where

$$\alpha_0 = \frac{\bar{N}}{1 + I_0/I_{\text{sat}}} \sigma, \quad (4.13)$$

whereas the modulated component obeys

$$\frac{d}{dz} I_1 = \alpha_1 I_1 \quad (4.14)$$

where

$$\alpha_1 = \alpha_0 - \sigma \frac{\bar{N}}{1 + I_0/I_{\text{sat}}} \left(\frac{I_0/I_{\text{sat}}}{1 + I_0/I_{\text{sat}} - i\delta T_1} \right) = \tag{4.15}$$

$$= \alpha_0 - \bar{N}\sigma \left(\frac{I_0/I_{\text{sat}}}{1 + I_0/I_{\text{sat}}} \right) \left(\frac{1 + I_0/I_{\text{sat}} + i\delta T_1}{(1 + I_0/I_{\text{sat}})^2 + (\delta T_1)^2} \right).$$
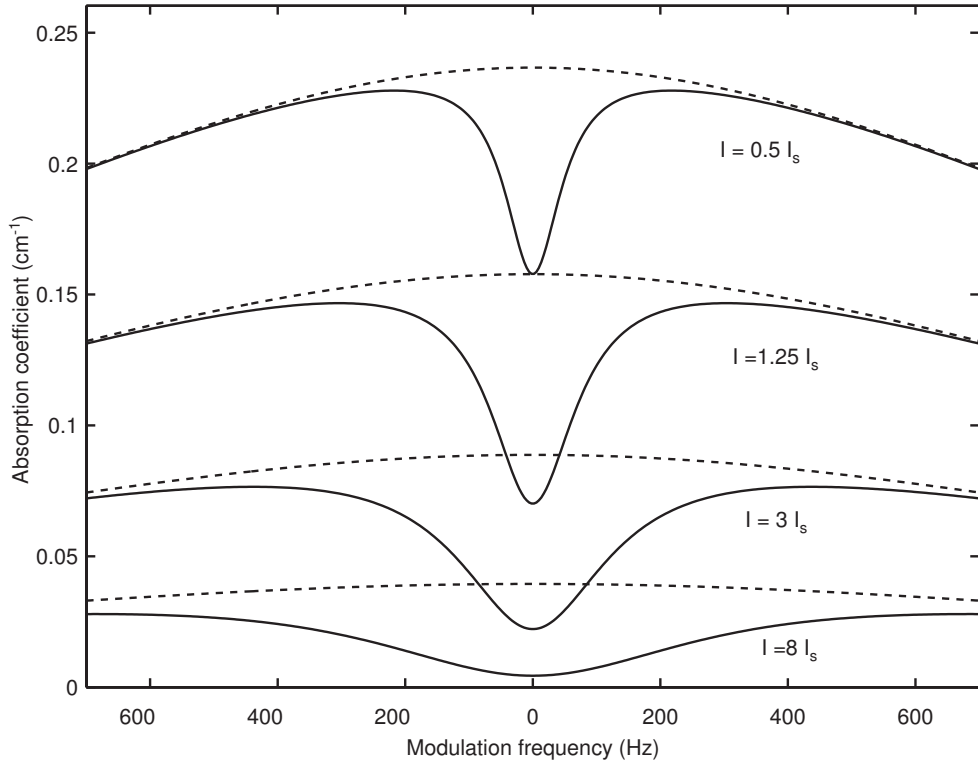
Figure 4.2: CPO holes for various values of pump intensity; for phase modulation there is no CPO hole (dashed lines), the CPO hole is present for amplitude modulation (solid lines).

Note that α_1 is complex. The real part of α_1, which is plotted for various values of the pump intensity in Figure (4.2), describes the attenuation of the modulated portion of the laser field, whereas its imaginary part describes a spatially varying change in

the phase of the modulation. We can describe spatial variation of the phase of the modulation in terms of a group velocity. In a time interval $T = 2\pi/\delta$, the modulated waveform will advance a distance $D = \pi/\alpha_1$. Thus the group velocity $v_g = D/T$ will be given by

$$v_g = \frac{(1 + I_0/I_{\mathrm{sat}})[(1 + I_0/I_{\mathrm{sat}})^2 + (\Delta T_1)^2]}{\bar{N}\sigma T_1(I_0/I_{\mathrm{sat}})}. \tag{4.16}$$

Equations 4.7 for the probe absorption and 4.8 for the modulation index thus descend directly from Equation 4.15.

The fact that slow-light CPO can be explained entirely within the context of a rate-equation model has been noted by other authors [136]. We want here to look at some specific aspects of CPO slow light that are particularly clear when the rate-equations model is used.

The first is that the properties of the laser light enter the model only in terms of the laser intensity. Thus, the spectral width of the light does not enter the model directly, and in particular the spectral width given by phase fluctuations is irrelevant. This explains the apparent contradiction that arises when slow-light effects are observed under conditions in which the line width of the incident laser radiation is much broader than the width of the induced transparency window [136]. For example, in work [30] the effective lifetime for the transition from the ground state to the $^4F_2$ absorption band in ruby is 4.45 ms, but the linewidth of the Ar^+ laser is on the order of 1 GHz.

The other conclusions is that we are indeed dealing with slow light even if the

laser linewidth exceeds the CPO linewidth. A pulse-on-a-background travelling in a saturable absorber is attenuated (Equation 4.7) and delayed (Equation 4.8) but does maintain its shape up to first-order effects.

4.1.2   Density-matrix approach to CPO

The density-matrix approach to CPO has two merits: it allows to treat the case in which pump and probe travel in different directions and shows that when pump and probe do travel in the same direction there are two physical effects that cannot be separated, CPO itself and four-wave mixing.

We start our treatment with non-collinear CPO (Figure 4.3). A good reason to consider the case in which pump and probe do not propagate in the same direction is the following. Absorption of the pump beam limits the maximum delay that can be obtained with the CPO technique. The pump decays more quickly than the probe because it feels only the effect of saturated absorption; as the pump intensity decays the CPO hole and the associated slowing down of the probe disappear. A possible solution to this problem is to replenish the pump; this, for example, could be done more easily if the direction of propagation of the pump and probe are different. Papers that have shown experimentally CPO in a non-collinear configuration are [137] and [138].

The effect can be described by applying the density matrix formalism to a two-level atom; we modify the treatment of [133] to obtain the phase and group velocity
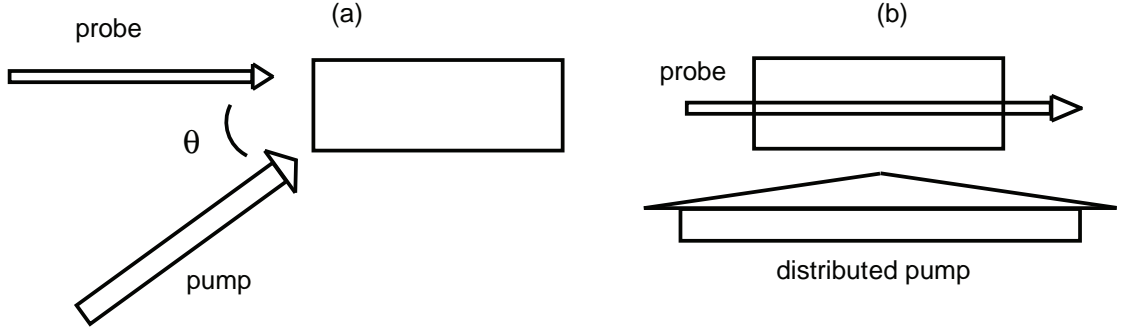
Figure 4.3: (a) non-collinear CPO; (b) distributed pump.

of the probe.

The two-level atom is described by a density matrix ρ_{ij}; $|a\rangle$ is the lower level and $|b\rangle$ is the upper level. The dipole matrix element is $\mu_{ba} = \mu_{ab}^* = \langle b| - ex |a\rangle$, T_1 is the population lifetime and T_2 is the dipole dephasing lifetime; $\bar{N}$ indicates the number density of atoms. The pump and probe fields are denoted respectively as

$$\tilde{E}\left(\tilde{\mathbf{r}}, t\right) = E_j e^{-i\omega_j t} + E_j^* e^{i\omega_j t} \tag{4.17}$$

where

$$E_j = A_j e^{i\tilde{\mathbf{k}}_j \cdot \tilde{\mathbf{r}}} \tag{4.18}$$

and j is equal to *pump* and *probe* respectively for the pump and probe fields. We assume that the pump field is tuned to the atomic resonance ω_{ba}. The frequency difference between the two fields is $\delta = \omega_{probe} - \omega_{pump}$.

When the dephasing width T_2^{-1} is large with respect to both the Rabi frequency

and the beat frequency δ the diagonal term of the density matrix can be expressed

as a function of the inversion as

$$\rho_{ba}(t) \approx -i\frac{\mu_{ba}T_2}{\hbar}\left(E_{pump}e^{-i\omega_{pump}t} + E_{probe}e^{-i\omega_{probe}t}\right)\left[\rho_{bb}(t) - \rho_{aa}(t)\right]. \qquad (4.19)$$

This allows one to obtain a simple formula for the population inversion, which can be

substituted back into Eq. (4.19) to obtain the polarization. We write the inversion as

in ref. [133], but we retain the phase difference between the pump and probe waves

that comes from their different spatial dependence. It is

$$\rho_{bb} - \rho_{aa} \simeq (\rho_{bb} - \rho_{aa})^{(dc)} + (\rho_{bb} - \rho_{aa})^{(\delta)}\,e^{i\delta t} + (\rho_{bb} - \rho_{aa})^{(-\delta)}\,e^{-i\delta t} \qquad (4.20)$$

with

$$(\rho_{bb} - \rho_{aa})^{(dc)} = \frac{(\rho_{bb} - \rho_{aa})^{(0)}}{\beta T_1} \qquad (4.21)$$

$$(\rho_{bb} - \rho_{aa})^{(\delta)} = -\frac{(\rho_{bb} - \rho_{aa})^{(0)}}{T_1}\gamma\frac{1 - i\delta/\beta}{\delta^2 + \beta^2} \qquad (4.22)$$

$$(\rho_{bb} - \rho_{aa})^{(-\delta)} = -\frac{(\rho_{bb} - \rho_{aa})^{(0)}}{T_1}\gamma^*\frac{1 + i\delta/\beta}{\delta^2 + \beta^2}. \qquad (4.23)$$

The quantities β and γ are given by

$$\beta = \frac{1}{T_1} + \frac{4T_2|\mu_{ba}|^2}{\hbar^2}|E_{pump}|^2 \tag{4.24}$$

$$\gamma = \frac{4T_2|\mu_{ba}|^2}{\hbar^2}E_{pump}E_{probe}^*; \tag{4.25}$$

$(\rho_{bb} - \rho_{aa})^{(0)}$ is the equilibrium value of the inversion.

The polarization of the two-level atom medium, $P = \bar{N}\rho_{ba}\mu_{ab}$ contains a term that oscillates at ω_{pump} and a term that oscillates at ω_{probe}:

$$P(\omega_{pump}) = \frac{-i\bar{N}|\mu_{ab}|^2 T_2}{\hbar} \frac{(\rho_{bb} - \rho_{aa})^{(0)}}{1 + \frac{4}{\hbar^2}|\mu_{ab}|^2|E_{pump}|^2 T_1 T_2} E_{pump} \tag{4.26}$$

$$P(\omega_{probe}) = \frac{-i\bar{N}|\mu_{ab}|^2 T_2}{\hbar}(\rho_{bb} - \rho_{aa})^{(0)} \times$$
$$\left[\frac{1}{1 + \frac{4}{\hbar^2}|\mu_{ab}|^2|E_{pump}|^2 T_1 T_2} - \frac{4T_2|\mu_{ba}|^2}{\hbar^2 T_1}|E_{pump}|^2 \frac{1 + i\delta/\beta}{\delta^2 + \beta^2}\right]E_{probe} \tag{4.27}$$

where we have retained only terms that are first order in E_{probe}. The polarization given by Eqs. (4.26) and (4.27) can be substituted in the wave equation

$$-\nabla^2 E + \frac{1}{c^2}\frac{\partial^2 E}{\partial t^2} = -\frac{4\pi}{c^2}\frac{\partial^2 P}{\partial t^2}. \tag{4.28}$$

The wave equation contains components of the polarization that are phase matched

with E_{pump} and E_{probe} respectively and which are functions of the pump wave intensity; E_{pump} and E_{probe} vary slowly along their respective direction of propagation because of these polarization components. It is possible to derive separate equations for E_{pump} and E_{probe}, as described for example in section 7.4 of ref [33]. The equation for E_{pump} shows saturable absorption, while the equation for E_{probe} is

$$\frac{\partial E_{probe}}{\partial z} = \frac{2\pi\omega}{c} \left(\frac{\bar{N} \left| \mu_{ba} \right|^2 T_2}{\hbar} \right) (\rho_{bb} - \rho_{aa})^{(0)} \times$$

$$\left[\frac{1}{1 + \frac{4}{\hbar^2} \left| \mu_{ab} \right|^2 \left| E_{pump} \right|^2 T_1 T_2} - \frac{4T_2 \left| \mu_{ba} \right|^2}{\hbar^2 T_1} \left| E_{pump} \right|^2 \frac{1 + i\delta/\beta}{\delta^2 + \beta^2} \right] E_{probe}. \quad (4.29)$$

In Eq. (4.29) we recognize the saturation of the absorption due to the pump wave and the population oscillations. The phase delay due to population oscillations leads to a group velocity for a probe wave whose intensity is modulated at a frequency 2δ given, in the approximation $v_g << c$, by

$$v_g = \frac{2 \left(1 + I_{pump}/I_{sat} \right) \left[\left(1 + I_{pump}/I_{sat} \right)^2 + (\delta T_1)^2 \right]}{\bar{N} \sigma T_1 \left(I_{pump}/I_{sat} \right)}. \quad (4.30)$$

In order to obtain expression (4.30) we have recognized the cross section $\sigma = (4\pi\omega/c) \left(\left| \mu_{ba} \right|^2 T_2/\hbar \right)$ and the ratio between the pump intensity and saturation intensity $I_{pump}/I_{sat} = \left(4 \left| \mu_{ab} \right| \left| E_{pump} \right|^2 / \hbar^2 \right) T_1 T_2$ in Eq. (4.29) and we have set $(\rho_{bb} - \rho_{aa})^{(0)} = -1$.

Comparing Equations 4.30 and 4.16 we note that in the case of noncollinear propagation the probe is twice faster than in the case of collinear propagation. The reason is that in the case of collinear propagation the contribution of four-wave mixing (4WM)

cannot be separated from the contribution of CPO, while the two effects are distinct in the case of noncollinear propagation. More precisely the wave-vector of the CPO component of the nonlinear polarization is $\mathbf{k}_{\text{CPO}} = \mathbf{k}_{pump} - \mathbf{k}_{pump} + \mathbf{k}_{probe} = \mathbf{k}_{probe}$ (always) while the wave-vector of the 4WM component is $\mathbf{k}_{4\text{WM}} = 2\mathbf{k}_{pump} - \mathbf{k}_{probe}$ which is in the same direction as $\mathbf{k}_{probe}$ only for collinear propagation. If pump and probe are co-propagating the 4WM term contributes to the modulation velocity in two ways: it contributes to the modulation itself and it affects the propagation of the probe.

The situation can be analyzed mathematically starting from Equation 4.28 and inserting in the nonlinear polarization P both the CPO and the 4WM terms. A straightforward way to do this is realizing that the Equations for the population inversion obtained applying the rate equation approximation in the density matrix formalism (equation (3c) of [133])

$$\dot{\rho}_{bb} - \dot{\rho}_{aa} = (-1/T_1) \left[\rho_{bb} - \rho_{aa} - (\rho_{bb} - \rho_{aa})^0 \right] + 2i\hbar^{-1} \left(V_{ab}\rho_{ba} - \rho_{ab}V_{ba} \right) \quad (4.31)$$

and Equation 4.9 are the same equation; in verifying that the two equations are identical one is helped by the identifications

$$\frac{I}{I_s} = \Omega^2 T_1 T_2 \quad (4.32)$$

where Ω is the Rabi frequency defined by

$$\Omega = \frac{2\,|\mu_{ab}|\,|E|}{\hbar} \tag{4.33}$$

and

$$I_s = \hbar\omega/(2\sigma T_1). \tag{4.34}$$

Equation 4.9 has already been solved for a modulated optical intensity and the solution is Equation 4.10.

If the electric field is expressed by

$$E = (A_0 + A_1 \exp\left(-i\delta t\right) + A_{-1} \exp\left(i\delta t\right)) \exp\left(-i\omega_0 t\right) \tag{4.35}$$

where A_i are the slowly varying amplitudes then the corresponding modulated intensity is

$$I = \frac{c}{2\pi} \left[|A_0|^2 + \left(A_0^* A_1 + A_0 A_{-1}^*\right) \exp\left(-i\delta t\right) + (A_0 A_1^* + A_0^* A_{-1}) \exp\left(i\delta t\right)\right] =$$

$$= I_0 + I_1 \exp\left(-i\delta t\right) + I_{-1} \exp\left(i\delta t\right). \tag{4.36}$$

The wave equation in the slowly varying amplitude approximation can be written as

$$\frac{\partial A}{\partial z} = \frac{\sigma}{2} A \left(\bar{N} - 2N \right),$$ (4.37)

because the rate equation approximation permits to calculate the atomic coherence ρ_{ba} as a function of the inversion $\rho_{bb} - \rho_{aa}$.

Form 4.37 permits one to use immediately the solution 4.10 for the population and obtain separate equations for each slowly varying amplitude:

$$
\begin{aligned}
\frac{\partial A_0}{\partial z} &= \frac{\sigma}{2} A_0 \left(\bar{N} - 2N_0 \right) \\
\frac{\partial A_1}{\partial z} &= \frac{\sigma}{2} A_1 \left(\bar{N} - 2N_0 \right) - \sigma A_0 N_1 \\
\frac{\partial A_{-1}}{\partial z} &= \frac{\sigma}{2} A_{-1} \left(\bar{N} - 2N_0 \right) - \sigma A_0 N_{-1}.
\end{aligned}
$$ (4.38)

We can write down explicitly the equation for A_1. We have

$$\frac{\sigma}{2} A_1 \left(\bar{N} - 2N_0 \right) = -\frac{1}{2} \frac{\sigma \bar{N}}{1 + \frac{I_0}{I_s}} A_1 = -\frac{1}{2} \frac{\alpha_0}{1 + \frac{I_0}{I_s}} A_1$$ (4.39)

and

$$-\sigma A_0 N_1 = \sigma A_0 \frac{I_1}{2I_s} \frac{\bar{N}}{1+\frac{I_0}{I_s}} \frac{\frac{I_0}{I_s}+1+i\delta T_1}{(\delta T_1)^2 + \left(\frac{I_0}{I_s}+1\right)^2} \tag{4.40}$$

$$= \sigma A_0 \frac{c}{2\pi} \frac{\left(A_0^* A_1 + A_0 A_{-1}^*\right)}{I_s} \frac{\bar{N}}{1+\frac{I_0}{I_s}} \frac{\frac{I_0}{I_s}+1+i\delta T_1}{(\delta T_1)^2 + \left(\frac{I_0}{I_s}+1\right)^2}$$

$$= \frac{\alpha_0}{2} \frac{1}{\frac{I_0}{I_s}+1} \left(\frac{I_0 A_1}{I_s} + \frac{c}{2\pi} \frac{A_0^2 A_{-1}^*}{I_s}\right) \frac{\frac{I_0}{I_s}+1+i\delta T_1}{(\delta T_1)^2 + \left(\frac{I_0}{I_s}+1\right)^2}$$

where we have used $\sigma \bar{N} = \alpha_0$. We recognize in equation (4.39) saturated absorption and in equation (4.40) the effects of CPO and 4WM. In order to calculate how an intensity modulation will propagate the 4WM term cannot be taken out of the equation because even if the second sideband is not present in the input fields it will always develop during propagation. To see this explicitly at this we derive the equation for the propagation of an intensity modulation starting from the equations for the amplitudes. It is

$$\begin{aligned}
\frac{\partial I_1}{\partial z} &= \frac{c}{2\pi} \frac{\partial}{\partial z} \left(A_1 A_0^* + A_{-1}^* A_0\right) \tag{4.41}\\
&= \frac{c}{2\pi} \frac{\partial A_1}{\partial z} A_0^* + A_1 \frac{\partial A_0^*}{\partial z} + \frac{\partial A_{-1}^*}{\partial z} A_0 + A_{-1}^* \frac{\partial A_0}{\partial z}\\
&= \sigma I_1 \left(\bar{N} - 2N_0\right) - 2\sigma N_1 I_0\\
&= -\frac{\alpha_0}{\frac{I_0}{I_s}+1} I_1 + \frac{\alpha_0}{\frac{I_0}{I_s}+1} \frac{I_0}{I_s} \frac{\frac{I_0}{I_s}+1+i\delta T_1}{(\delta T_1)^2 + \left(\frac{I_0}{I_s}+1\right)^2} I_1
\end{aligned}$$

(recalling that $N_{-1}^* = N_1$). We have recovered (as we should) Equation 4.14 closing in this way the link between the rate equations and the density matrix treatments of CPO and clarifying the reason of the different group velocity of the modulation in the two cases.

4.2   Quantum dots as ultrafast saturable absorbers

As an application of the concepts of the previous section I have, together with Aaron Schweinsberg, used quantum dots to slow down the propagation of infrared pulses of ps duration. From the discussion in the previous section follows that they key parameter in determining the maximum bandwidth of the modulation that can be slowed down by a given material is given by the inverse of its recovery time; additional conditions are that the saturation intensity should be low and that the non-saturable losses should be low.

Several papers have shown light modulated at GHz frequencies slowed down by CPO [137,139–142]; material systems used included semiconductor quantum wells and a quantum dot optical amplifier. Selecting an appropriate material for this demonstration has been made easier by the fact that recovery time and saturation intensity are crucial parameters for the saturable absorbers that are used to mode-lock ultrafast lasers and therefore a vast literature can guide research on the topic. The aim was to slow down the pulses emitted by the EKSPLA ps OPA that was also used in the experiments with the gold nanoparticles, which have a duration of around 25 ps

(the duration varies as a function of wavelength). Normally grown semiconductors are unsuitable because they have two recombination times [143], one in the tens to hundred of femtoseconds (intraband thermalization) and one in the nanosecond range (recombination) while we are interested in recovery times around 10 ps. Better materials are low-temperature grown semiconductors [144, 145], quantum wells (QWs) and quantum dots (QDs) (a book which presents QWs and QDs and their optical properties is [15]).

The selection has been made even easier considering that the mode-locker used in the EKSPLA ps laser is a glass with quantum dots embedded into it. A discussion of saturable absorption in a similar system appears in [146]; the recovery time that these authors have measured is in the order of tens of ps. For our study we acquired PbS QDs produced by Evident Technologies ("Snake Eyes NIR") suspended in toluene and with an absorption peak centered at 795 nm. Figure 4.4 shows the absorption spectrum of a 1 cm thick sample.
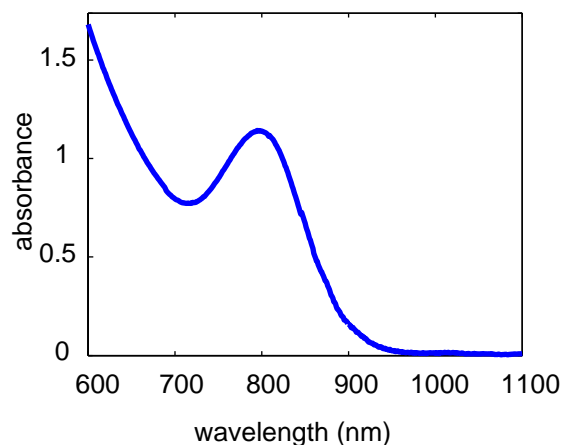

Figure 4.4: Absorption spectrum of the PbS quantum dots.

We found the saturation fluence of the QDs for our pulses to be on the order of $4 \, \mathrm{mJ/cm^2}$, and that for higher fluences the material shows induced absorption. CPO is a pump-probe effect but the dynamics of the collinear pump-probe configuration can be realized with a single pulse experiment; the delay of a single pulse through the material as a function of the pulse energy is related to the saturation intensity and tests whether the recovery time is well matched to the pulse duration.

Measuring the delay of 25 ps pulses with low repetition rate can be accomplished only with a cross-correlation experiment. Electronics is too slow to be able to record a time-resolved trace of the optical pulse (with the exception of extremely expensive streak cameras or sampling oscilloscopes). On the other hand the technique of spectral interferometry utilized in [147] is not suitable in our case because the spectrum of our pulses (< 0.5nm FWHM) cannot be resolved with the spectrometers available in our laboratory.

The delay experiment consists therefore in placing the 1 cm thick QD sample in one arm of an intensity autocorrelator and taking autocorrelation (or better, cross-correlation) traces of pulses of different energies.

Figure 4.5 shows a cross-correlation scan at low intensity, in which there are no nonlinear effects, and a scan at an energy that corresponds to the saturation fluence. The comparison between the two scans shows that the high energy pulse is delayed by 2.8 ps and broadened with respect to the low energy pulse. The delay (10 % of the pulse FWHM) is in good agreement with the model of Selden [148] for a saturation

recovery time of 30 ps.

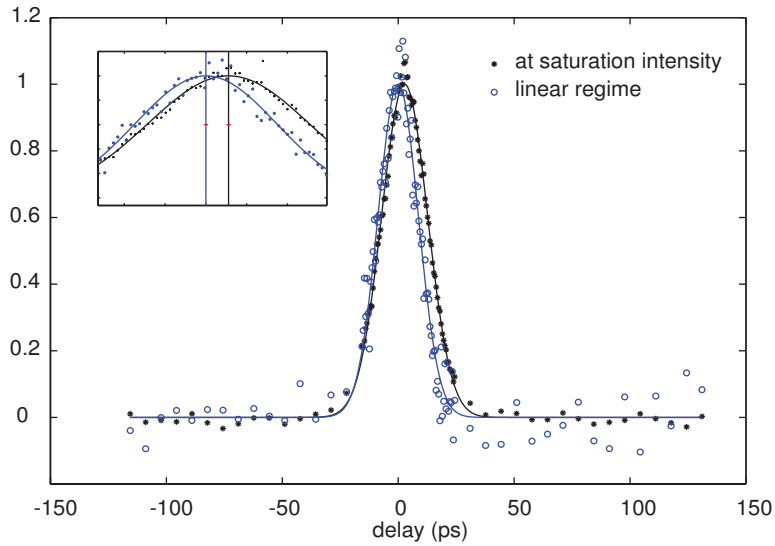Figure 4.5: Autocorrelation trace of two pulses that have travelled through a PbS QD sample.

This work could be extended to different wavelengths by selecting quantum dots of different size and composition; for example PbS dots can be made to absorb at 1500 nm. Moreover the quantum dots can be embedded in a solid matrix, as it is done in the paper by Dementjev et al. [146] to build a solid-state device.

Chapter 5

Conclusions

In this thesis I have presented the results of measurements of nonlinear absorption on composite materials constituted by a collection of gold nanoparticles dispersed into silica and a demonstration of slow propagation of ps pulses using the mechanism of coherent population oscillations.

Combining gold with glass produces a "composite material" whose properties are remarkably different from the properties of either gold or glass. In particular at certain frequencies the material presents enhanced attenuation that is accompanied by a large concentration of the electric field in the metallic component. This phenomenon is called "plasmon resonance"; it is connected to the bulk plasma oscillations; in the case of metal nanoparticles the free electrons in the metal oscillate in unison and these oscillations are coupled to travelling electromagnetic waves.

The large field concentration in the metal component leads to the enhancement

of the nonlinear optical properties of the composite with respect to the properties of pure metal (whose nonlinearity is much larger than that of glass).

I have measured, using the open-aperture z-scan technique, the nonlinear absorption coefficient β in a large range of compositions (gold volume fraction ranging from 0.05 to 0.55) for samples prepared with the technique of magnetron co-sputtering and for wavelengths around the plasmon resonance which for gold is situated at 532 nm. I have also measured (always with the open-aperture z-scan) the nonlinear absorption coefficient of two samples prepared with the technique of laser ablation.

The sample prepared by sputtering is a saturable absorber at all fill fractions and at all wavelengths for which I have performed measurements. This behaviour must be compared and contrasted to the one of pure gold that at the same wavelengths is an optical limiter.

The effective third-order nonlinear susceptibility of the composite material, at least when the gold content is low, can be expressed in the frame of an effective-medium theory, first derived for the linear case by J. C. Maxwell Garnett in 1904. Using this theory the apparent paradox that mixing gold and glass, both of which are optical limiters, gives as a result a saturable absorber, is explained as a consequence of local field effects. I have shown that the same equations of the same theory can be interpreted in another way and more precisely the saturable absorption can be seen as an effect of plasmon damping.

A modified version of the Maxwell Garnett theory that takes into account the

geometry of the composite fits the data at low gold concentration very well. The interpretation of the effective nonlinearity as a consequence of plasmon damping is valid beyond the range of validity of the Maxwell Garnett theory.

The samples prepared with laser ablation are optical limiters at a wavelength of 532 nm. Since this wavelength falls off the plasmon resonance of these samples this fact is not in contradiction with the theory that explains saturable absorption of the other kind of samples.

Another part of my thesis has dealt with the use of fast saturable absorbers for slowing down the propagation of pulses of ps duration.

The technique of coherent population oscillations can be applied to slow down optical pulses in a pump-probe configuration. A pulse can be efficiently slowed down with this technique if its duration is of the order of the recovery time of the saturable absorber in which the population oscillations take place.

It is therefore necessary to find, for slowing down a pulse that is approximately 20 ps long, a saturable absorber with a recovery time of approximately 20 ps; PbS quantum dots possess approximately this recovery time.

As a demonstration I, working together with Aaron Schweinsberg, delayed a single strong 28-ps long pulse (without the use of a pump) by 10% of its FWHM. The experiment is not strictly a demonstration of CPO but tests the nonlinear response of the quantum dots system in such a way that the success of a pump-probe CPO experiment is guaranteed.

I have also clarified some theoretical aspects of CPO, in particular questions linked to the effect of the additional bandwidth imparted to laser light by phase fluctuations.

The future of these topics and the perspective for future research as I see them are the following.

Mixed metal-dielectric materials will have a mixed success. The main difficulty for nanoparticle systems with high metal content is that they are extremely susceptible to optical damage, and it will be necessary to find a way around this problem in order to use them in practical applications. But, for example, there are wavelength ranges at the side of the plasmon resonance in which these materials should have a strong refractive nonlinearity without the full at-resonance absorption and these are worth investigating in my opinion. Layered composites have already proven to be superior to nanoparticle systems from this point of view and one should try to make a practical device based on them. Moreover the nonlinear optical effects connected with the percolation threshold have not yet been fully investigated experimentally and they should provide an interesting challenge to physicists.

The mechanism of Coherent Population Oscillations has played a key role in the development of research in the field of slow light. At the moment it seems to me that other physical effects and mechanisms are better suited for practical applications; of course I could be proved wrong.

Bibliography

[1] B. R. Masters. *Handbook of Biomedical Nonlinear Optical Microscopy.* Oxford University Press.

[2] C. Rulliere, editor. *Femtosecond Laser Pulses: Principles and Experiments.* Springer, 2nd edition, 2004.

[3] V. G. Dmitriev, G. G. Gurzadyan, and D. N. Nikogosyan. *Handbook of Nonlinear Optical Crystals.* Springer Series in Optical Sciences. Springer, 3rd rev. edition, 1999.

[4] L. Li and J. T. Fourkas. Multiphoton polymerization. *Materials Today*, 10:30–37, 2007.

[5] R. W. Boyd and S. J. Bentley. Recent progress in quantum and nonlinear optical lithography. *Journal of Modern Optics*, 53:713718, 2006.

[6] G. S. He, L.-S. Tan, Q. Zheng, and P. N. Prasad. Multiphoton absorbing materials: Molecular designs, characterizations, and applications. *Chemical Review*, 108:1245–1330, 2008.

[7] J. A. Miragliotta. Analytical and device-related applications of nonlinear optics. *Johns Hopkins APL Technical Digest*, 16(4):348–357, 1995.

[8] J. E. Midwinter, editor. *Photonics in Switching.* Quantum Electronics - Principles and Applications. Academic Press, 1993.

[9] G. P. Agrawal. *Applications of Nonlinear Fiber Optics.* Optics and Photonics Series. Academic Press, 2001.

[10] G. P. Agrawal. *Lightwave technology - components and devices.* Wiley-Interscience, 2004.

[11] A. Shacham, K. Bergman, and L. P. Carloni. The case for low-power photonic networks-on-chip. In *Proceedings of Design Automation Conference*, 2007.

[12] A. Sugar. Ultrafast (femtosecond) laser refractive surgery. *Current Opinion in Ophthalmology*, 13:246–249, 2002.

[13] D. Cotter, R. J. Manning, K. J. Blow, A. D. Ellis, A. E. Kelly, D. Nesset, I. D. Phillips, A. J. Pustie, and D. C. Rogers. Nonlinear optics for high-speed digital information processing. *Science*, 286:1523–1527, 1999.

[14] H. Singh Nalwa and S. Miyata, editors. *Nonlinear Optics of Organic Molecules and Polymers*. CRC Press, 1997.

[15] N. Peyghambarian, S. W. Koch, and A. Mysyrowicz. *Introduction to semiconductor optics*. Prentice Hall Series in Solid State Physical Electronics. Prentice Hall, 1993.

[16] V. G. Taeed, N. J. Baker, L. Fu, K. Finsterbusch, M. R. E. Lamont, D. J. Moss, H. C. Nguyen, B. J. Eggleton, D. Y. Choi, S. Madden, and B. Luther-Davies. Ultrafast all-optical chalcogenide glass photonic circuits. *Optics Express*, 15:9205–9221, 2007.

[17] M. Soljačić and J. D. Joannopoulos. Enhancement of nonlinear effects using photonic crystals. *Nature Materials*, 3:211–219, 2004.

[18] J. García, P. Sanchis, A. Martínez, and J. Martí. 1d periodic structures for slow-wave induced non-linearity enhancement. *Optics Express*, 16:3146–3160, 2008.

[19] J. Heebner, R. Grover, and T. Ibrahim. *Optical Microresonators: Theory, Fabrication, and Applications*. Springer Series in Optical Sciences. Springer, 1st edition, 2007.

[20] T. Tokizaki, A. Nakamura, S. Kaneko, K. Uchida, S. Omi, H. Tanji, and Y. Asaharaaj. Subpicosecond time response of third-order optical nonlinearity of small copper particles in glass. *Applied Physcs Letters*, 65:941–943, 1994.

[21] V. M. Shalaev. *Nonlinear Optics of Random Media*. Springer-Verlag, 2000.

[22] R. S. Bennink, Y.-K. Yoon, and R. W. Boyd. Accessing the optical nonlinearity of metals with metal-dielectric photonic bandgap structures. *Optics Letters*, 24(20):1416–1418, 1999.

[23] D. L. Feldheim and C. A. Foss Jr. editors. *Metal Nanoparticles - Synthesis, Characterization, and Applications*. Marcell Dekker, 2002.

[24] L. A. Lyon, M. D. Musick, and M. J. Natan. Colloidal au-enhanced surface plasmon resonance immunosensing. *Analytical Chemistry*, 70:5177–5183, 1998.

[25] P. Fortina, L. J. Kricka, D. J. Graves, J. Park, T. Hyslop, F. Tam, N. Halas, S. Surrey, and S. A. Waldman. Applications of nanoparticles to diagnostics and therapeutics in colorectal cancer. *Trends in Biotechnology*, 25:145–152, 2007.

[26] D. Ricard, P. Roussignol, and C. Flytzanis. Surface-mediated enhancement of optical phase conjugation in metal colloids. *Optics Letters*, 10(10):511–513, 1985.

[27] C. Min, P. Wang, C. Chen, Y. Deng, Y. Lu, H. Ming, T. Ning,Y. Zhouand, and G. Yang. All-optical switching in subwavelength metallic grating structure containing nonlinear optical materials. *Optics Letter*, 33:869–871, 2008.

[28] R. W. Boyd and D. J. Gauthier. "slow" and "fast" light. *Progress In Optics, Volume 43*, 43:497–530, 2002.

[29] L. V. Hau, S. E. Harris, Z. Dutton, and C. H. Behroozi. Light speed reduction to 17 metres per second in an ultracold atomic gas. *Nature*, 397:594–598, 1999.

[30] M. S. Bigelow, N. N. Lepeshkin, and R. W. Boyd. Observation of ultraslow light propagation in a ruby crystal at room temperature. *Physical Review Letters*, 90(11):113903, 2003.

[31] D. D. Smith, G. Fischer, R. W. Boyd, and D. A. Gregory. Cancellation of photoinduced absorption in metal nanoparticle composites through a counterintuitive consequence of local field effects. *Journal of the Optical Society of America B*, 14(7):1625–1631, 1997.

[32] D. D. Smith, Y. Yoon, R. W. Boyd, J. K. Campbell, L. A. Baker, R. M. Crooks, and M. George. z-scan measurement of the nonlinear absorption of a thin gold film. *Journal of Applied Physics*, 86(11):6200–6205, 1999.

[33] R. W. Boyd. *Nonlinear Optics*. Academic Press, second edition, 2003.

[34] R. J. Gehr and R. W. Boyd. Optical properties of nanostructured optical materials. *Chemistry of Materials*, 8(8):1807–1819, 1996.

[35] Z. Hashin and S. Shtrikman. A variational approach to the theory of the effective magnetic permeability of multiphase materials. *Journal of Applied Physics*, 33(10):3125–3131, 1962.

[36] D. J. Bergman. Variational bounds on some bulk properties of a two-phase composite material. *Physical Review B*, 14(4):1531–1542, 1976.

[37] G. W. Milton. Bounds on the complex dielectric constant of a composite material. *Applied Physics Letters*, 37(3):300–302, 1980.

[38] D. J. Bergman. Exactly solvable microscopic geometries and rigorous bounds for the complex dielectric constant of a two-component composite material. *Physical Review Letters*, 44(19):1285–1287, 1980.

[39] J. C. Maxwell Garnett. Colours in metal glasses and in metallic films. *Philosophical Transactions of the Royal Society of London. Series A, Containing Papers of a Mathematical or Physical Character*, 203:385–420, 1904.

[40] D. A. G. Bruggeman. Berechnung verschieder physikalischer Konstanten von heterogenen Substanzen I. Dielektrizitätskonstanten und Leitfähigkeiten der Mischkörper aus isotropen Substanzen. *Annalen der Physik (Leipzig)*, 24:636, 1935.

[41] R. Landauer. The electrical resistance of binary metallic mixtures. *Journal of Applied Physics*, 23(7):779–784, 1952.

[42] D. L. Turcotte. *Fractals and Chaos in Geology and Geophysics.* Cambridge University Press, 2nd edition, 1997.

[43] P. Sheng. Pair-cluster theory for the dielectric constant of composite media. *Physical Review B*, 22(12):6364–6368, 1980.

[44] P. Sheng. Theory for the dielectric function of granular composite media. *Physical Review Letters*, 45(1):60–63, 1980.

[45] V. M. Shalaev and A. K. Sarychev. Nonlinear optics of random metal-dielectric films. *Physical Review B*, 57(20):13265–13288, 1998.

[46] P. J. Reynolds, W. Klein, and H. E. Stanley. A real-space renormalization group for site and bond percolation. *Journal of Physics C: Solid State Physics*, 10:L167–L172, J. Phys. C: Solid State Phys., Vol. 10, 1977.

[47] A. K. Sarychev. Scaling invariance and percolation in a random field. *Zhurnal Eksperimentalnoi i teoreticheskoi fiziki*, 72(3):1001–1004, 1977.

[48] P. Gadenne and J. C. Rivoal. *Surface-Plasmon-Enhanced Nonlinearities in Percolating 2-D Metal-Dielectric Films: Calculation of the Localized Giant Field and Their Observation in SNOM*, volume 82 of *Topics in Applied Physics*, pages 185–215. Springer-Verlag, 2002.

[49] K. Seal, M. A. Nelson, Z. C. Ying, D. A. Genov, and D. A. Sarychev and V. M. Shalaev. Growth, morphology, and optical and electrical properties of semicontinuous gold films. *Physical Review B*, 67:035318, 2003.

[50] R. W. Boyd and J. E. Sipe. Nonlinear optical susceptibilities of layered composite materials. *Journal of the Optical Society of America B*, 11:297–303, 1994.

[51] G. L. Fischer, R. W. Boyd, R. J. Gehr, S. A. Jenekhe, J. A. Osaheni, J. E. Sipe, and L. A. Weller-Brophy. Enhanced nonlinear optical response of composite materials. *Phys. Rev. Lett.*, 74:1871 – 1874, 1995.

[52] N. N. Lepeshkin, A. Schweinsberg, G. Piredda, R. S. Bennink, and R. W. Boyd. Enhanced nonlinear optical response of one-dimensional metal-dielectric photonic crystals. *Physical Review Letters*, 93(12):123092, 2004.

[53] N. W. Ashcroft and N. D. Mermin. *Solid State Physics*. Harcourt College Publishers, 1976.

[54] M. Born and E. Wolf. *Principles of Optics*. Cambridge University Press, 6th (with corrections) edition, 1980.

[55] P B. Johnson and R. W. Christy. Optical constants of the noble metals. *Physical Review B*, 6(12):4370–4379, 1972.

[56] C. Kittel. *Introduction to Solid State Physics*. Wiley, 7th edition, 1996.

[57] H. Raether. *Surface plasmons on smooth and rough surfaces and on gratings*, volume 111 of *Springer tracts in modern physics*. Springer-Verlag, 1987.

[58] J. M. Pitarke, V. M. Silkin, E. V. Chulkov, and P. M. Echenique. Surface plasmons in metallic structures. *Journal of Optics A: Pure and Applied Optics*.

[59] F. Hache, D. Ricard, C. Flytzanis, and U. Kreibig. The optical kerr effect in small metal particles and metal colloids. *Applied Physics A*, 47:347–357, 1988.

[60] F. Hache, D. Ricard, and C. Flytzanis. Optical nonlinearities of small metal particles: surface-mediated resonance and quantum size effects. *Journal of the Optical Society of America B*, 3(12):1647–1655, 1986.

[61] M. Perner, P. Bost, U. Lemmer, G. von Plessen, J. Feldmann, U. Becker, M. Mennig, M. Schmitt, and H. Schmidt. Optically induced damping of the surface plasmon resonance in gold colloids. *Physical Review Letters*, 78(11):2192–2195, 1997.

[62] R. Rosei. Temperature modulation of the optical transitions involving the fermi surface in ag: Theory. *Physical Review B*, 10(2):474–483, 1974.

[63] R. Rosei, C. H. Culp, and J. H. Weaver. Temperature modulation of the optical transitions involving the fermi surface in ag: Experimental. *Physical Review B*, 10(2):484–489, 1974.

[64] R. Rosei and D. W. Lynch. Thermomodulation spectra of al, au, and cu. *Physical Review B*, 5(10):3883–3894, 1972.

[65] G. L. Eesley. Generation of nonequilibrium electron and lattice temperatures in copper by picosecond laser pulses. *Physical Review B*, 33(4):2144–2151, 1986.

[66] H. E. Elsayed-Ali, T. B. Norris, M. A. Pessot, and G.A. Mourou. Time-resolved observation of electron-phonon relaxation in copper. *Physical Review Letters*, 58(12):1212–1215, 1987.

[67] S. D. Brorson, J. G. Fujimoto, and E. P. Ippen. Femtosecond electronic heat-transport dynamics in thin gold films. *Physical Review Letters*, 59(17):1962–1965, 1987.

[68] C.-K. Sun, F. Valle, L. Acioli, E. P. Ippen, and J. G. Fujimoto. Femtosecond investigation of electron thermalization in gold. *Physical Review B*, 48(16):12365–12368, 1993.

[69] C.-K. Sun, F. Valle, L. H. Acioli, E. P. Ippen, and J. G. Fujimoto. Femtosecond-tunable measurement of electron thermalization in gold. *Physical Review B*, 50:15337–15348, 1994.

[70] H. Inouye, K. Tanaka, I. Tanahashi, and K. Hirao. Ultrafast dynamics of nonequilibrium electrons in a gold nanoparticle system. *Physical Review B*, 57:11334–11340, 1998.

[71] A. Sihvola. *Electromagnetic mixing formulas and applications*. IEE Electromagnetic Waves Series. The Institution of Electrical Engineers, 1999.

[72] D. E. Aspnes. Local-field effects and effective-medium theory: A microscopic perspective. *American Journal of Physics*, 50(8):704–709, 1982.

[73] G. A. Niklasson, C. G. Granqvist, and O. Hunderi. Effective medium models for the optical properties of inhomogeneous materials. *Applied Optics*, 20(1):26–30, 1981.

[74] G. B. Smith. Dielectric constants for mixed media. *Journal of Physics D: Applied Physics*, 10:L39–L42, 1977.

[75] G. B. Smith. The scope of effective medium theory for fine metal particle solar absorbers. *Applied Physics Letters*, 35(9):668–670, 1979.

[76] P. Mallet, C. A. Guérin, and A. Sentenac. Maxwell-garnett mixing rule in the presence of multiple scattering: Derivation and accuracy. *Physical Review B*, 72:014205, 2005.

[77] R. H. Doremus. Optical properties of small gold particles. *Journal of Chemical Physics*, 40:2389–2396, 1964.

[78] R. H. Doremus. Optics properties of small silver particles. *Journal of Chemical Physics*, 42:414–417, 1965.

[79] C. F. Bohren and D. R. Huffman. *Absorption and Scattering of Light by Small Particles*. Wiley-VCH, 2004.

[80] R. H. Doremus. Optical properties of thin metallic films in island form. *Journal of Applied Physics*, 37:2775–2781, 1966.

[81] C. G. Granqvist and O. Hunderi. Optical properties of ultrafine gold particles. *Physical Review B*, 16:3513–3534, 1977.

[82] R. W. Cohen, G. D. Cody, M. D. Coutts, and B. Abeles. Optical properties of granular silver and gold films. *Physical Review B*, 8(8):3689–3701, 1973.

[83] S. Cho, H. Limb, K.S. Lee, T.S. Lee, B. Cheong, W.M. Kim, and S. Leea. Spectro-ellipsometric studies of Au/SiO$_2$ nanocomposite films. *Thin Solid Films*, 475:133–138, 2005.

[84] B. Abeles and J. I. Gittleman. Composite material films: optical properties and applications. *Applied Optics*, 15:2328–2332, 1976.

[85] K. Kneipp, M. Moskovits, and H. Kneipp, editors. *Surface-enhanced raman scattering : physics and applications*. Springer, 2006.

[86] R. L. Sutherland. *Handbook of Nonlinear Optics*. Marcel Dekker, Inc., 1996.

[87] J. E. Sipe and R. W. Boyd. Nonlinear susceptibility of composite optical materials in the maxwell garnett model. *Physical Review A*, 46(3):1614–1629, 1992.

[88] L. Yang, K. Becker, F. M. Smith, R. H. Magruder III, Jr. R. F. Haglund, L. Yang, R. Dorsinville, R. R. Alfano, and R. A. Zuhr. Size dependence of the third-order susceptibility of copper nanoclusters investigated by four-wave mixing. *Journal of the Optical Society of America B*, 11(3):457–461, 1994.

[89] K. Uchida, S. Kaneko, S. Omi, C. Hata, H. Tanji, Y. Asahara, A. J. Ikushima, T. Tokizaki, and A. Nakamura. Optical nonlinearities of a high concentration of small metal particles dispersed in glass: copper and silver particles. *Journal of the Optical Society of America B*, 11(7):1236–1243, 1994.

[90] J. M. Ballesteros, J. Solis, R. Serna, and C. N. Afonso. Nanocrystal size dependence of the third-order nonlinear optical response of $Cu : Al_2O_3$ thin films. *Applied Physics Letters*, 74:2791–2793, 1999.

[91] V. Halt, J. Guille, J.-C. Merle, I. Perakis, and J.-Y. Bigot. Electron dynamics in silver nanoparticles: Comparison between thin films and glass embedded nanoparticles. *Physical Review B*, 60(16):11738–11746, 1999.

[92] H. B. Liao, R. F. Xiao, J. S. Fu, H. Wang, K. S. Wong, and G. K. L. Wong. Origin of third-order optical nonlinearity in $Au : SiO_2$ composite films on femtosecond and picosecond time scales. *Optics Letters*, 23(5):388–390, 1998.

[93] V. K. Mizrahi, K. W. Delong, G. I. Stegeman, M. A. Saifi, and M. J. Andrejco. Two-photon absorption as a limitation to all-optical switching. *Optics Letters*, 14:1140–1142, 1989.

[94] E. Cattaruzza, G. Battaglin, F. Gonella, G. Mattei, P. Mazzoldi, R. Polloni, and B.F. Scremin. Fast third-order optical nonlinearities in metal alloy nanocluster composite glass: negative sign of the nonlinear refractive index. *Applied Surface Science*, 247:390–395, 2005.

[95] R. Polloni, B. F. Scremin, P. Calvelli, E. Cattaruzza, G. Battaglin, and G. Mattei. Metal nanoparticles-silica composites: Z-scan determination of non-linear refractive index. *Journal of Non-Crystalline Solids*, 322:300–305, 2003.

[96] D. Faccio, P. Di Trapani, E. Borsella, F. Gonella, P. Mazzoldi, and A. M. Malvezzi. Measurement of the third-order nonlinear susceptibility of ag nanoparticles in glass in a wide spectral range. *Europhysics Letters*, 43(2):213–218, 1998.

[97] Y. Hamanaka, A. Nakamura, N. Hayashi, and S. Omi. Dispersion curves of complex third-order optical susceptibilities around the surface plasmon resonance in ag nanocrystal-glass composites. *Journal of the Optical Society of America B*, 20(6):1227–1232, 2003.

[98] Y. Takeda, O. A. Plaksin, and N. Kishimoto. Dispersion of nonlinear dielectric function of au nanoparticles in silica glass. *Optics Express*, 15:6010–6018, 2007.

[99] R. del Coso, J. Requejo-Isidro, J. Solis, J. Gonzalo, and C. N. Afonso. Third order nonlinear optical susceptibility of Cu : Al_2O_3 nanocomposites: From spherical nanoparticles to the percolation threshold. *Journal of Applied Physics*, 95(5):2755–2762, 2004.

[100] H.B. Liao, R.F. Xiao, J.S. Fu, and G.K.L.Wong. Large third-order nonlinear optical susceptibility of $Au - Al_2O_3$ composite films near the resonant frequency. *Applied Physics B*, 65(4-5):673676, 1997.

[101] H. B. Liao, R. F. Xiao, J. S. Fu, P. Yu, G. K. L. Wong, and P. Sheng. Large third-order optical nonlinearity in Au : SiO_2 composite films near the percolation threshold. *Applied Physics Letters*, 70(1):1–3, 1997.

[102] H. B. Liao, R. F. Xiao, H. Wang, K. S. Wong, and G. K. L. Wong. Large third-order optical nonlinearity in Au : TiO_2 composite films measured on a femtosecond time scale. *Applied Physics Letters*, 72(15):1817–1819, 1998.

[103] S. Ding, X. Wang, D. J. Chen, and Q. Q. Wang. Optical percolation and nonlinearity of sputtered Ag island films. *Optics Express*, 14:1541–1546, 2006.

[104] V. P. Safonov, V. M. Shalaev, V. A. Markel, Yu. E. Danilova, N. N. Lepeshkin, W. Kim, S. G. Rautian, and R. L. Armstrong. Spectral dependence of selective photomodification in fractal aggregates of colloidal particles. *Physical Review Letters*, 80:1102–1105, 1998.

[105] N. N. Lepeshkin, W. Kim, V. P. Safonov, J. G. Zhu, R. L. Armstrong, C. W. White, R. A. Zuhr, and V. M. Shalaev. Optical nonlinearities of metal-dielectric composites. *Journal of Nonlinear Optical Physics and Materials*, 8(2):191–210, 1999.

[106] M. Breit, V. A. Podolskiy, S. Gresillon, G. von Plessen, J. Feldmann, J. C. Rivoal, P. Gadenne, A. K. Sarychev, and V. M. Shalaev. Experimental observation of percolation-enhanced nonlinear light scattering from semicontinuous metal films. *Physical Review B*, 64:125106, 2001.

[107] A. Husakou and J. Herrmann. Steplike transmission of light through a metal-dielectric multilayer structure due to an intensity-dependent sign of the effective dielectric constant. *Physical Review Letters*, 99:127402, 2007.

[108] M. Nelson. *Physical Characterization of Semicontinuous Silver and Gold Films on Dielectric Substrates*. PhD thesis, New Mexico State University, 2004.

[109] M. Sheik-Bahae, A. A. Said, and E. W. Van Stryland. High-sensitivity, single-beam n_2 measurements. *Optics Letters*, 14(17):955–957, 1989.

[110] M. Sheik-Bahae, A. A. Said, T.-H. Wei, D. J. Hagan, and E. W. Van Stryland. Sensitive measurement of optical nonlinearities using a single beam. *IEEE Journal of Quantum Electronics*, 26(4):760–769, 1990.

[111] R. del Coso and J. Solis. Relation between nonlinear refractive index and third-order susceptibility in absorbing media. *Journal of the Optical Society of America B*, 21(3):640–644, 2004.

[112] R. G. Barrera, M. del Castillo-Mussot, G. Monsivais, P. Villaseñor, and W . L. Mochán. Optical properties of two-dimensional disordered systems on a substrate. *Physical Review B*, 43:13819–13826, 1991.

[113] R. Lazzari and I. Simonsen. Granfilm: a software for calculating thin-layer dielectric properties and fresnel coefficients. *Thin Solid Films*, 419:124–136, 2002.

[114] U. Kreibig and M. Vollmer. *Optical Properties of Metal Clusters*, volume 25 of *Springer Series in Materials Science*. Springer-Verlag, 1995.

[115] D. D. Smith, Y. Yoon, R. W. Boyd, J. K. Campbel, L.A. Baker, R. M. Crooks, and M. George. z-scan measurement of the nonlinear absorption of a thin gold film. *Journal of Applied Physics*, 86(11):6200–6205, 1999.

[116] L.J. Wang, A. Kuzmich, and A. Dogariu. Gain-assisted superluminal light propagation. *Nature*, 406:277–279, 2000.

[117] M. S. Bigelow, N. N. Lepeshkin, and R. W. Boyd. Superluminal and slow light propagation in a room-temperature solid. *Science*, 301:200–202, 2003.

[118] Joe T. Mok and Benjamin J. Eggleton. Expect more delays. *Nature*, 433:811–812, 2005.

[119] Y. Okawachi, M. S. Bigelow, J. E. Sharping, Z. Zhu, A. Schweinsberg, D. J. Gauthier, R. W. Boyd, and A. L. Gaeta. Tunable all-optical delays via brillouin slow light in an optical fiber. *Physical Review Letters*, 94:153902, 2005.

[120] J. Sharping, Y. Okawachi, and A. Gaeta. Wide bandwidth slow light using a Raman fiber amplifier. *Optics Express*, 13:6092–6098, 2005.

[121] R. Pant, M. D. Stenner, M. A. Neifeld, and D. J. Gauthier. Optimal pump profile designs for broadband sbs slow-light systems. *Optics Express*, 16:2764–2777, 2008.

[122] Z. Shi, R. Pant, Z. Zhu, M. D. Stenner, M. A. Neifeld, D. J. Gauthier, and R. W. Boyd. Design of a tunable time-delay element using multiple gain lines for increased fractional delay with high data fidelity. *Optics Letters*, 32:1986–1988, 2007.

[123] R. W. Boyd, D. J. Gauthier, A. L. Gaeta, and A. E. Willner. Maximum time delay achievable on propagation through a slow-light medium. *Physical Review A*, 71:023801, 2005.

[124] J. B. Khurgin. Performance limits of delay lines based on optical amplifiers. *Optics Letters*, 31:948–950, 2005.

[125] R. S. Tucker. The role of optics and electronics in high-capacity routers. *Journal Of Lightwave Technology*, 24:4655–4673, 2006.

[126] R. S. Tucker, P.-C. Ku, and C. J. Chang-Hasnain. Slow-light optical buffers: capabilities and fundamental limitations. *Journal of Lightwave Technology*, Volume 23, Issue 12,:4046 – 4066, 2005.

[127] D. A B. Miller. Fundamental limit to linear one-dimensional slow light structures. *Physical Review Letters*, 99:203903, 2007.

[128] Y. Okawachi, R. Salem, and A. L. Gaeta. Continuous tunable delays at 10-gb/s data rates using self-phase modulation and dispersion. *Journal of Lightwave Technology*, 25:3710–3715, 2007.

[129] M. S. Shahriar, G. S. Pati, R. Tripathi, V. Gopal, M. Messall, and K. Salit. Ultrahigh enhancement in absolute and relative rotation sensing using fast and slow light. *Physical Review A*, 75:053807, 2007.

[130] Z. Shi, R. W. Boyd, R. M. Camacho, P. K. Vudyasetu, and J. C. Howell. Slow-light Fourier transform interferometer. *Physical Review Letters*, 99:240801, 2007.

[131] L. Gao, S. I. Herriot, and K. H. Wagner. Sluggish light for radio-frequency true-time-delay applications with a large time-bandwidth product. *Optics Letters*, 31:3360–3362, 2006.

[132] S. E. Schwartz and T. Y. Tan. Wave interaction in saturable absorbers. *Applied Physics Letters*, 10:4, 1967.

[133] R. W. Boyd, M. G. Raymer, P. Narum, and D. J. Harter. Four-wave parametric interaction in a strongly driven two-level system. *Physical Review A*, 24(1):411–423, 1981.

[134] G. Piredda and R. W. Boyd. Slow light by means of coherent population oscillations: laser linewidth effects. *Journal of the European Optical Society - Rapid Publications*, 2:07004, 2007.

[135] M. S. Malcuit, R. W. Boyd, L. W. Hillmann, J. Krasinski, and C. R. Stroud Jr. Saturation and inverse-saturation absorption line shapes in alexandrite. *Journal of the Optical Society of America B*, 1(1):73–75, 1984.

[136] V. S. Zapasskii and G. G. Kozlov. A saturable absorber, coherent population oscillations and slow light. *Optics and Spectroscopy*, 100(3):419–424, 2006.

[137] P.-C. Ku, F. Sedgwick, C. J. Chang-Hasnain, P. Palinginis, T. Li, H. Wang, S.-W. Chang, and S.-L. Chuang. Slow light in semiconductor quantum wells. *Optics Letters*, 29(19):2291–2293, 2004.

[138] H. Su and S. L. Chuang. Room-temperature slow light with semiconductor quantum-dot devices. *Optics Lett.*, 31:271–273, 2006.

[139] P. Palinginis, S. Crankshaw, F. Sedgwick, E.-T. Kim, M. Moewe, and C. J. Chang-Hasnain. Ultraslow light (¡200 m/s) propagation in a semiconductor nanostructure. *Applied Physics Letters*, 87:171102, 2005.

[140] M. van der Poel, J. Mork, and J. M. Hvam. Controllable delay of ultrashort pulses in a quantum dot optical amplifier. *Optics Express*, 13(20):8032–8037, 2005.

[141] X. Zhao, P. Palinginis, B. Pesala, C. J. Chang-Hasnain, and P. Hemmer. Tunable ultraslow light in vertical-cavity surface-emitting laser amplifier. *Optics Express*, 13(20):7899–7904, 2005.

[142] J. Mork, R. Kjaer, M. van der Poel, and K. Yvind. Slow light in a semiconductor waveguide at gigahertz frequencies. *Optics Express*, 13(20):8136–8145, 2005.

[143] U. Keller, K. J. Weingarten, F. X. Kartner, D. Kopf, B. Braun, I. D. Jung, R. Fluck, C. Honninger, N. Matuschek, and J. Aus der Au. Semiconductor saturable absorber mirrors (SESAM's) for femtosecond to nanosecond pulse generation in solid-state lasers. *IEEE Journal of Selected Topics in Quantum Electronics*, 2(3):435–453, 1996.

[144] E. S. Harmon, M. R. Melloch, J. M. Woodall, D. D. Nolte, N. Otsuka, and C. L. Chang. Carrier lifetime versus anneal in low temperature growth gaas. *Applied Physics Letters*, 63(16):2248–2250, 1993.

[145] U. Siegner, R. Fluck, G. Zhang, and U. Keller. Ultrafast high-intensity nonlinear absorption dynamics in low-temperature grown gallium arsenide. *Applied Physics Letters*, 69(17):2566–2568, 1996.

[146] A. Dementjev, V. Gulbinas, L. Valkunas, I. Motchalov, H. Raaben, and A. Michailovas. Mode-locking of neodymium lasers by glasses doped with pbs nanocrystals. *Applied Physics B*, 77:595–599, 2003.

[147] J. E. Sharping, Y. Okawachi, and A. L. Gaeta. Wide bandwidth slow light using a raman fiber amplifier. *Optics Express*, 13:6092–6098, 2005.

[148] A. C. Selden. Pulse transmission through a saturable absorber. *British Journal of Applied Physics*, 18:743–748, 1967.

[149] G. Piredda, D. D. Smith, B. Wendling, and R. W. Boyd. Nonlinear optical properties of a gold-silica composite with high gold fill fraction and the sign change of its nonlinear absorption coefficient. *Journal of the Optical Society of America B*, 25(6):945–950, 2008.

[150] D. Weaire, B. S. Wherrett, D. A. B. Miller, and S. D. Smith. Effect of low-power nonlinear refraction on laser-beam propagation in insb. *Optics Letters*, 4:331–333, 1974.

[151] Q. Lin, J. Zhang, G. Piredda, R. W. Boyd, P. M. Fauchet, and G. P. Agrawal. Dispersion of silicon nonlinearities in the near infrared region. *Applied Physics Letters*, 91:021111, 2007.

Appendix A

The intensity-dependent refractive

index

In this Appendix we review the concepts of nonlinear optics which lead to the definition of the intensity-dependent refractive index and we list some relevant formulae.

A precise definition of the intensity-dependent refractive index can be given in the perturbative formalism of nonlinear optics. The following discussion is based on Boyd's book on nonlinear optics [33].

For a lossless and dispersionless medium the polarization $\tilde{P}(t)$ can be expressed as a power series in the field $\tilde{E}(t)$ (let us indicate with a tilde the full dependence on time of a physical quantity, including its rapidly oscillating behaviour):

$$\tilde{P}(t) = \chi^{(1)} \tilde{E}(t) + \chi^{(2)} \tilde{E}^2(t) + \chi^{(3)} \tilde{E}^3(t) + ... \qquad (A.1)$$

The "perturbative" approach to nonlinear optics assumes that the series A.1 converges fairly quickly and uses each term to define a separate nonlinear susceptibility: in particular $\chi^{(2)}$ is the second-order susceptibility (from which second-harmonic generation and optical rectification result for example) and $\chi^{(3)}$ is the third-order susceptibility which gives rise to many phenomena among which is the one, the intensity-dependent refractive index, in which we are interested.

If the medium is lossy and is dispersive (these two characteristics are linked in linear optics by the Kramers-Kronig relations in linear optics but the situation in nonlinear optics is more complicated) the relationship between polarization and electric field can be expressed more synthetically in the frequency domain rather than in the time domain. In particular it is possible to associate a nonlinear susceptibility coefficient to each distinct product of frequency components of the electric field and to distinguish in this way between different nonlinear optical effects; for example the generation of a certain frequency that did not exist in the incident fields could be attributed to a second- or third-order effect and starting with this attribution one can calculate, for example, how the generation will vary if the directions of one of possibly several interacting beams vary.

In particular the intensity-dependent refractive index comes from the following part of nonlinear polarization:

$$P^{\text{NL}}(\omega) = 3\chi^{(3)}(\omega = \omega + \omega - \omega)\,|E(\omega)|^2\,E(\omega)\,, \qquad\qquad \text{(A.2)}$$

where the frequency arguments that accompany $\chi^{(3)}$ remind that it is the coefficient of the combination $|E(\omega)|^2 E(\omega)$ in the perturbative expansion of the polarization in the frequency domain. In Equation A.2 we have assumed that light is linearly polarized and we have ignored the tensor nature of $\chi^{(3)}$. The frequency components of the electric field are defined in such a way that for a monochromatic field $\tilde{E}(t) = E(\omega) e^{-i\omega t} + E(-\omega) e^{i\omega t}$, and for the other physical quantities one adopts the same convention.

The total polarization at frequency ω can then be written as

$$P^{\mathrm{TOT}}(\omega) = \chi^{(1)} E(\omega) + 3\chi^{(3)} |E(\omega)|^2 E(\omega) = \chi_{\mathrm{eff}} E(\omega), \tag{A.3}$$

where we have introduced the effective susceptibility

$$\chi_{\mathrm{eff}} = \chi^{(1)} + 3\chi^{(3)} |E(\omega)|^2. \tag{A.4}$$

The definition of an effective susceptibility leads to the definition of an effective refractive index as

$$n^2 = 1 + 4\pi\chi_{\mathrm{eff}}, \tag{A.5}$$

and individuating in the effective index n the part that depends on $|E(\omega)|^2$ leads to the following equation:

$$\bar{n}_2 = \frac{3\pi\chi^{(3)}}{n_0}.$$ (A.6)

We need to note that a factor of two is inserted inside the equation that defines the dependence of the refractive index on the square of the field

$$n = n_0 + 2\bar{n}_2 \left|E\left(\omega\right)\right|^2$$ (A.7)

because in this way $\bar{n}_2$ is the linear coefficient of the dependence of the refractive index on the average of the square of the field:

$$n = n_0 + \bar{n}_2 \left\langle \tilde{E}^2 \right\rangle.$$ (A.8)

The effective refractive index can be written as a function of intensity rather than square of the field:

$$n = n_0 + n_2 I.$$ (A.9)

Taking into account the relationship between intensity and field

$$I = \frac{n_0 c}{2\pi} \left|E\left(\omega\right)\right|^2$$ (A.10)

one can express n_2 as a function of either $\bar{n}_2$ or $\chi^{(3)}$:

$$n_2 = \frac{4\pi}{n_0 c}\bar{n}_2 \tag{A.11}$$

and

$$n_2 = \frac{12\pi^2}{n_0^2 c}\chi^{(3)}. \tag{A.12}$$

The last two equations have to be modified for absorbing media and in particular Equation A.12 becomes

$$n_2 = \frac{12\pi^2}{n_0 \mathrm{Re}\left\{n_0\right\} c}\chi^{(3)}. \tag{A.13}$$

The consequences of the difference between Equations A.12 and A.13 have been examined in detail by Smith and coauthors [32] and del Coso and Solis [111]; in particular the imaginary part of $\chi^{(3)}$ can lead to nonlinear refraction and conversely the real part of $\chi^{(3)}$ to nonlinear absorption.

The scalar formulation of the intensity-dependent refractive index is adequate to describe the experiment presented in this thesis that were performed with one beam of linearly polarized light.

Appendix B

The model of Maxwell Garnett

We present the derivation for two forms of the Maxwell Garnett theory. The original theory [39] deals with spherical inclusions and is appropriate to treat bulk composite media. In [149] we applied the same ideas to a collection of infinitely long cylinders whose axis is perpendicular to the applied field immersed in a host medium. David D. Smith proposed this geometry to take into account in a simplified way of one important feature of thin films that differentiates them from bulk media. In bulk media the neighbors to each particle are distributed in three dimensions around it, while in a thin film the neighbors are distributed in a correspondingly thin disk. The calculation of the local field must take this into account. We finally interpolate the formulae for the three-dimensional and two-dimensional cases with a single expression.

B.0.1   Standard Maxwell Garnett theory

Let us start with the standard three-dimensional case. Our aim is to calculate the polarization density in the medium when a macroscopic field $\mathbf{E}$ is measured inside the medium. The macroscopic field is the field averaged over a region large with respect to a nanoparticle.

The polarization density is given by the sum of the polarization density of the host and the one of the nanoparticles as

$$\mathbf{P}_{MG} = \chi_h \mathbf{E} + N\alpha_i \mathbf{E}_{loc}, \tag{B.1}$$

where χ_h is the susceptibility of the host, α_i is the polarizability of a single nanoparticle, N is the number of nanoparticles per unit volume and $\mathbf{E}_{loc}$ is the Lorentz local field; the Lorentz local field is the field experienced by the nanoparticle, that is the macroscopic field minus the field of the nanoparticle itself.

In the Clausius-Mossotti theory the Lorentz local field has a "microscopic" character because it is the field felt by a single gas molecule; in the Maxwell Garnett theory it has a mesoscopic character because includes fields generated by objects of nanometer size, but it is calculated in the same way. Here is a way to calculate it.

The field in any point $\mathbf{r}$ in the medium is equal to the field generated by the dipoles contained in a sphere centered around the point itself $\mathbf{r}$ plus the field generated by all the other sources. As the diameter of the sphere becomes smaller and smaller "the field produced by all the other sources" becomes closer and closer to the local

field $\mathbf{E}_{loc}$ because the field produced by the dipoles contained in the sphere becomes closer and closer to the field of the single dipole placed at $\mathbf{r}$. The reason why this limit procedure works is that the field generated by a spherical distribution of dipoles inside the sphere where the dipoles are contained is independent of the radius of the sphere; this field is

$$\mathbf{E}_{sph} = -\frac{4\pi}{3}\frac{1}{\varepsilon_h}\mathbf{P}_{np};\qquad\text{(B.2)}$$

in the case of the Maxwell Garnett medium we take $\mathbf{P}_{np}$ as the dipole density due to the nanoparticles

$$\mathbf{P}_{np} = N\alpha_i\mathbf{E}_{loc} = N\alpha_i\left(\mathbf{E} + \frac{4\pi}{3}\frac{1}{\varepsilon_h}\mathbf{P}_{np}\right).\qquad\text{(B.3)}$$

The expression for the static polarizability of a sphere of radius R and dielectric constant ε_i immersed in a host of dielectric constant ε_h is

$$\alpha_i = R^3\varepsilon_h\frac{\varepsilon_i - \varepsilon_h}{\varepsilon_i + 2\varepsilon_h}.\qquad\text{(B.4)}$$

We solve Equation B.1 for $\mathbf{P}_{np}$ and we insert expression B.4 to obtain the polarization density of the nanoparticles as a function of the macroscopic field:

$$\mathbf{P}_{np} = \frac{N\alpha_i}{1 - \frac{4\pi}{3}\frac{N\alpha_i}{\varepsilon_h}}\mathbf{E} = \frac{3f}{4\pi}\varepsilon_h\frac{\frac{\varepsilon_i-\varepsilon_h}{\varepsilon_i+2\varepsilon_h}}{1 - f\frac{\varepsilon_i-\varepsilon_h}{\varepsilon_i+2\varepsilon_h}}\mathbf{E}\qquad\text{(B.5)}$$

where we have noted that the volume fill fraction f is equal to $N\frac{4\pi}{3}R^3$.

Following Equation B.1 we sum the polarization density of the host to that of the nanoparticles; we then obtain the effective susceptibility of the Maxwell Garnett composite material as

$$\chi_{MG} = \chi_h + \chi_{np} = \chi_h + \frac{3f}{4\pi} \frac{\frac{\varepsilon_i - \varepsilon_h}{\varepsilon_i + 2\varepsilon_h}}{1 - f\frac{\varepsilon_i - \varepsilon_h}{\varepsilon_i + 2\varepsilon_h}}. \tag{B.6}$$

Passing from susceptibilities to dielectric constants we obtain

$$\frac{\varepsilon_{MG} - \varepsilon_h}{\varepsilon_{MG} + 2\varepsilon_h} = f\frac{\varepsilon_i - \varepsilon_h}{\varepsilon_i + 2\varepsilon_h} \tag{B.7}$$

which is the Maxwell Garnett result expressed as a linear equation.

As a general note on the procedure that we have followed, we first "average" (start with macroscopic fields) then "solve" (work out the Lorentz local field). The review paper by Aspnes [72] shows that it is possible to do the opposite, that is first "solve" (calculate the local fields starting from an external applied field and the response of the dipoles in the system) and then average the fields to obtain the macroscopic fields. In this way one avoids the step in which all dipoles, does not matter how far away they are, seem to give the same contribution to the local field (Equation B.2).

An important quantity in the theory of composites materials is the mesoscopic local field inside the components. It can be calculated considering once more the electrostatic problem. The field inside a sphere subject to an incident uniform electric

field $\mathbf{E}_{loc}$ is

$$\mathbf{E}_{in} = \frac{3\varepsilon_h}{\varepsilon_i + 2\varepsilon_h}\mathbf{E}_{loc} \tag{B.8}$$

which becomes after substitution of expression B.2 for the local field and application of the Maxwell Garnett equation 2.6 becomes

$$\mathbf{E}_{in} = \frac{\varepsilon + 2\varepsilon_h}{\varepsilon_i + 2\varepsilon_h}\mathbf{E} = q_i\mathbf{E}. \tag{B.9}$$

The proportionality factor q_i between the mesoscopic field inside the nanoparticles and the macroscopic field is called the "local field factor".

B.0.2 Maxwell Garnett theory for a two-dimensional system

We approximate the two-dimensional medium as a three-dimensional system with translational symmetry along one axis: a collection of infinitely long cylinders parallel to each other with their axes perpendicular to the applied field and immersed in a host medium (see Figure B.1).

If a cylinder of radius R and dielectric constant ε_i, immersed in a medium of dielectric constant ε_h, is subject to an electric field $\mathbf{E}$ perpendicular to its axis, it acquires a polarization per unit length

$$\mathbf{\Pi}_{cyl} = \varepsilon_h \frac{R^2}{2}\frac{\varepsilon_i - \varepsilon_h}{\varepsilon_i + \varepsilon_h}\mathbf{E} = \alpha_{cyl}\mathbf{E}. \tag{B.10}$$
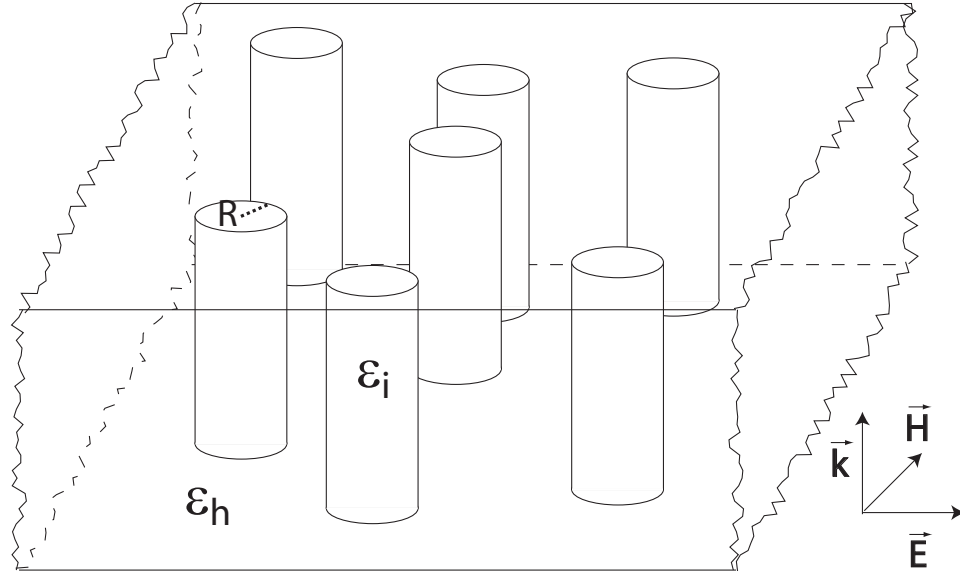
Figure B.1: Section of the model for a Maxwell Garnett two-dimensional composite, a host with infinitely long cylindrical inclusions.

The polarization density of the medium, when the macroscopic electric field is $\mathbf{E}$, is

$$\mathbf{P} = \mathbf{P}_h + N\mathbf{\Pi}_{cyl} = \chi_h\mathbf{E} + N\alpha_{cyl}\mathbf{E}_{loc}, \tag{B.11}$$

where N is the number of cylindrical inclusions per unit area and $\mathbf{E}_{loc}$ is the Lorentz local field.

The Lorentz local field is the field to which each inclusion is subject, that is the macroscopic field minus the field generated by the inclusion itself. It can be calculated by eliminating the inclusions from a cylindrical region, creating in this way a cylindrical cavity, and leaving all the rest, and in particular the polarization of

the other inclusions, unchanged; in this cavity the Lorentz field is uniform and given by

$$\mathbf{E}_{loc} = \mathbf{E} + \frac{2\pi\mathbf{\Pi}}{\varepsilon_h}. \tag{B.12}$$

Inserting Eq. (B.12) in (B.11) we obtain the following expression for the susceptibility χ of the composite medium:

$$\chi = \chi_h + \frac{N\alpha_{cyl}}{1 - \frac{2\pi N\alpha_{cyl}}{\varepsilon_h}}. \tag{B.13}$$

Rewriting Eq. (B.13) in terms of the dielectric constants we obtain for the two-dimensional Maxwell Garnett composite the following relation:

$$\frac{\varepsilon - \varepsilon_h}{\varepsilon + \varepsilon_h} = f \frac{\varepsilon_i - \varepsilon_h}{\varepsilon_i + \varepsilon_h} \tag{B.14}$$

.

The local field $\mathbf{E}_i$ inside the cylindrical inclusions is given by

$$\mathbf{E}_i = q_i\mathbf{E}, \tag{B.15}$$

where

$$q_i = \frac{\varepsilon + \varepsilon_h}{\varepsilon_i + \varepsilon_h} \tag{B.16}$$

is the local field factor.

B.0.3   Interpolation between the 2- and 3-dimensional models

Comparing Equation (B.14) to the Maxwell Garnett result for spherical inclusions we see that both the two- and three-dimensional relations have the form

$$\frac{\varepsilon - \varepsilon_h}{\varepsilon + (D-1)\,\varepsilon_h} = f\,\frac{\varepsilon_i - \varepsilon_h}{\varepsilon_i + (D-1)\,\varepsilon_h}, \tag{B.17}$$

where D is the dimensionality of the system. In an analogous way we have for the local field factor

$$q_i = \frac{\varepsilon + (D-1)\varepsilon_h}{\varepsilon_i + (D-1)\varepsilon_h}. \tag{B.18}$$

In Eqs. (B.17) and (B.18) the dimensionality D can be treated as a free parameter ranging between 2 and 3 to represent composite media whose characteristics are intermediate between the two- and three-dimensional cases.

B.0.4   Extension to a nonlinear optical response

An expression for the effective third-order nonlinearity for the Maxwell Garnett composite in the case in which only the inclusions are nonlinear can be obtained by considering that the Maxwell Garnett expression must remain valid as the electric field increases and the dielectric constant of the inclusions change. We can then

equate the variation in both sides of Eq. (B.17) obtaining

$$\frac{\partial}{\partial \varepsilon} \left(\frac{\varepsilon - \varepsilon_h}{\varepsilon + (D-1)\,\varepsilon_h} \right) \Delta\varepsilon = f \frac{\partial}{\partial \varepsilon_i} \left(\frac{\varepsilon_i - \varepsilon_h}{\varepsilon_i + (D-1)\,\varepsilon_h} \right) \Delta\varepsilon_i, \qquad \text{(B.19)}$$

and after a few simplifications we obtain a concise expression for the change of the effective dielectric constant ε as a function of the change of the dielectric constant of the inclusions ε_i:

$$\Delta\varepsilon = f q_i^2 \Delta\varepsilon_i. \qquad \text{(B.20)}$$

If the inclusions have a Kerr nonlinearity then $\Delta\varepsilon_i$ can be written as a function of the local field in the inclusions as $\Delta\varepsilon_i = 4\pi\chi_i^{(3)} |E_i|^2 = 4\pi\chi_i^{(3)} |q_i|^2 |E|^2$. Inserting this last expression in Eq. (B.20) we obtain the effective nonlinearity of the composite as

$$\chi^{(3)} = f \chi_i^{(3)} q_i^2 |q_i|^2. \qquad \text{(B.21)}$$

Appendix C

The z-scan technique

The z-scan technique [109, 110] is a sensitive, single beam technique to measure the real and imaginary part of the nonlinear refractive index.

There are two basic versions of the z-scan technique, the open-aperture and the closed-aperture technique; the closed-aperture technique is a method to extract phase information from power measurements, while the open-aperture technique is a refinement of transmittance measurements.

In the closed-aperture z-scan technique one measures the transmittance of a sample through an aperture placed in the far-field as the sample is translated across the focus of a gaussian beam. Figure C.1 shows the reason why in this configuration a power measurement is able to detect the phase changes associated with a nonlinear refractive index.

If a sample with positive intensity-dependent refractive index (n_2) is placed in
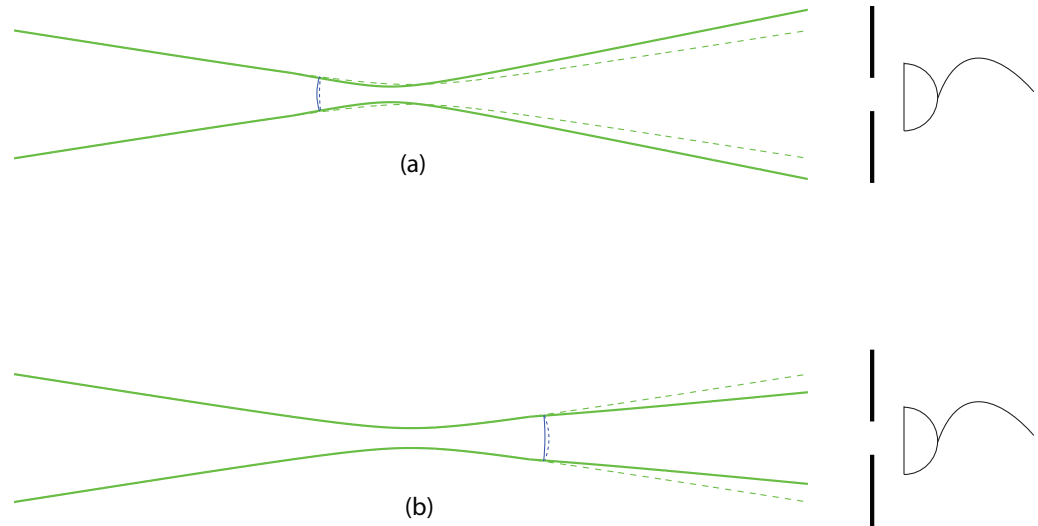
Figure C.1: Schematic representation of a closed-aperture z-scan experiment. Part (a) represents the effect of a sample with positive intensity-dependent refractive index placed before the beam waist; part (b) represents the effect of the same sample placed after the beam waist. The blue lines indicate the wavefronts at the sample position. The propagation of a low-power beam of light is represented with dashed lines while solid lines represent the propagation of a high-power beam.

a Gaussian beam the light acquires a positive amount of phase in addition to the phase given by linear propagation while travelling through the sample; this additional "nonlinear" phase is a function of intensity and therefore of transverse position across the beam, larger at the center of the beam and smaller at the wings. When the sample is placed before the waist (part (a) of Figure C.1) the nonlinear phase tends to increase the curvature of the wavefronts of the Gaussian beam, while when the sample is placed after the beam waist ((part (b) of Figure C.1)) the additional phase

tends to "flatten" the wavefronts.

In case (a) the beam that has gone through the nonlinear sample (solid line) focuses more tightly than the linearly propagating beam (dashed line) and in the far field diverges with a larger angle; the amount of energy that passes through an aperture in the far field is therefore smaller than the energy that passes through the same aperture in the linear regime. In case (b) the beam, after passing through the nonlinear sample, looks like a beam that propagated out of a wider waist than the waist given by linear propagation; it therefore diverges less and more energy passes through the far-field aperture. The opposite happens for a sample possessing a negative intensity-dependent refractive index.

If one plots the transmittance as a function of position for the two different kind of samples (positive and negative n_2) two different curves are obtained; for the positive n_2 the curve consists of a valley followed by a peak, and the opposite for the negative n_2 case.

The curves of transmittance as a function of sample position are influenced not only by nonlinear refraction but also by nonlinear absorption. Saturable absorption tends to enhance the peak and suppress the valley, and optical limiting acts in the opposite sense.

An expression for the transmittance through a far-field aperture of a Gaussian beam that underwent nonlinear refraction and absorption can be obtained in series form using the "Gaussian decomposition" method [150]. We follow here the treatment

given by Sheik-Bahae et al. in their detailed description of the z-scan method [110].

For a cubic nonlinearity the index of refraction can be expressed through the equation [33]

$$n = n_0 + n_2 I \qquad \text{(C.1)}$$

where n_0 is the linear index of refraction, I is the optical intensity and n_2 is the intensity-dependent refractive index; if comparing to reference [110] note that in [110] the symbol n_2 denotes the lowest order of the dependence of the refractive index on the average of the square of the electric field, while the symbol γ is used in place of our symbol n_2.

The electric field of a Gaussian beam incident on the nonlinear sample is written as

$$E\left(z, r, t\right) = E_0\left(t\right) \frac{w_0}{w\left(z\right)} \exp\left(-\frac{r^2}{w^2\left(z\right)} - \frac{ikr^2}{2R\left(z\right)}\right) \exp\left(-i\phi\left(z, t\right)\right). \qquad \text{(C.2)}$$

In Equation C.2 $k = 2\pi/\lambda$ is the wavenumber of a light wave of wavelength λ, w_0 is the beam waist, $w\left(z\right)$ is the beam radius and $R\left(z\right)$ the radius of curvature of the wavefront, all given in free space; $E_0\left(t\right)$ contains the temporal envelope of the laser pulse and in the term $\exp\left(-i\phi\left(z, t\right)\right)$ we have expressed all phase variations that do not depend on the spatial transverse coordinate. Expressions for $w\left(z\right)$ and $R\left(z\right)$ are

respectively

$$w^2(z) = w_0^2 \left(1 + \frac{z^2}{z_0^2}\right) \tag{C.3}$$

$$R(z) = z \left(1 + \frac{z^2}{z_0^2}\right) \tag{C.4}$$

with $z_0 = kw_0^2/2$.

If a sample is thin enough the modification of a beam that has travelled through it can be expressed by a multiplicative term:

$$E_e(z, r, t) = E(z, r, t) e^{-\alpha L/2} e^{i\Delta\phi(z,r,t)} \tag{C.5}$$

where α is the sample linear absorption coefficient and L the sample length. The "phase shift" term $\Delta\phi(z, r, t)$ contains both nonlinear absorption and nonlinear refraction and is given by the expression

$$\Delta\phi(z, r, t) = \Delta\phi_0(z, t) \exp\left(-\frac{2r^2}{w^2(z)}\right) \tag{C.6}$$

with

$$\Delta\phi_0(z, t) = \frac{\Delta\Phi_0(t)}{1 + z^2/z_0^2}. \tag{C.7}$$

$\Delta\Phi_0$ is the on-axis phase shift at focus:

$$\Delta\Phi_0\left(t\right) = kn_2I_0\left(t\right)L_{eff} \tag{C.8}$$

with $L_{eff} = \left(1 - e^{-\alpha L}\right)/\alpha$ an effective length that takes into account linear losses within the sample and I_0 the optical intensity on axis and at focus.

The "Gaussian decomposition" method of [150] prescribes expanding the exponential that contains the nonlinear phase into a Taylor series as

$$e^{i\Delta\phi(z,r,t)} = \sum_{m=0}^{\infty} \frac{\left[i\Delta\phi_0\left(z,t\right)\right]^m}{m!} \, e^{-2mr^2/w^2(z)}. \tag{C.9}$$

The beam profile after the sample is thus expressed as a superposition of Gaussian beams that can be propagated to the far field and then resummed to reconstruct the beam.

Two limiting cases are of particular interest. The first one is of a very small aperture, pure refractive nonlinearity and small nonlinear phase shift $\Delta\Phi_0$; in this case an approximated expression can be obtained for the normalized transmission as a function of position that allows a quick and often precise estimation of the value of n_2 and gives an immediate "feeling" for characteristic experimental results:

$$T\left(z,\Delta\Phi_0\right) \cong 1 + \frac{4\Delta\Phi_0 x}{\left(x^2 + 9\right)\left(x^2 + 1\right)} \tag{C.10}$$

where $x = z/z_0$ and z is the sample position (not to be confused with the z used in the expression for the Gaussian beam). In Figure C.2 we show a graph of Equation

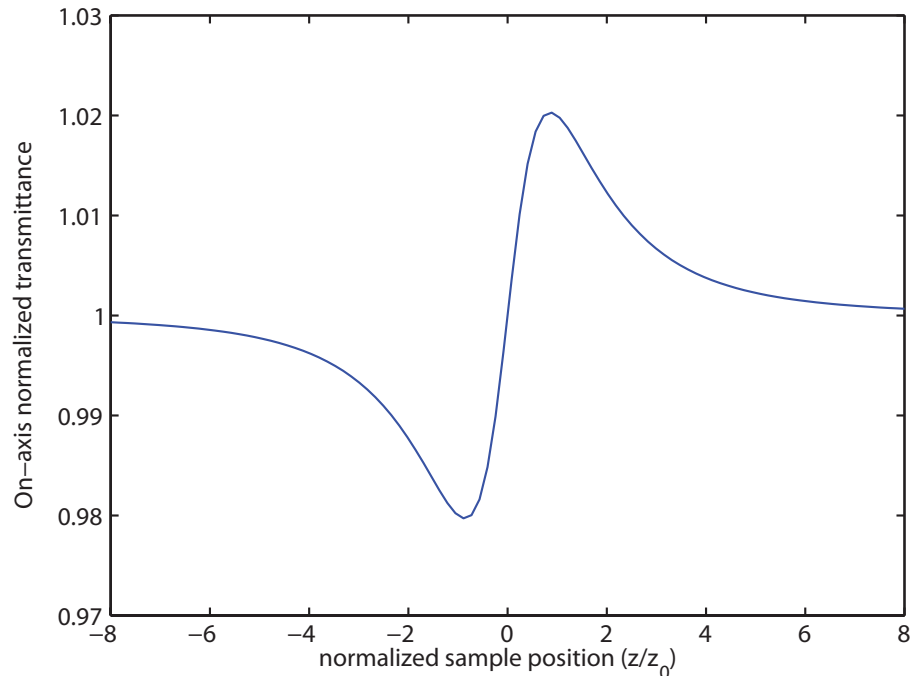C.10 for a sample exhibiting a positive n_2.

Figure C.2: The characteristic "valley and peak" aspect of the on-axis irradiance in the far field as a sample possessing a purely real intensity-dependent refractive index is translated through the focus of a Gaussian beam.

The second case is the one of an aperture that is large enough to capture all of the energy of the beam. In this case the only effect that can contribute to a variation in transmission is nonlinear absorption. This is the configuration that has been used for the experiment of this thesis.

The theoretical treatment suggested by [110] for this experimental configuration goes a bit beyond the thin-sample approximation (Equation C.5) by taking into account that the intensity change as the light travels along the sample is given not only by linear but also by nonlinear absorption; it still ignores diffraction on the length

scale of the sample. The amplitude $\sqrt{I}$ and phase of the light are then governed by the equations

$$\frac{d\Delta\phi}{dz'} = kn_2 I \tag{C.11}$$

and

$$\frac{dI}{dz'} = -(\alpha + \beta I)I \tag{C.12}$$

with z' the propagation distance in the sample (again not to be confused with sample position z). Note that if $\beta = 0$ Equations C.12 and C.11 yield again the simplest form of the thin-sample approximation.

The beam phase and intensity as the light exits the sample are given by

$$\Delta\phi\left(z, r, t\right) = \frac{kn_2}{\beta} \ln\left[1 + q\left(z, r, t\right)\right] \tag{C.13}$$

$$I_e\left(z, r, t\right) = \frac{I\left(z, r, t\right)e^{-\alpha L}}{1 + q\left(z, r, t\right)}. \tag{C.14}$$

The complex field pattern at the far-field aperture can be expressed again by a superposition of Gaussian beams, but since we are interested only in the total transmitted energy we only need to integrate Equation C.14 over the transverse coordinate r. The result of the integration is the transmitted power

$$P(z,t) = P_i(t) e^{-\alpha L} \frac{\ln[1 + q_0(z,t)]}{q_0(z,t)} \qquad (C.15)$$

where $q_0(z,t) = \beta I_0(t) L_{eff}/(1 + z^2/z_0^2)$ and $P_i(t) = \pi w_0^2 I_0(t)/2$ is the instantaneous input power.

If we assume a temporally Gaussian pulse and we integrate Equation C.15 over time we obtain the normalized energy transmission

$$T(z) = \frac{1}{\sqrt{\pi} q_0(z,0)} \int_{-\infty}^{\infty} \ln\left[1 + q_0(z,0) e^{-\tau^2}\right] d\tau. \qquad (C.16)$$

For $|q_0| < 1$ this transmittance can be expressed as the series

$$T(z) = \sum_{m=0}^{\infty} \frac{[-q_0(z,0)]^m}{(m+1)^{3/2}}. \qquad (C.17)$$

It is interesting to note that the series expression can fit normalized z-scan transmission curves that do not peak to more than ≈ 2.61 (in the case of saturable absorption) or dip more than ≈ 0.77 (in the case of optical limiting); one can verify this limits substituting $q_0 = -1$ and 1 respectively and summing the series (I did it with a computer program). The other important observation is that series C.17 converges very quickly and one needs just the first two terms to fit well z-scans curves with normalized transmittances between 0.90 and 1.10. A typical curve obtained from an open-aperture z-scan experiment is shown in Figure C.3

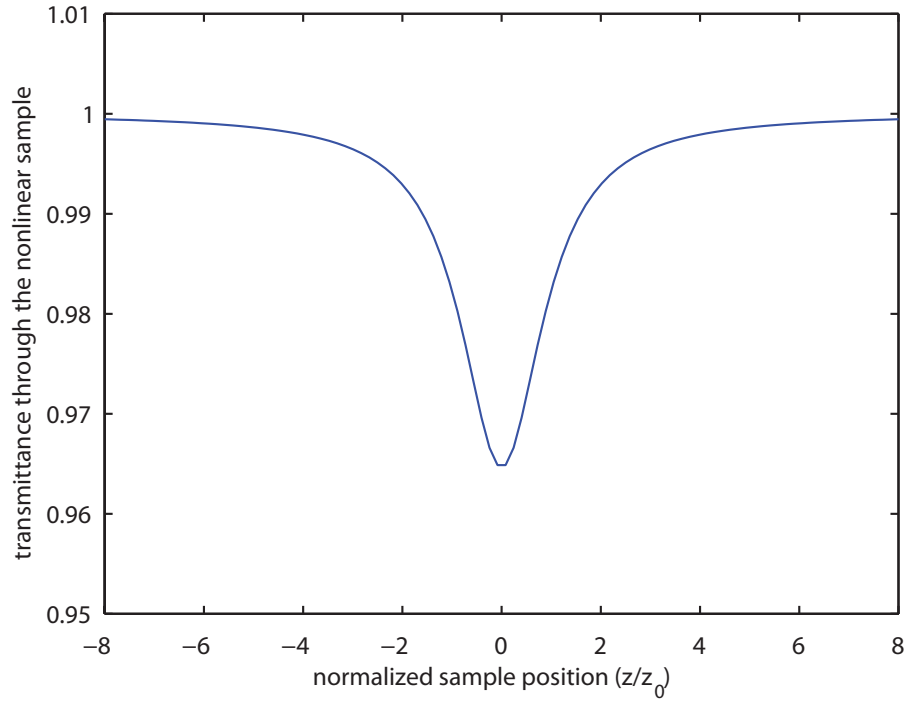Finally, an expression for the z-scan curve that takes into account both nonlinear

Figure C.3: The curve resulting from an open-aperture z-scan experiment on an optical limiter.

absorption and nonlinear refraction (according to Equations C.11 and C.12) and the effect of a finite aperture in the far field is [151]

$$T\left(z\right) = 1 - \frac{I_0 L_{eff}\left(\beta D_r - 2kn_2 D_i\right)}{2\sqrt{2}S\left(1 + x^2\right)} \tag{C.18}$$

where S is the transmittance of the on-axis aperture and D_r and D_i are defined by

$$D_r + iD_i = 1 - \exp\left[\frac{2\left(x - i\right)\left(x + 3i\right)}{x^2 + 9}\ln\left(1 - S\right)\right]; \tag{C.19}$$

Expression C.18 corresponds to the far-field propagation of the first term of expres-

sions (27) and (28) in reference [110].